

Redesign of the Poly Picosatellite Orbital Deployer for the
Dnepr Launch Vehicle

A Thesis
Presented to
The Faculty of
California Polytechnic State University, San Luis Obispo

In Partial Fulfillment
of the Requirements for the Degree
Master of Science in Aerospace Engineering

By
Armen Toorian
February 2007

One day you'll read this and smile...

Authorization

Redesign of the Poly Picosatellite Orbital Deployer for the Dnepr Launch Vehicle

By

Armen Toorian

I grant permission for the reproduction of this thesis in its entirety or any of its parts,
without further authorization from me.

Signature

Date

Approval

TITLE: Redesign of the Poly Picosatellite Orbital Deployer for the Dnepr Launch Vehicle

AUTHOR: Armen Toorian

DATE: February 8, 2007

Dr. Jordi Puig-Suari

Date

Dr. Eric Mehiel

Date

Dr. James Meagher

Date

Abstract

Redesign of the Poly Picosatellite Orbital Deployer for the Dnepr Launch Vehicle

Armen Toorian

The CubeSat Program is an international collaboration of 80+ universities, companies, and government organizations building a class of tiny spacecraft — CubeSats. The CubeSat Program aims to make launches readily available for universities and allow students to experience a complete mission life cycle. A key enabler is the use of a standard deployment system. The Poly Picosatellite Orbital Deployer (P-POD) is a square, tubular structure capable of deploying three CubeSats into space.

Following one successful launch, the P-POD design was iterated to improve on lessons learned and ensure compatibility with the Dnepr launch vehicle. Five P-PODs carrying 14 CubeSats were built, tested, and shipped to Baikonur for integration and launch on a Dnepr launch vehicle.

The P-POD allowed Cal Poly to demonstrate the feasibility of low cost CubeSat missions, show benefits of standardization in space, simplified the export process, allowed CubeSat payloads to be swapped between launch vehicles only months before launch, and provided students with invaluable experience.

Acknowledgments

Dr. Jordi Puig-Suari, Cal Poly CubeSat PI —

For fostering the CubeSat project at Cal Poly. Your guidance and leadership has helped the CubeSat Program become a great success at Cal Poly and abroad. P.S., I reserve the right to show up unannounced with a forty of your favorite malt liquor.

Bob Twiggs, Stanford University —

For having the ingenuity to look at a beany-baby box and see a potential class of tiny satellites instead of a ridiculous toy. Thank you for sharing your vision.

Jill Keezer, Cal Poly Sponsored Programs Director —

For helping us navigate the daunting seas of ITAR paperwork. We would have never had a chance without you.

Simon “Snuggles” Lee and Roland “Rolaid” Coelho —

For the endless support and motivation. Working as a team made the impossible possible. Thanks for the privilege of working with you.

CubeSat and PolySat Teams —

For being a crutch, a sounding block, a motivator, and a constant source of inspiration, all at the appropriate times. Thanks for being friends instead of colleagues.

Cal Poly Multidisciplinary Space Technology Lab —

For being my home away from home. I can't begin to count the number of sleepless nights. I'd rather not know, it's bad enough we added up the cleanroom hours... Thank you to those in the administration that supported the CubeSat Program, and thank you to all the professors for their help and guidance, especially Dr. Meagher and Dr. Mehiel.

My Family —

I could say so much... Thanks for too many years of unquestioned love and support.

Contents

List of Figures	xiii
List of Tables	xix
1 Introduction	1
1.1 The CubeSat Program	1
1.2 The Poly Picosatellite Orbital Deployer	3
1.3 History	4
1.4 The Dnepr Launch Opportunity	7
2 Requirements Definition	9
2.1 Safety Requirements	9
2.2 Operational Requirements	11
2.3 Environmental Requirements	11
2.3.1 Static Loads	13
2.3.2 Dynamic Loads	13
2.3.3 Thermal Loads	14
2.3.4 Other Considerations	14
2.4 Changes to the P-POD	16
3 Design Tools and Philosophy	17

3.1	Computer Aided Engineering	17
3.2	Finite Element Analysis	18
3.3	Prototyping	19
3.4	Testing	20
3.5	On Reliability	21
3.6	On Simplicity	21
4	Redesigning the P-POD	23
4.1	Coordinate Systems	23
4.2	Launch Vehicle Interface	23
4.2.1	Mechanical Interface	25
4.2.2	Electrical Interface	27
4.3	Release Mechanism	28
4.3.1	Planetary Systems Corp. Line Cutter	29
4.3.2	Mechanism Type Survey	30
4.3.3	Mechanism Trade Study	33
4.3.4	Starsys Research Corp. Qwknut	35
4.3.5	Qwknut Mounting Scheme	37
4.4	Top Panel	40
4.5	Release Mechanism Bracket	41
4.6	Door	42
4.6.1	Flex Problem with Original Door	42
4.6.2	Rib Design	43
4.6.3	Bolt Clearance During Release	45
4.6.4	Ability to Open 270°	46

4.7	Torsion Springs	46
4.8	Main Spring	47
4.9	Kick Springs	49
4.10	Back Panel	51
4.11	Pusher Plate	53
4.12	Telemetry System	54
4.12.1	Optical Sensors	55
4.12.2	Hall Effect Sensors	56
4.12.3	Limit Switch in Back of P-POD	56
4.12.4	Break Wire	57
4.12.5	Limit Switch on Door	57
4.13	Stopper Bracket	58
4.14	View Ports	60
5	Prototype Testing	61
5.1	Test Flow	61
5.2	Vibration Testing	62
5.2.1	Dnepr Qualification	63
5.2.2	NASA GEVS Qualification	63
5.3	Finite Element Model Verification	65
5.3.1	Finite Element Models	65
5.3.2	P-POD Frame FEA Results	67
5.3.3	P-POD Door FEA Results	70
5.3.4	Release Mechanism Subassembly Results	71
5.3.5	Comparison to Experimental Data	72

5.4	Thermal and Vacuum Testing	74
5.5	Functional	76
5.5.1	Geometry	76
5.5.2	Deployment	76
5.6	Problems with the Qwknut	77
6	Post Failure Design Iteration	79
6.1	Detailed Analysis of the Problem	79
6.1.1	How Curiosity Killed the Qwknut	79
6.1.2	Test versus Flight Circuits	81
6.1.3	Shear Stress	82
6.1.4	Low Grade Fasteners	83
6.1.5	Qwknut Misalignment	83
6.2	Rework of Parts	84
6.2.1	Shear Plate	84
6.2.2	Bracket Locator Pins	86
6.2.3	Mounting Screw Sizing	86
6.2.4	Spherical Washers	86
6.3	Requalification	87
6.3.1	NASA X Axis Qualification	87
6.3.2	Full NASA Qualification	87
6.3.3	Vibration and Thermal Vacuum	88
6.3.4	Dnepr Vibration Qualification	88
7	The “Dnepr Launch 1” Mission	89
7.1	Assembly and Qualification	90

7.2	P-POD / Launch Vehicle Fit Check	91
7.3	CubeSat / P-POD Fit Check	92
7.4	Integration	93
7.5	Acceptance	94
7.6	Launch Swapping	95
7.7	Launch Campaign	96
8	Conclusion	100
8.1	Future Recommendations	101
8.1.1	Design	101
8.1.2	Analysis	104
8.1.3	Testing	105
8.1.4	Long Term Improvements	106
A	Aluminum 7075-T73 Properties	110
B	Design Load Definition	112
C	Fastener Design Methodology	114
C.1	Fastener Specifications	114
C.2	Shear Strength	116
C.3	Combined Shear and Tension	116
C.4	Preload	117
C.5	Tensile Strength	119
C.6	Thread Stripping: Fastener to Heli-Coil	120
C.7	Thread Stripping: Heli-Coil to P-POD	121
C.8	Final Fastener Selection	121

C.9	Torque Specification	122
D	P-POD Deployment Simulation	124
D.1	Deployment Simulation Block Diagram	125
D.2	Deployment Simulation Integration Blocks	126
D.3	Simulation Parameter Code	127
D.4	Deployment Simulation Separated Case Blocks	129
D.5	Deployment Simulation Compressed Case Blocks	130
D.6	Compressed Case Code	131
D.7	Deployment Simulation Visualization Blocks	132
D.8	Position Plot for Nominal Case	133
D.9	Velocity Plot for Nominal Case	134
D.10	Velocity Plot for Light Case	135
D.11	Velocity Plot for Heavy Case	136
E	Finite Element Analysis Results	137
E.1	Restraint Models	137
E.1.1	P-POD Frame	138
E.1.2	P-POD Door	148
E.1.3	P-POD Release Mechanism Subassembly (RMS)	151
F	Vibration Test Data	153
F.1	Random Vibration Profiles	154
F.2	Sample Vibration Data	155
F.3	Reduced Natural Frequency Data	157
G	Dnepr Launch Failure Analysis	159

List of Figures

1.1	Cal Poly's first satellite (CP1) shown for scale.	1
1.2	Members of the Cal Poly CubeSat and PolySat teams.	2
1.3	Cal Poly's role in the CubeSat Program.	3
1.4	Stanford's OPAL satellite.	4
1.5	OPAL picosatellite deployer.	5
1.6	Rokot upper stage with CubeSats integrated.	6
1.7	Current CubeSat class deployment systems.	6
1.8	Model of the SS-18 missile at Yuzhnoe State Design Office, Ukraine.	7
1.9	Integrated Dnepr space head module for fourth launch.	8
1.10	Cluster (left) and piggyback (right) mission configurations.	8
2.1	Dnepr launch vehicle deployment sequence.	12
3.1	Design loop for P-POD Mk. II development.	18
3.2	Stages of prototyping for the P-POD Mk. II door.	19
3.3	Cal Poly environmental test facilities.	20
4.1	Dnepr launch vehicle coordinate system.	24
4.2	P-POD Mk. II coordinate system.	24
4.3	P-POD Mk. II mounting hole pattern.	25

4.4	Diagram of LVI with two P-PODs attached.	26
4.5	Picture of LVI with two P-POD mass models attached.	26
4.6	Diagram of P-POD electrical interface.	27
4.7	The P-POD Deployment Electronics Package (P-DEP).	27
4.8	Picture of P-POD electrical connections.	28
4.9	P-POD Mk. I with line cutter attached.	29
4.10	A pin puller mechanism manufactured by TiNi Aerospace.	31
4.11	A cable release mechanism manufactured by G&H Technologies.	32
4.12	A separation nut mechanism manufactured by NEA Electronics.	32
4.13	The Starsys Qwknut 3k release mechanism.	36
4.14	Prototype fixture for mounting the Qwknut to the P-POD.	38
4.15	Fitting the Qwknut to the P-POD with the prototype door and bracket.	38
4.16	Free body diagram of door.	39
4.17	Old (left) and new (right) P-POD top panels.	40
4.18	Left mounting bracket for the Qwknut release mechanism.	41
4.19	FEA of the left bracket under static lateral loading.	42
4.20	Old (left) and new (right) P-POD doors.	42
4.21	Integrated P-POD Mk. I door showing a “healthy bow.”	43
4.22	Cross sections of old (left) and new (right) P-POD doors.	44
4.23	FEA of old (left) and new (right) P-POD doors under static loading.	44
4.24	Close-up of P-POD door hinge.	46
4.25	Deployment simulation block diagram.	48
4.26	Results of P-POD deployment simulation.	48
4.27	Difference between old (top) and new (bottom) P-POD main springs.	49
4.28	Diagram and internal view of a spring plunger.	50

4.29	Torque data, courtesy of Heli-Coil and Emhart.	50
4.30	Old (left) and new (right) P-POD back panels.	51
4.31	Internal P-POD rails cut to accommodate kick springs.	52
4.32	Side view of kick springs integrated into the P-POD.	53
4.33	P-POD pusher plate.	53
4.34	A photodiode could be used to sense deployment.	55
4.35	A hall effect sensor could be triggered by a magnet in the pusher plate.	56
4.36	Various styles of mechanical limit switches.	57
4.37	Saia-Burgess F4 series microswitch.	58
4.38	Telemetry switches and guide rail.	58
4.39	P-POD with stopper bracket attached.	59
4.40	Theoretical view through P-POD view port.	60
5.1	Vibration testing on the Cal Poly shake table.	62
5.2	Dnepr two stage random vibration qualification profile.	64
5.3	NASA GEVS random vibration qualification profile.	64
5.4	Fundamental shearing mode in an unrestrained case.	68
5.5	Fundamental shearing mode with bottom panel restrained.	68
5.6	First breathing mode in an unrestrained case.	69
5.7	First breathing mode with bottom panel restrained.	69
5.8	Second breathing mode with bottom panel restrained.	70
5.9	P-POD door fundamental bending mode.	71
5.10	P-POD RMS second mode shape.	71
5.11	P-PODs being prepared for thermal vacuum testing.	75
5.12	Thermal vacuum bakeout profile.	76

6.1	Schematic of Qwknut circuits	81
6.2	Two side views of the Qwknut and release bolt.	82
6.3	Cross section of the reworked release mechanism assembly.	84
6.4	P-POD Mk. II shear plate.	85
6.5	Picture of release bolt and spherical washer set.	87
6.6	Strategically placed accelerometers during a vibration test.	88
7.1	CubeSat triple mass model used for P-POD qualification.	91
7.2	Mass simulator for the P-POD Mk. II.	92
7.3	P-PODs being integrated with CubeSats at Cal Poly.	93
7.4	P-POD bagged for cleanliness, ready for testing.	94
7.5	P-PODs awaiting integration at Baikonur Cosmodrome.	96
7.6	Installation of P-PODs onto the SHM.	97
7.7	Silo launch of the Dnepr launch vehicle.	98
7.8	Dnepr vehicle crash site.	99
C.1	Common failure points for bolted joints [16].	115
C.2	Design curves for combined (tension and shear) loading [3].	117
C.3	Loading diagram for P-POD interface joints.	119
D.1	Block diagram of deployment simulation components.	125
D.2	Integration section of deployment simulation.	126
D.3	Section of simulation to accommodate full extension of springs.	129
D.4	Section of simulation to accommodate full compression of springs.	130
D.5	Various visualization options for simulation results.	132
D.6	Position vs. Time for nominal weight CubeSats ($m = 1.0 \text{ kg}$).	133
D.7	Velocity vs. Time for nominal weight Cubesats ($m = 1.0 \text{ kg}$).	134

D.8	Velocity vs. Time for underweight CubeSats ($m = 0.7$ kg).	135
D.9	Velocity vs. Time for overweight CubeSats ($m = 1.3$ kg).	136
E.1	P-POD Frame Restrained, 1st mode, 430.96 Hz.	139
E.2	P-POD Frame Restrained, 2nd mode, 582.92 Hz.	139
E.3	P-POD Frame Restrained, 3rd mode, 760.6 Hz.	139
E.4	P-POD Frame Restrained, 4th mode, 858.39 Hz.	140
E.5	P-POD Frame Restrained, 5th mode, 887.64 Hz.	140
E.6	P-POD Frame Restrained, 6th mode, 934.36 Hz.	140
E.7	P-POD Frame Restrained, 7th mode, 947.29 Hz.	141
E.8	P-POD Frame Restrained, 8th mode, 962.98 Hz.	141
E.9	P-POD Frame Restrained, 9th mode, 1011.3 Hz.	141
E.10	P-POD Frame Restrained, 10th mode, 1064.7 Hz.	142
E.11	P-POD Frame Restrained, 11th mode, 1109.8 Hz.	142
E.12	P-POD Frame Restrained, 12th mode, 1220.2 Hz.	142
E.13	P-POD Frame Restrained, 13th mode, 1229.9 Hz.	143
E.14	P-POD Frame Restrained, 14th mode, 1255.5 Hz.	143
E.15	P-POD Frame Restrained, 15th mode, 1262.9 Hz.	143
E.16	P-POD Frame Restrained, 16th mode, 1283.6 Hz.	144
E.17	P-POD Frame Restrained, 17th mode, 1472.6 Hz.	144
E.18	P-POD Frame Restrained, 18th mode, 1479.1 Hz.	144
E.19	P-POD Frame Restrained, 19th mode, 1518.7 Hz.	145
E.20	P-POD Frame Restrained, 20th mode, 1533.1 Hz.	145
E.21	P-POD Frame Restrained, 21st mode, 1611.3 Hz.	145
E.22	P-POD Frame Restrained, 22nd mode, 1646 Hz.	146

E.23 P-POD Frame Restrained, 23rd mode, 1797.8 Hz.	146
E.24 P-POD Frame Restrained, 24th mode, 1863.9 Hz.	146
E.25 P-POD Frame Restrained, 25th mode, 1938.9 Hz.	147
E.26 P-POD Door Restrained, 1st mode, 613.04 Hz.	149
E.27 P-POD Door Restrained, 2nd mode, 719.63 Hz.	149
E.28 P-POD Door Restrained, 3rd mode, 1137.3 Hz.	149
E.29 P-POD Door Restrained, 4th mode, 1343.4 Hz.	150
E.30 P-POD Door Restrained, 5th mode, 1954.4 Hz.	150
E.31 P-POD RMS Restrained, 1st mode, 951.78 Hz.	152
E.32 P-POD RMS Restrained, 2nd mode, 1255.8 Hz.	152
E.33 P-POD RMS Restrained, 3rd mode, 1975.5 Hz.	152
F.1 VIbration test accelerometer locations.	153
F.2 Composite plot of various random vibration profiles.	154
F.3 Sample plot of P-POD sine sweep test data.	155
F.4 Sample PSD plot of P-POD random vibration test data.	156
F.5 Histogram of vibration accelerometer data.	157
F.6 Composite scatter plot of vibration accelerometer data.	158

List of Tables

4.1	Release mechanism trade study summary.	35
4.2	Qwknut 3k specifications summary.	37
6.1	Common fastener grades and prices (McMaster Carr, 2007).	83
B.1	Dnepr LV maximum structural load factors.	112
C.1	Strength of metric grade fasteners.	114
C.2	Modulus of elasticity for aluminum and steel.	118
E.1	Finite element analysis properties for restrained P-POD frame.	138
E.2	Finite element analysis properties for restrained P-POD door.	148
E.3	Finite element analysis properties for restrained P-POD RMS.	151

Chapter 1

Introduction

1.1 The CubeSat Program

The CubeSat Program is an international collaboration of more than 80 universities, private companies, and government organizations building a class of small spacecraft — CubeSats. These picosatellites adhere to the CubeSat Design Specification (CDS) [6], which defines interfaces and operational requirements for developers.

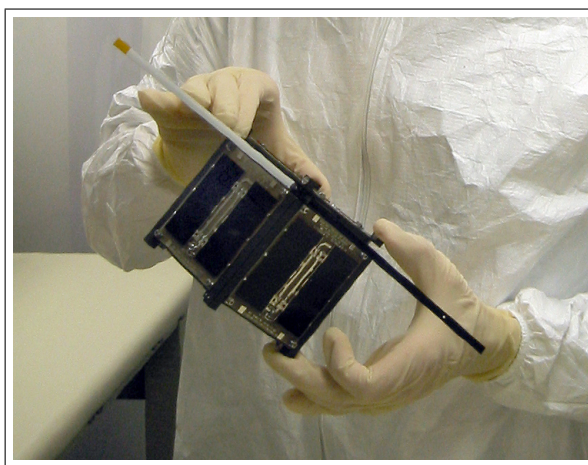


Figure 1.1: Cal Poly’s first satellite (CP1) shown for scale.

The CubeSat Program started as a collaboration between the California Polytechnic State University Multidisciplinary Space Technology Lab (MSTL) and the Stanford Uni-

versity Space Systems Development Laboratory (SSDL). The objectives of the CubeSat Program are to provide a standard platform for launching CubeSats [12]. The CubeSat standard enables rapid, low cost missions with regular launch opportunities.

The motivation of the CubeSat Program is to make space flight accessible for universities with varying degrees of Aerospace expertise and allow students to experience the complete life cycle of a real space mission. CubeSat missions can be completed within a nominal two year graduate program, allowing students to participate in:

- Mission requirements development
- Design, analysis, & testing
- Fabrication, assembly, & quality control
- Systems engineering
- Integration and launch
- Spacecraft operations



Figure 1.2: Members of the Cal Poly CubeSat and PolySat teams.

Low cost and regular launches produce an environment that is cooperative rather than competitive. Universities share information and work together to further technology, pro-

cesses, and standards. In addition, when groups of CubeSats are launched simultaneously, developers share mission costs.

1.2 The Poly Picosatellite Orbital Deployer

A unique feature of the CubeSat Program is the use of a standard deployment system known as the Poly Picosatellite Orbital Deployer (P-POD). The P-POD is a square, tubular structure capable of holding three CubeSats during launch and releasing them once in orbit. The P-POD acts as the interface between CubeSats and launch vehicles, and uses concepts of standardization to meet program goals.

Since the P-POD is a secondary payload aboard larger missions, the safety of the launch vehicle and primary payload are the primary concern. A failure of even a single P-POD could jeopardize future launch opportunities for the entire CubeSat Program. The P-POD mission statement is comprised of three basic philosophies (in order of priority):

1. Protect the launch vehicle and primary payload(s)
2. Provide a safe and reliable deployment system for CubeSats
3. Enable launches on a variety of launch vehicles through flexibility

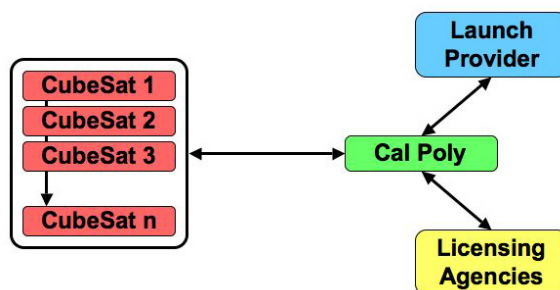


Figure 1.3: Cal Poly's role in the CubeSat Program.

Cal Poly's current roles are to maintain the CubeSat Standard, coordinates launch opportunities, and continue to improve and support the P-POD. This framework allows developers to build and launch CubeSats, without worrying about the specifics of coordinating a launch.

1.3 History

Launching tiny satellites was pioneered by the Orbiting Picosatellite Launcher (OPAL) spacecraft built by Stanford University. OPAL's primary mission was to test a number of low-cost, commercial sensors for attitude control. The sensor suite consisted of various accelerometers, gyros, and magnetometers.

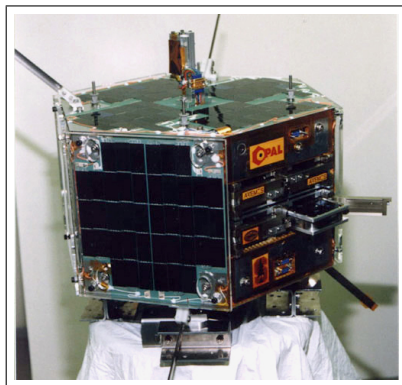


Figure 1.4: Stanford's OPAL satellite.

The OPAL project began in 1995, and the satellite was launched in 2000. In addition to its primary mission, OPAL was carrying four picosatellites (roughly the size of sardine cans) and a custom deployment system [7]. These picosatellites were successfully ejected into orbit using the launcher seen in Figure 1.5.

Cal Poly was drawn to the CubeSat Program to build, fly, and operate satellites. The program was originally modeled so that universities would build the satellites and an intermediary company would coordinate the launches. One Stop Satellite Solutions

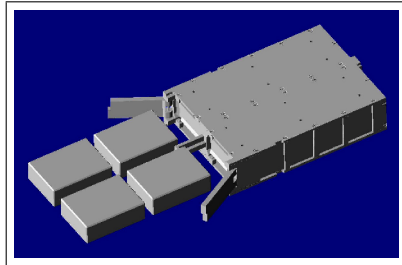


Figure 1.5: OPAL picosatellite deployer.

(OSSS) — pronounced O-S-cubed — was one such company established to provide low cost launch opportunities for CubeSats and other smallsats. OSSS began negotiating a launch with International Space Company (ISC) Kosmotras of the Russian Federation.

Some time around 2001, OSSS filed for Chapter 11 bankruptcy. Since OSSS was the only company performing this type of service at the time, their downfall jeopardized the launch opportunity with ISC Kosmotras, forced OSSS to default on loans fronted by universities and businesses, and shattered the hopes and dreams of the students and faculty banking on their success.

Around this time, the University of Toronto Institute for Aerospace Studies, Space Flight Lab (UTIAS/SFL) had begun work on their CanX-1 CubeSat project, in addition to their primary project — the Microvariability and Oscillations of STars (MOST) microsatellite.

Out of frustration at the lack of concrete launch opportunities for CubeSats, UTIAS/SFL decided to push for the inclusion of CubeSat payloads on the same launch as the MOST mission. On June 30, 2003, six CubeSats were placed into low earth orbit via a Rokot launch vehicle out of Plesetsk, Russia. Four of these CubeSats were coordinated by UTIAS/SFL and deployed from P-PODs; the other two were coordinated by Japanese university CubeSat projects and utilized custom deployers.

While University of Toronto prepared for their launch, Cal Poly contemplating their



Figure 1.6: Rokot upper stage with CubeSats integrated.

role in the future of the CubeSat Program. In early 2003, Cal Poly began negotiations with ISC Kosmotras, and in July of the same year, four Cal Poly students headed for Rome, Italy to meet face to face with Kosmotras representatives.

The progression of these events started an international movement, and established the CubeSat Program as a modest, but permanent chapter in space history. To date, there have been five CubeSat missions placing 11 CubeSats into low earth orbit. The CubeSat Program has become truly international, reaching across dozens of nations and affecting thousands of students worldwide.

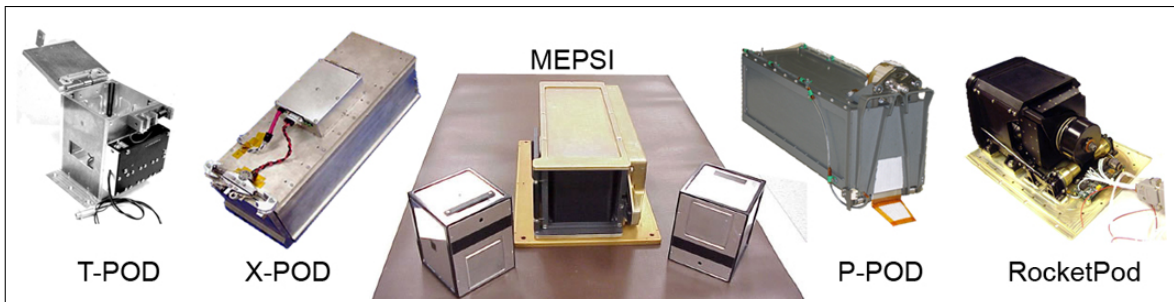


Figure 1.7: Current CubeSat class deployment systems.

1.4 The Dnepr Launch Opportunity

The Dnepr launch vehicle is a converted SS-18 Inter-Continental Ballistic Missile (ICBM).

With a diameter of three meters, the SS-18 was the largest — some say the deadliest — ICBM to ever be put into service worldwide [23]. The SS-18 was developed as a first-strike weapon capable of showering enemies with multiple nuclear payloads half way across the globe. Its size and devastating ability to deploy Multiple Independently targetable Reentry Vehicles (MIRV) earned it the NATO designation of “Satan” during the Cold War. Ironically, it is this MIRV capability that makes cluster launches possible at such low cost. For this mission, Kosmotras provided launch services for USD 10,000 per kilogram.

The Dnepr is a launch vehicle variant of the SS-18, developed as part of the START-II program to disarm Soviet and U.S. nuclear weapons, and was named after the city in the Ukraine which served as the Soviet Union’s missile development and manufacturing center. As a launch vehicle, the Dnepr is considered a medium lift vehicle [23].



Figure 1.8: Model of the SS-18 missile at Yuzhnoe State Design Office, Ukraine.

Since the SS-18 was developed for missions with delicate payloads, the Dnepr vehicle is able to provide a surprisingly benign launch environment. Fourteen CubeSats housed in five P-PODs were manifested on the 6th Dnepr mission in addition to five other small satellites, for a record-breaking total of 23 payloads on a single launch.



Figure 1.9: Integrated Dnepr space head module for fourth launch.

Kosmotras refers to these missions as “cluster launches”, containing many small payloads with no clearly defined primary customer. Manifesting many small payloads allows Kosmotras to provide launch opportunities for small payloads while still covering costs. An additional benefit to this approach, as opposed to the “piggyback” approach, is that no risk is added to expensive missions with large primary spacecraft.

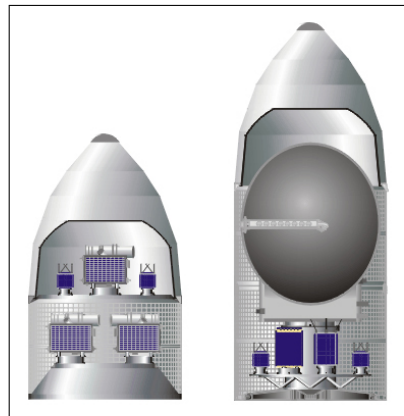


Figure 1.10: Cluster (left) and piggyback (right) mission configurations.

Chapter 2

Requirements Definition

A number of requirements drove the design of the P-POD Mk. II, including safety requirements, operational requirements, and environmental requirements. These requirements were clearly defined at the beginning of the redesign process, and were derived from:

- P-POD mission statement
- Requirements established when designing the P-POD Mk. I
- Requirements imposed by Kosmotras
- Self-imposed requirements to maximize launch vehicle compatibility

2.1 Safety Requirements

As secondary payloads do pose additional risk to any mission, it is important to mitigate concerns by creating a standardized secondary payload that launch providers know and trust. Interfaces between the P-POD and launch vehicle are independent of CubeSat design. This approach works because hazard analysis of the P-POD is very similar from mission to mission, and credibility can be established by flying the same hardware repeat-

edly. The goal is to convince launch providers and primary payloads that the P-POD can remain safe no matter what is placed inside.

The P-POD must maintain its structural integrity despite any structural failures that the P-POD or CubeSats may experience. Encapsulation of CubeSats within the P-POD mechanically and electrically isolates the CubeSats from the rest of the launch vehicle, reducing risk of damage due to:

- Accidental activation of CubeSat electronics.
- Debris produced by CubeSat structural damage.
- Premature deployment of CubeSat antennas or booms.

A more likely failure is the premature deployment of the P-POD, releasing entire CubeSats into the fairing during launch. This failure mode is addressed by using proven, reliable release mechanisms verified by rigorous testing. Premature deployment of the P-POD could be caused by:

- A signal sent from the launch vehicle at the incorrect time.
- Incorrectly setting the release mechanism during integration.
- Launch loads exceeding the capabilities of the P-POD.

In addition to producing physical debris, CubeSats can generate Electro-Magnetic Interference (EMI). Forcing CubeSats to remain powered off while in the P-POD mitigates this risk. Designing the P-POD to act as a faraday cage provides additional EMI protection. P-POD panels are electrically connected to help block accidental transmissions produced by CubeSats. It must be noted, that EMI attenuation properties of the P-POD have not been tested.

Propellants, pressure vessels, and explosives also pose significant risk. These issues are currently avoided altogether by restricting their use. These issues will have to be addressed in the future, as CubeSats are starting to evolve to a point where there is some interest in flying these types of systems.

2.2 Operational Requirements

The large number of objects in a cluster launch increases the number of potential collisions. Likewise, limited fuel available for attitude control of the launch vehicle decreases the allowable deployment time per payload. Kosmotras set limits on ejection velocity and deployment time to ensure successful deployment.

- The velocity vector magnitude of the CubeSats must be less than 2 m/s in relation to the upper stage at the time of separation.
- The P-PODs must be completely empty within one second.

In order to understand this requirement, it is important to know a little about the launch vehicle trajectory. As mentioned above, the Dnepr LV is based on the SS-18 ICBM and its associated MIRV technology. After the vehicle reaches its desired trajectory — in this case, low earth orbit — it separates the fairing then performs a 180° rotation maneuver. At this point, it starts accelerating (backwards relative to the upper stage) and dropping off payloads one at a time. A timeline is shown in Figure 2.1.

2.3 Environmental Requirements

Environmental design and testing loads were derived from a number of different sources; most important was the Dnepr Users Guide [14], which served as the official source for the

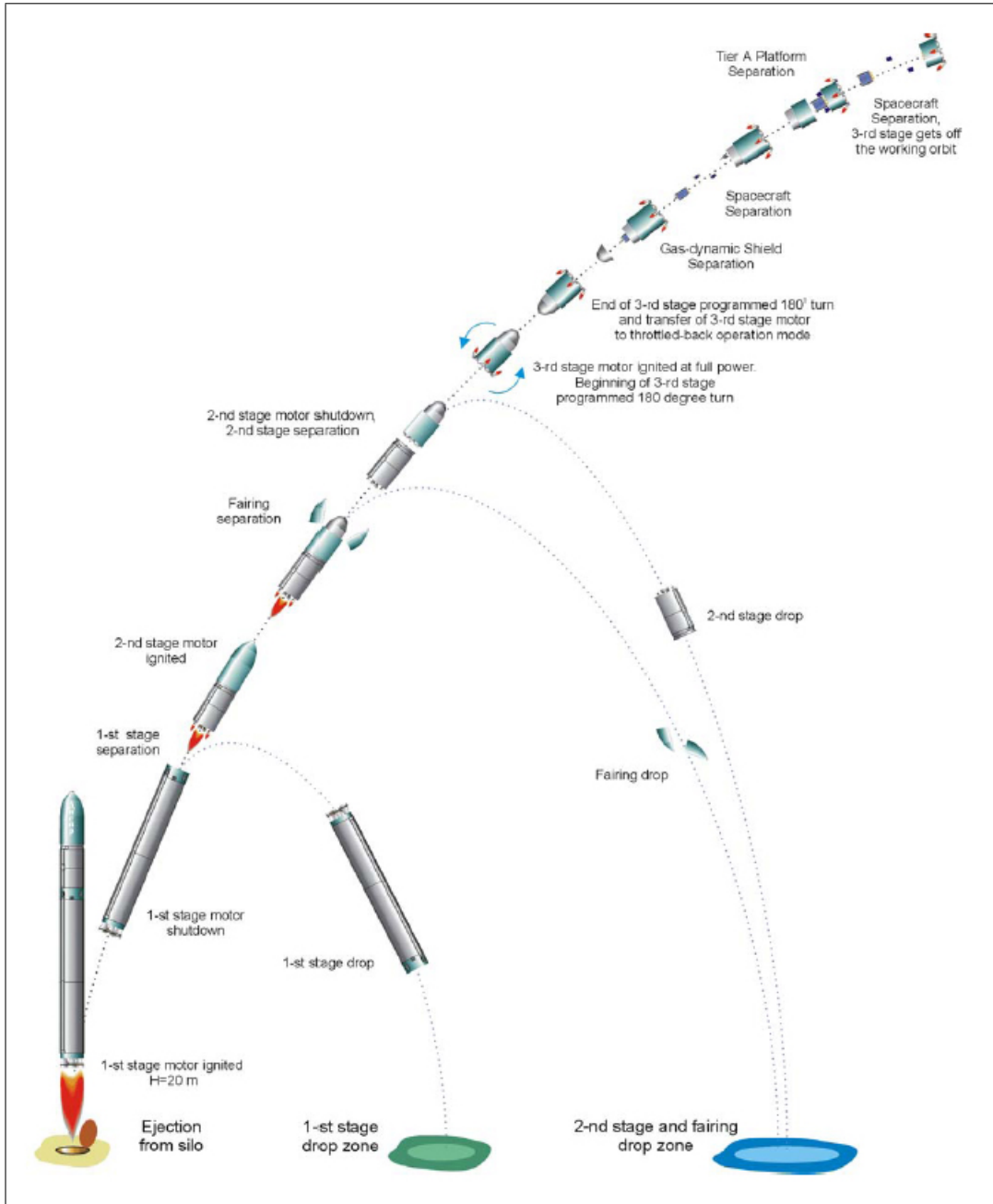


Figure 2.1: Dnepr launch vehicle deployment sequence.

upcoming launch. In addition, various vehicle users guides and NASA specifications were consulted to keep the P-POD design compatible with a variety of vehicles. Primarily, the NASA General Environmental Verification Standard (GEVS) is worth mentioning [19]. The NASA GEVS document outlines testing requirements for payloads and defines test profiles that envelope NASA approved launch vehicles.

2.3.1 Static Loads

The P-POD is subjected to static loads caused by launch vehicle acceleration. These loads are based on the acceleration properties and trajectory of the launch vehicle. In this case, static loading was simple to account for, as the CubeSats are pushed towards the back of the P-POD, thus relieving stress on the door. Maximum axial acceleration during launch is 7.8 G's and occurs during second stage burn. Many launch vehicles have similar maximum axial accelerations.

2.3.2 Dynamic Loads

Dynamic loads are produced by vibration, shock, and acoustic stimuli. Pure acoustic loads were ignored, as their impact is negligible on small systems such as the P-POD. Shock loads were considered briefly, as the P-POD only experiences small or indirect shock events. Random vibration was treated as the major potential cause for failure, and attention was given accordingly.

Random Vibration

Random vibration was an important design driver for the P-POD redesign effort. Two random vibration profiles were used for analysis and testing: the Dnepr profile and NASA GEVS profile. The Dnepr vehicle is a silo ejected, liquid fuel rocket. Its vibration environment is described as a combination of the liftoff phase and the remainder of the flight. This profile was used during prototype testing as well as qualification of the flight units. Qualification testing levels are defined to be 150% of the flight levels [14].

Section 2.4.2 of the NASA GEVS document outlines requirements for vibration testing of payloads for NASA missions. A simple profile is provided which envelopes the environments of a number of launch vehicles. The testing requirements defined in this document

are conservative and fairly severe. The qualification profile defined in the GEVS document was used extensively for design and testing of prototypes.

Shock

Shock loads are high frequency, short duration events. These transient vibration loads are usually caused by shipping accidents, motor ignition and cutoff, and pyrotechnic separation events. Assuming that proper packaging can negate transportation shock events, the P-PODs will experience the greatest shock during payload separation.

Kosmotras uses large pyrotechnic bolts left over from Cold War days to initiate fairing separation and spacecraft deployment. These mechanisms are proven and reliable, but are quite violent. Fortunately, the P-PODs incorporate low shock release mechanisms, and will only experience indirect shock events as other spacecraft are deployed.

2.3.3 Thermal Loads

The P-PODs stay attached to the launch and only have to function until the CubeSats are deployed. During the fifteen minute launch, P-PODs will be exposed to thermal loads produced by aero-drag and solar radiation. Dominant thermal loads are transferred via conduction through any mounting adapter and radiation from the fairing.

2.3.4 Other Considerations

A number of other factors contribute to the launch environment. The following factors do not have a significant impact on the P-POD.

Pressure

Payloads will experience a rapid drop in pressure during launch. The P-POD does not contain any pressurized components and is fully outgassed prior to delivery.

Gas Dynamic Effects

Payloads will briefly fly through the plume of the 3rd stage thrusters during deployment.

After consulting with Kosmotras, it was decided that the plume would not apply significant forces to the CubeSats, nor would it produce significant contaminant deposits on the CubeSats.

Electro-Magnetic Interference (EMI)

The CubeSat Specification Document explicitly states that CubeSats must be powered off during launch and may only activate after deployment from the P-POD. This self-imposed requirement alleviates any concerns with electromagnetic interference between the CubeSats and other payloads.

Humidity

The P-PODs and CubeSats will be exposed to environments of varying humidity during integration and just prior to launch. The Dnepr Users Guide defines humidity ranges experienced during operations and launch, which do not pose a risk to the P-POD.

Transportation

P-PODs will be subjected to environmental loads during transportation. Many launch sites are in remote locations only accessible by harsh roads, and the Dnepr launch facility at Baikonur Cosmodrome is no exception. Vibration and shock loading information for the transportation environment was obtained from the Dnepr Users Guide and deemed negligible compared to launch loads. Thermal loads during transportation were also deemed acceptable.

2.4 Changes to the P-POD

The space industry has a strong bias towards “flight proven” hardware. Since reliability is of the utmost importance, it is always preferred to use space qualified technology and components. At the time of this redesign, two P-PODs had flown on the 2003 mission, giving the P-POD Mk. I this status.

During the preliminary design phase of the P-POD Mk. II, it was decided that changes would be kept to a minimum in number and scope. The changes were derived from requirements set by launch providers as well as lessons learned from the first launch. A total of 12 changes differentiate the P-POD Mk. I from the P-POD Mk. II.

Chapter 3

Design Tools and Philosophy

A number of tools were used to take the P-POD from concept to reality. Virtual models, physical prototypes, or both were used to visualize design concepts. Likewise, a healthy balance of computer simulation and environmental testing were used to validate the design changes. These elements were combined into a spiral development process (Figure 3.1) allowing the system to be fine tuned before components were fabricated.

3.1 Computer Aided Engineering

Computer Aided Engineering (CAE) tools provide many benefits to the design process. One major benefit to the CAE approach is the reduction in program cost. CAE minimizes the number of physical models and prototypes needed to effectively evaluate a design. Changes to virtual models are quick and easy, allowing engineers to focus on the design rather than building prototypes.

PTC Pro ENGINEER (Pro/E) was the CAE package used for the redesign. The primary reason for using Pro/E is that the original P-POD model files had been developed in Pro/E and were available in that format. In addition, Pro/E is a powerful tool and an

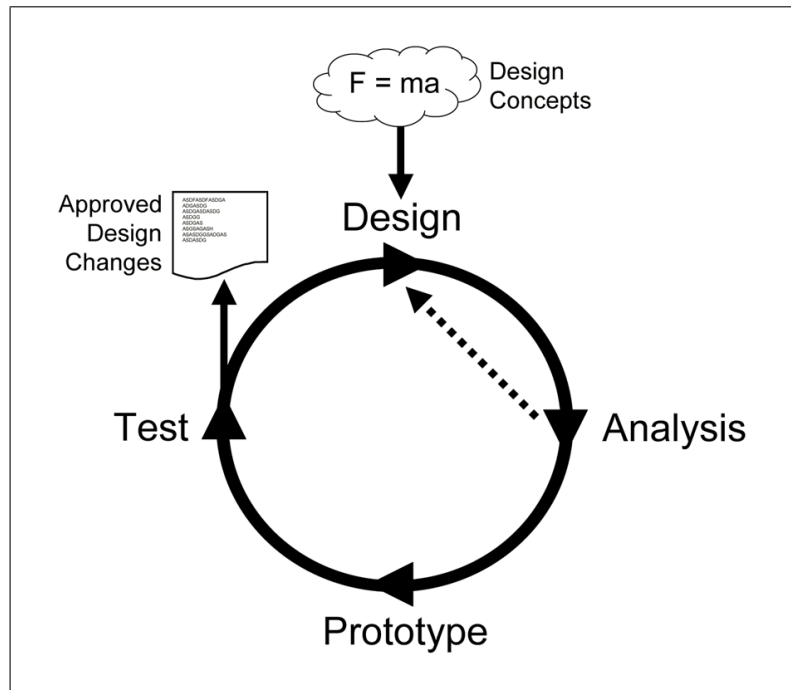


Figure 3.1: Design loop for P-POD Mk. II development.

industry standard. It is also fairly simple to learn. Finally, licenses were readily available for campus use and computers in the MSL already had Pro/E running.

CAE allowed consideration of multiple designs without significantly increasing project costs. CAE tools also proved to be a very effective way to perform virtual fit checks. These fit checks made it very easy to understand how components would fit together when assembled, minimizing the need for rework or modification of parts.

3.2 Finite Element Analysis

Most CAE packages utilize Finite Element Analysis (FEA) algorithms to simulate a model's response to structural and thermal loading. The FEA package used for this redesign was Pro Mechanica and is packaged with Pro/E.

Although analysis was originally performed in Pro Mechanica, due to a software license issue, Pro Mechanica was not available at the time of writing this paper. As a result,

COSMOSWorks was used to reproduce the analysis and depict the results graphically.

FEA was extremely useful for quick checks of component strength under various static and dynamic loading conditions. FEA results helped quickly identify stress concentrations and safety factors in the design. This analysis was performed early and often and served to feed back into subsequent iterations of the design loop.

3.3 Prototyping

The existence of first generation P-POD parts helped tremendously when evaluating design changes, and could easily be modified to test out ideas. Every design change was prototyped to some degree before being incorporated into the final design. Some changes were minor enough to be made right on the P-POD Mk. I parts, while other modifications required ordering prototypes from machine shops to fully evaluate.

Extensive prototyping was used to offset any oversights caused by inexperience with CAE tools. Prototyping was interwoven with the design process and was started very early on to flush out interference problems between components.

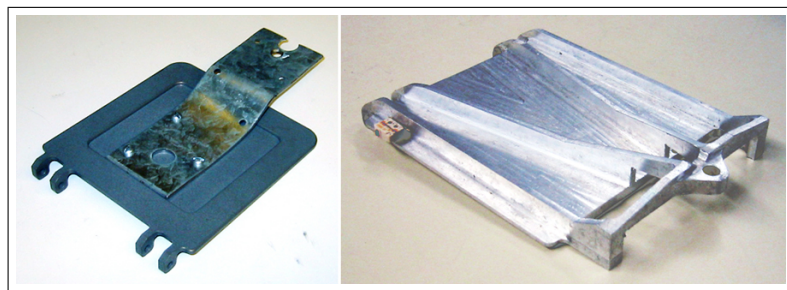


Figure 3.2: Stages of prototyping for the P-POD Mk. II door.

Like finite element analysis, successes and failures experienced through prototyping fed back into the design loop. A number of different prototyping methods were used depending on the scope of the modification and phase of the redesign. These prototypes ranged in

fidelity from rough concepts made from Commercial Off the Shelf (COTS) parts, to rapid prototypes, to parts manufactured on campus, to prototypes outsourced to machine shops.

3.4 Testing

Testing was an irreplaceable part of the P-POD redesign effort. Access to the Mechanical Engineering Department vibrations lab, and the CubeSat project's thermal vacuum chamber made it easy to perform tests often and with minimal notice for resource coordination.



Figure 3.3: Cal Poly environmental test facilities.

A component-centric redesign approach was used to develop a prototype P-POD. Modifications were first tested individually on a P-POD Mk. I chassis. This made it easy to see how modifications impacted the overall system and facilitated troubleshooting tasks. Testing included environmental tests (in the form of vibration and thermal vacuum tests) as well as functional tests of the deployment system. After testing each modification separately, the prototype parts were combined to create a full P-POD Mk. II prototype.

Testing was also used to verify computer simulations and models. Even experienced engineers cannot always predict every single environmental condition. The only way to account for unpredictable environmental conditions is to complement analysis with rigorous testing.

Most importantly, a “test as you fly, fly as you test” philosophy was adopted, which

states that hardware should be tested in a flight-like state, with no differences between engineering and flight units. This philosophy also looks down on implementing last minute changes, and is a good approach to developing reliable systems.

3.5 On Reliability

Although the P-POD is a relatively simple system, reliability is of the utmost importance. There is much at stake if the P-POD fails to perform its mission. On one hand, CubeSat developers are relying on the P-POD to successfully deploy their satellites. On the other hand, the primary customer of the launch and the launch provider are expecting the P-POD to stay intact during launch and not interfere with the launch vehicle or the primary spacecraft in any way.

As a result, reliability has always been and should always be the primary design driver for the P-POD. To meet this end, proven technologies and accepted methods were used whenever possible. This approach makes the P-POD an acceptable risk to launch providers and primary payloads, so that CubeSat developers can build high-risk, high-gain satellites. NASA and military standards were common references during design and testing of the P-POD.

3.6 On Simplicity

The concept of simplicity is embedded deep within the fabric of the Cal Poly CubeSat project. The philosophy of designing simple and elegant systems is evident throughout the MSTL. This no frills mentality was the key to designing a reliable system with a limited budget and aggressive schedule. Eliminating unnecessary features and trading luxury for simplicity bred reliability and confidence.

Minimizing the number of changes maximized the amount of time that could be devoted per modification. Every change was meticulously examined and rushing was avoided. A lot of time was spent refining the design of the P-POD; a bulk of that time was spent analyzing high-risk areas such as the release mechanism.

An approach of fewer high quality components, rather than many low cost components, was favored. Minimizing the number of components resulted in a bigger budget per component.

Finally, keeping the number and complexity of modifications low meant less time spent designing and more time spent testing. This approach was embraced to ensure that every part of the design was properly tested and that no corners were cut.

Chapter 4

Redesigning the P-POD

4.1 Coordinate Systems

It was important to define coordinate systems before beginning the design process to avoid confusion later on. The LV coordinate system (shown in Figure 4.1) is defined in the Dnepr User's Guide.

The P-POD coordinate system was defined somewhat arbitrarily, using a right handed coordinate system as shown in Figure 4.2.

4.2 Launch Vehicle Interface

The first topic considered in the redesign was the interface between the launch vehicle and the P-POD. Although the interface was designed specifically for the Dnepr launch vehicle, a lot of thought was put in to keeping the interface generic enough to be compatible with a wide range of vehicles in order to avoid limiting options for future launches.

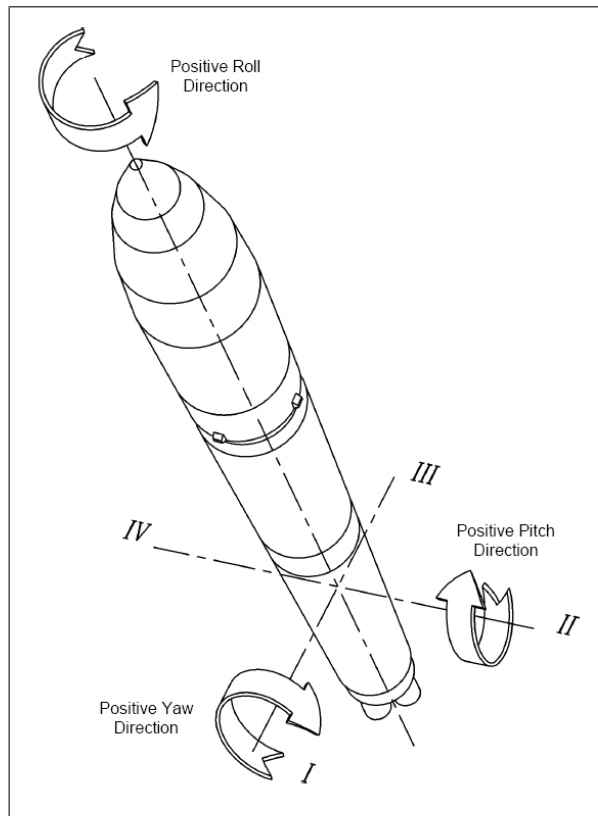


Figure 4.1: Dnepr launch vehicle coordinate system.

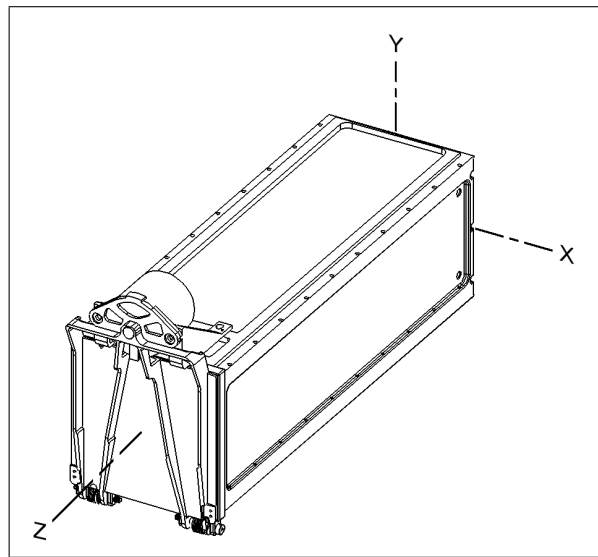


Figure 4.2: P-POD Mk. II coordinate system.

4.2.1 Mechanical Interface

The P-POD has a very versatile mechanical interface based mainly on the fact that all four sides of the P-POD have similar features. Each panel has a set of rails along its longitudinal edges. These rail sections are thick enough to support threaded holes, which can be used for mounting the P-POD to the launch vehicle adapter. In the case of the Dnepr mission, six M6x1 fasteners were used to attach each P-POD to the Dnepr launch vehicle interface. These fasteners were threaded into tapped holes on the bottom panels of the P-PODs.

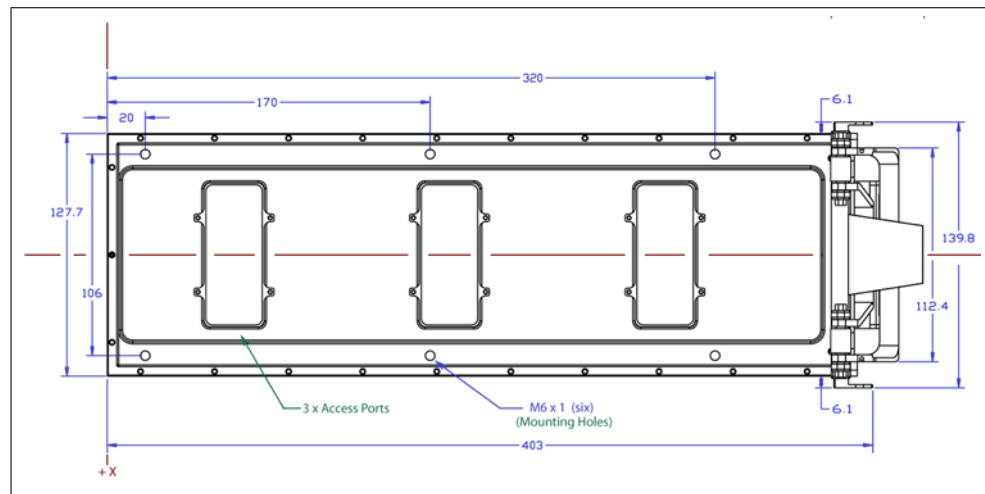


Figure 4.3: P-POD Mk. II mounting hole pattern.

The hole pattern and fastener specifications were jointly agreed upon by Cal Poly and Kosmotras. Cal Poly was responsible for certifying the soundness of the mechanical interface and providing Kosmotras with analysis to show that the interface could survive launch loads. Definition of design loads for the interface and selection of fasteners based on various criteria are discussed in detail in Appendix B and Appendix C respectively.

The mounting holes in the P-POD utilize threaded inserts — Heli-Coils — so that the threads could be repaired, if need be, without disassembly of the hardware. Benefits and considerations of using Heli-Coils are also discussed in Appendix C.

As part of their standard service, Kosmotras designed an adapter between the P-POD and Dnepr Space Head Module (SHM). The Launch Vehicle Interface (LVI) was designed to carry all five P-PODs on one adapter with the +Z axis of the P-POD facing the front of the rocket.

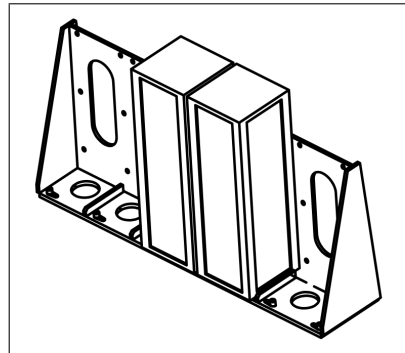


Figure 4.4: Diagram of LVI with two P-PODs attached.

The LVI is basically a glorified L-bracket with triangular supports on each side. It is constructed out of machined aluminum alloy and welded at the seams. The LVI can be seen in Figure 4.5 with two P-POD mass models attached and installed into the Dnepr SHM.

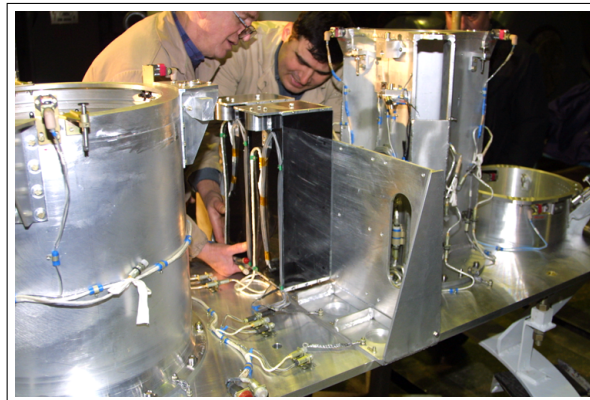


Figure 4.5: Picture of LVI with two P-POD mass models attached.

4.2.2 Electrical Interface

The electrical interface was designed specifically for the Dnepr launch vehicle, but the release mechanism used is capable of accepting a wide variety of separation signals. Components were chosen that are widely utilized in the aerospace industry and are designed to work with standard launch vehicle electrical buses.

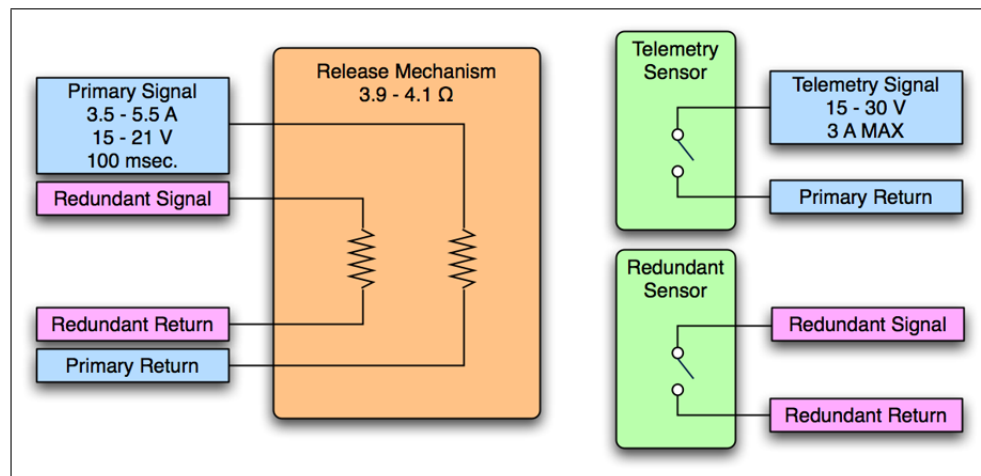


Figure 4.6: Diagram of P-POD electrical interface.

The capability of directly accepting standard separation signals eliminated the need for the P-POD Deployment Electronics Package (P-DEP), which was necessary to interface the P-POD Mk. I to launch vehicles. This resulted in mass savings of 200 grams, and reduced risk inherent in using student designed hardware.

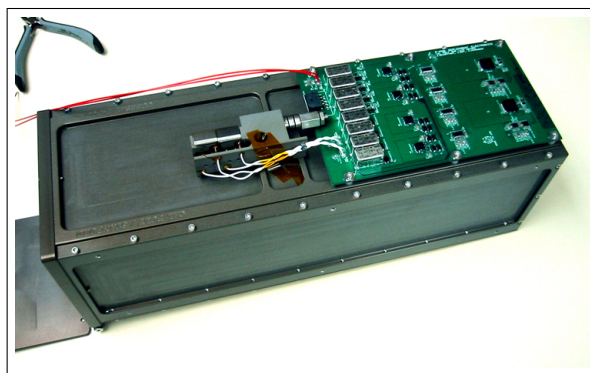


Figure 4.7: The P-POD Deployment Electronics Package (P-DEP).

The electrical interface for the Dnepr launch was defined by selecting the most appropriate release mechanism, then consulting with Kosmotras to verify compatibility with launch vehicle electronics. The resulting interface has three connections: a primary and redundant separation signal, a primary and redundant telemetry signal, and a grounding bolt. Discussions with other launch providers have shown this interface to be compatible with many launch vehicles.

Signal cables were provided by ISC Kosmotras, and connectors were all placed at the back of the P-POD. The release signal cable, telemetry signal cable, and grounding bolt are shown in Figure 4.8.



Figure 4.8: Picture of P-POD electrical connections.

4.3 Release Mechanism

The release mechanism is the most critical component on the P-POD Mk. II because it is responsible for:

- Initiating deployment of the CubeSats upon receipt of a separation signal.
- Preventing the deployment of CubeSats until a separation signal is received.

A release mechanism failure could cause catastrophic effects, not only for CubeSats, but for the primary spacecraft or launch vehicle as well. This mechanism needed to be robust and extremely reliable.

Because of the emphasis on reliability, a decision was made to purchase a release mechanism rather than build one at Cal Poly. This makes it easier to convince primary payloads and launch providers that P-PODs do not add significant risk to their missions.

4.3.1 Planetary Systems Corp. Line Cutter

The release mechanism used on the P-POD Mk. I was a Line Cutter developed by Planetary Systems Corporation. Developed primarily for the Lightband series of separation systems, the Line Cutter uses radiant heaters to raise the temperature of a vectran line until the line fails in tension. Vectran is a high-performance, thermoplastic, multi-filament yarn with a very high tensile strength.

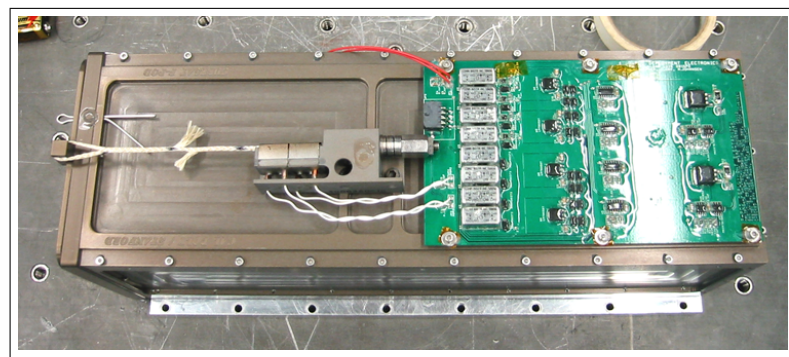


Figure 4.9: P-POD Mk. I with line cutter attached.

Although this mechanism is simple and efficient, the decision to use the Line Cutter was primarily a financial one. These mechanisms were provided for low cost and Planetary Systems Corp. offered significant support in the implementation and testing of the system. Despite their many benefits, the Line Cutter proved to be incompatible with the upcoming Dnepr mission.

Benefits

The line cutter does offer some significant benefits other than cost. The mechanism has good reliability due to its simplicity and redundant heating mechanisms. In addition, the mechanism can be reset by the user with simple tools and extra vectran lines. The Line Cutter is straightforward to use and is easily integrated into the P-POD design.

Incompatibilities

During preliminary discussions, Kosmotras identified two compatibility issues with the Line Cutter: nominal actuation time and variance in actuation time (30 ± 5 seconds). Due to the number of payloads on the launch, there would not be enough fuel to maintain attitude control throughout the deployment sequence. Even staggering the separation signals 10 seconds apart — instead of waiting the full 30 seconds — did not solve this problem.

The initial hope was to find a solution that worked with the Line Cutter, however, eventually a decision was made to consider mechanisms with shorter actuation times.

4.3.2 Mechanism Type Survey

Historically, separation mechanisms have been pyrotechnic in nature. These “pyros” use explosive charges to actuate a separation event. They are widely used on older systems, as well on many new systems, and are a proven, reliable technology with an exceptional energy to size ratio [5].

Due to their explosive nature, these mechanisms induce high levels of shock into nearby components. Additionally, pyros pose a safety hazard to engineers and technicians working with or around these mechanisms. As a result, a number of alternatives have been developed; most of these devices are thermally actuated, either by burning a fuse, or changing

an actuators shape. Due to their hazardous properties, pyrotechnic mechanisms were not considered in this study. Additionally, slow mechanisms, such as paraffin-actuated devices, were not considered. Finally, motor driven mechanisms were not considered, as they are either very expensive or relatively risky for aerospace applications. Three categories of mechanisms were considered: pin pullers, cable release mechanisms, and separation nuts.

Pin Pullers

Pin pullers are a class of release mechanisms that retract (or extend) a pin upon receipt of a separation signal. Pin pullers can be pyro, SMA, or paraffin actuated, and are usually small, lightweight devices. However, the pins are not designed to take very large shear loads, and additional components would be necessary to integrate a pin puller into the P-POD.



Figure 4.10: A pin puller mechanism manufactured by TiNi Aerospace.

Cable Release

This class of mechanism releases, cuts, or burns through a cable in tension. The cables used in these devices can often carry large loads. The drawback is usually that there is a free floating cable that has to be dealt with after deployment.

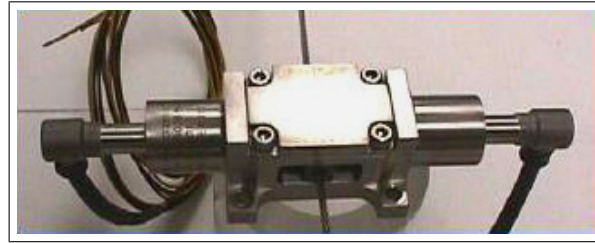


Figure 4.11: A cable release mechanism manufactured by G&H Technologies.

Separation Nut Mechanisms

Separation nuts are very common in aerospace applications where panels or appendages need to be deployed. They are also very common in payload and fairing separation systems.

The basic function of a separation nut is to hold a threaded bolt in place, then release the bolt upon receipt of a separation signal. Various methods are used to restrain the bolts and actuate these mechanisms, but their overall functionality is very similar.

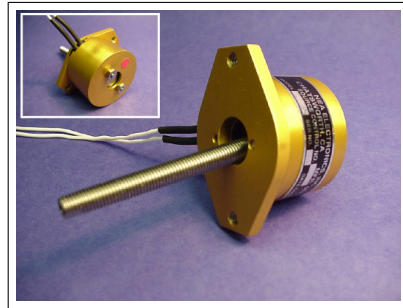


Figure 4.12: A separation nut mechanism manufactured by NEA Electronics.

The greatest benefit to these mechanisms is that they are strong enough to support the required loads in the P-POD with no additional moving parts. Separation nuts required the least number of moving parts to integrate onto the P-POD, and create a more solid connection than cable release type mechanisms. Separation nuts were determined to be the best match for this application.

4.3.3 Mechanism Trade Study

Based on the survey above, a number of compatible devices were chosen for further study.

A simple trade study was performed on four mechanisms (three separation nuts, one cable release mechanism). The Line Cutter was included in the study as reference. No sensitivity analysis was performed, however a number of design concept sketches were made for each device. These sketches were used to examine how well each device could be integrated into the existing P-POD design.

Reliability

Due to the criticality of this component's operation, reliability was the primary design driver. The mechanism should be produced by a reputable aerospace vendor, have flight heritage, average or better reliability for this market (99.9% reliability with 95% confidence is typical).

Actuation Time

The primary requirement from the launch provider was actuation time of the mechanism. The mechanism should actuate in well under 1 second.

Simplicity

Simplicity is very important in mechanisms as added complexity adds risk, cost, or both to the design. Effects of various mechanism types on the simplicity of the overall P-POD design were considered in addition to simplicity of the mechanisms themselves. Most importantly, the need for support electronics was considered a drawback as it added mass and risk to the design.

Testability

Many aerospace mechanisms are single use devices, which are either disposed of or refurbished by the manufacturer after use. Reset costs and schedule impacts were taken into account in this study. The ability to thoroughly test a mechanism was considered extremely important to offset the inexperience of this primarily undergraduate design team. Mechanisms capable of being reset by the end user had a clear advantage in this category.

Cost

Surprisingly, cost was fairly low on the list for a university aerospace project. Reliable mechanisms are never inexpensive, but the investment seemed worthwhile to protect the reputation of Cal Poly and the CubeSat Program in general. Nevertheless, cost was definitely a consideration in this study.

Mass

Mass affected the decision process in the form of launch costs. With launch costs of \$10,000 per kilogram, lighter mechanisms had the potential for significant cost savings.

Redundancy

Redundancy was a favored quality in this study, as it increases reliability. Most mechanisms are redundant in actuation, not restraint. Premature actuation was the primary concern, so the benefits of redundancy were marginal. Full redundancy would require two independent mechanisms, which the budget could not support.

Technical Support

Anticipated technical support was important since the team had very limited experience with aerospace mechanisms. This parameter was judged based on early conversations with applications engineers.

Schedule

At the time of this study, there was plenty of schedule margin to support even the longest lead times.

Table 4.1: Release mechanism trade study summary.

	G&H 8036-500	NEA 9101	PSC Line Cutter	Starsys Qwknut	TiNi ERM500
Reliability	GREAT	GREAT	GOOD	GREAT	GREAT
Actuation Time	25 msec.	25 msec.	30 ± 5 sec.	35 msec.	30 msec.
Simplicity	GOOD	GREAT	GREAT	FAIR	FAIR
Testability	POOR	POOR	GOOD	GREAT	GREAT
Cost	\$7,000	\$5,000	\$1,500	\$6,000	\$5,000
Mass	250 g	120 g	200 g	225 g	74 g
Redundancy	YES	NO	YES	YES	YES
Tech Support	POOR	GOOD	GREAT	GOOD	—
Schedule	3-6 mo.	3-6 mo.	0 mo.	3-6 mo.	3-6 mo.

4.3.4 Starsys Research Corp. Qwknut

Based on the research conducted, the Starsys Qwknut was chosen as the replacement for the Line Cutter. The Qwknut met all the requirements listed above, and was known to

be a reliable mechanism with extensive flight heritage. The price of the Qwknut was also close to most other similar mechanisms.

Micro Qwknut

The ideal mechanism in the Qwknut family is the small and lightweight Micro Qwknut. When contacted about this mechanism, Starsys mentioned that this model was not in production. The Micro Qwknut had been funded half way through development by a customer, but never made it past the prototype phase. Starsys predicted that it would cost about \$60,000 to bring the Micro Qwknut up to production level.

Qwknut 3k

At that price, it was much more practical to use the Qwknut 3k, which is the next size up from the Micro Qwknut. Even with the weight penalty, it would take a lot of flights to make up the cost of development. In addition, the Qwknut 3k was already space qualified hardware and a very commonly used and well supported product.



Figure 4.13: The Starsys Qwknut 3k release mechanism.

The Qwknut 3k is an Shape Memory Alloy (SMA) actuated separation nut that is capable of releasing a 1/4-28 bolt within a nominal 35 milliseconds after receiving a signal. The Qwknut 3k was the most appropriate mechanism for this application.

Table 4.2: Qwknut 3k specifications summary.

Release Time	50 ms MAX at 3.5 A
Nominal Preload	3000 lb _f
Resettable	End user reset capability
Operating Lifetime	100 preloaded deployments MIN
Storage Lifetime	5 years MIN
Mass	225 g MAX
Operating Temp.	-45 °C to 65 °C
Non-operating Temp.	-80 °C to 75 °C

The primary benefit of choosing this mechanism is its reset capability. Resetting the mechanism is a quick and easy process requiring a very simple tool provided by Starsys. In addition to the flight units, an engineering unit was acquired early on to assist in the design and testing process. The system was tested many times during various stages of development.

4.3.5 Qwknut Mounting Scheme

Having selected a mechanism, the task became to integrate the Qwknut into the P-POD while adding the minimum number of parts, and zero moving parts if possible. In addition, the Qwknut mounting system was designed to accept a number of other similar mechanisms with only minor modification. This designed in flexibility would allow some immunity from possible supply chain problems.

After reviewing many concepts, the Qwknut was placed as close to the front of the P-POD as possible. In this configuration, no additional moving parts would be necessary and the release bolt would pass directly through the P-POD door.



Figure 4.14: Prototype fixture for mounting the Qwknut to the P-POD.

Integrating the Qwknut would require modification of the door and addition of a bracket to hold the mechanism in place. The detailed design process for the bracket and door is discussed later.

A demo unit was loaned out by Starsys and proved very useful while designing. A very simple but effective prototype was built using scrap pieces of metal and a spare early generation door. Having a prototype on hand to experiment with helped visualize the deployment kinematics and made the design process much easier.

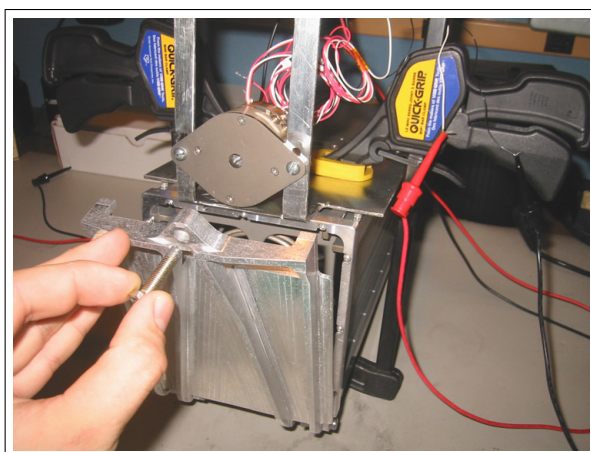


Figure 4.15: Fitting the Qwknut to the P-POD with the prototype door and bracket.

To determine how the loads would propagate to the mechanism, Equation 4.1 was used to calculate a design load of $F_{D,cubes} = 1800$ Newtons. G_{\oplus} is acceleration of gravity on earth, N is the maximum acceleration as defined in Appendix B, M_{cubes} is the mass of three CubeSats, M_{pusher} is the mass of the pusher plate, SF is the safety factor, $(k\delta)_{main}$ is the product of spring ratio and deflection for the main spring, $(k\delta)_{kick}$ is the product of spring ratio and deflection for the kick springs, and $(k\delta)_{sep}$ is the product of spring ratio and deflection for the separation springs. Acceleration of the door was assumed to be negligible.

$$F_{D,cubes} = G_{\oplus}N(M_{cubes} + M_{pusher})(SF) + (k\delta)_{main} + 4(k\delta)_{kick} + 6(k\delta)_{sep} \quad (4.1)$$

With a general idea of how the components would fit together, the design load was used to calculate the approximate forces on the release mechanism bolt. The door was assumed to have a high enough stiffness for a statically determinate analysis. Moments were taken about the hinge at the bottom of the door,

$$\sum M_{hinge} = (F \times r)_{bolt} - (F \times r)_{cubes} \quad (4.2)$$

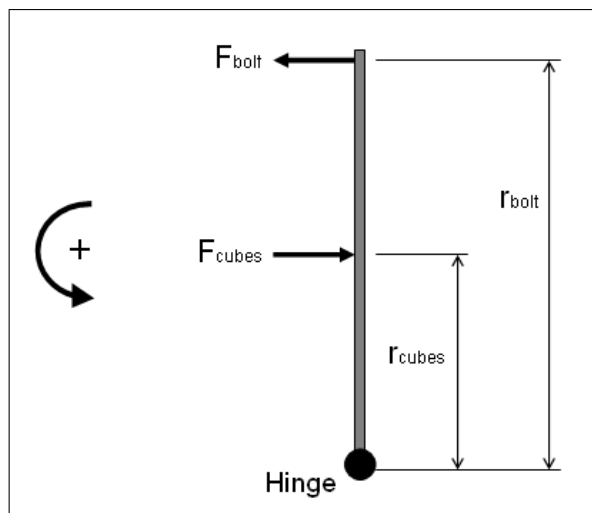


Figure 4.16: Free body diagram of door.

Payload generated forces acting on the release bolt would not exceed $F_{bolt} = 1300$ Newtons. This translates to a minimum required preload of 1000 Newtons. The Qwknut 3k is designed to handle a nominal preload of 13,350 Newtons. For the reasons cited in Appendix C.4, it was decided to set the preload just slightly under the recommended nominal amount.

4.4 Top Panel

The P-POD top panel is different than the other panels in that it has a series horizontal ribs to allow mounting of a release mechanism. For the Line Cutter, these ribs were placed in the center of the panel, with the vectran line extending to the front of the P-POD.

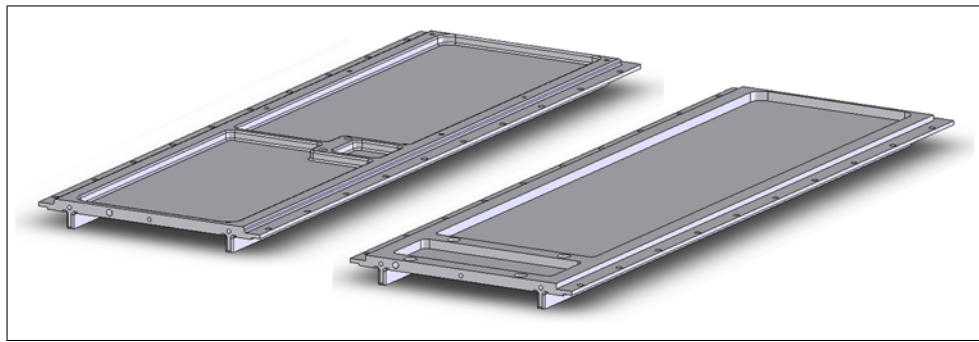


Figure 4.17: Old (left) and new (right) P-POD top panels.

The center ribs were removed and replaced with two ribs at the front of the panel. One of the ribs is built into the edge of the panel to save weight. The mounting bolt locations were defined somewhat arbitrarily at this point, based on the diameter of the Qwknut plus some additional width for the bracket. As the Qwknut is among the widest of these separation nut mechanisms, this configuration would allow the use of any separation nut of comparable or smaller diameter.

4.5 Release Mechanism Bracket

Mounting the Qwknut required the addition of a bracket. The bracket would have to be strong enough to survive the launch environment, but as lightweight as possible to minimize launch costs.

With the forces acting on the bracket defined, a simple bracket was conceptualized, then the design was optimized for mass. Splitting the bracket into two pieces eliminated a lot of unnecessary material, but the mounting plate of the Qwknut would now be subjected to static and dynamic loads. Since the Qwknut is oversized for this application, it was determined that the stress induced on the Qwknut would be minimal based on its design criteria.

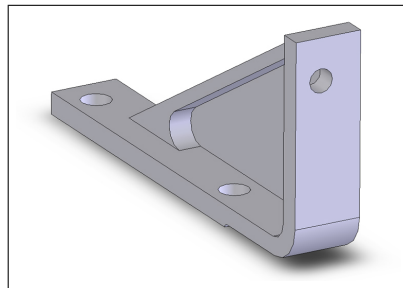


Figure 4.18: Left mounting bracket for the Qwknut release mechanism.

The bracket design was analyzed to predict its response under load. Static and quasi-static loads were first considered. The brackets were tuned to deflect less than 1 mm when statically loaded with the full weight of the Qwknut and both brackets under maximum acceleration.

As with most of the P-POD components, designing for maximum allowable deflection ensures low overall stress in the part — excluding stress concentrations of course.

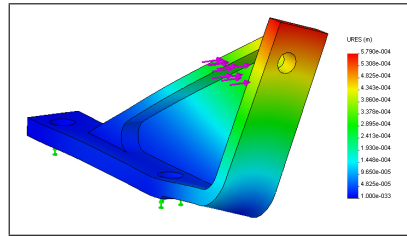


Figure 4.19: FEA of the left bracket under static lateral loading.

4.6 Door

A significant amount of time was spent redesigning the P-POD door. The door was identified as one of the main problem areas with the first generation P-POD design.

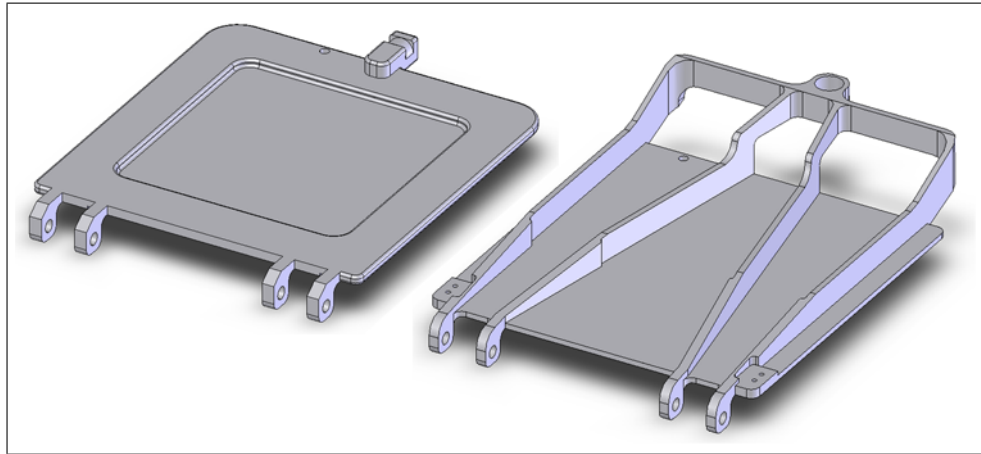


Figure 4.20: Old (left) and new (right) P-POD doors.

4.6.1 Flex Problem with Original Door

The original door was designed mostly as a flat plate, which made the door very lightweight, but did not do much for its stiffness. The door was susceptible to warping and bending when subjected to vibration environments. Even when exposed to the static loads seen during integration, the door exhibited what was known around the lab as “a healthy bow.” Although there was no risk of fracture under these loads, increased cyclic stress in the door made fatigue a concern. Additionally, flex in the door would lower natural frequencies and

possibly induce higher loads to the CubeSats. Finally, it just did not look right, and would not be very confidence inspiring to safety engineers.

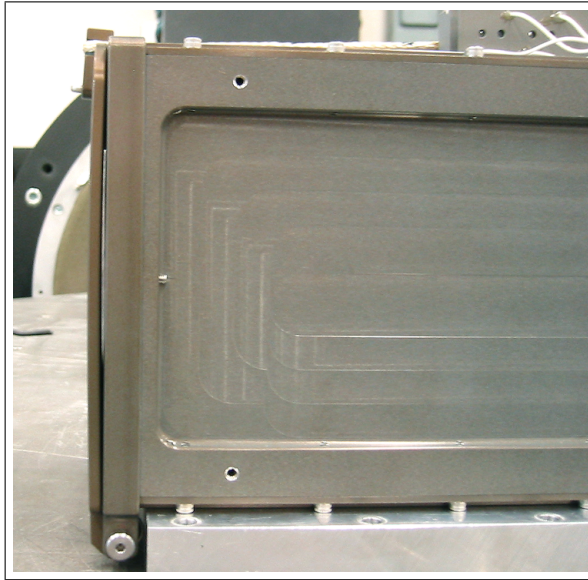


Figure 4.21: Integrated P-POD Mk. I door showing a “healthy bow.”

4.6.2 Rib Design

The approach taken was to increase the door’s stiffness about the flexing axis by increasing the cross section height. In order to keep the additional mass to a minimum, a set of ribs were designed in to the door. The moment of inertia is much more dependent on an objects cross-sectional height than width. Tall slender ribs significantly increased the stiffness of the door while keeping the mass of the door relatively low.

$$I_x = \int y^2 dA \quad (4.3)$$

The placement and dimensions of the ribs went through much iteration. The end result was a set of four ribs. Two ribs cross through the locations where the CubeSat standoffs apply a force on the inside of the P-POD and provide stiffness to the edges of the door. Likewise, two more ribs provide stiffness to the middle portion of the door and traverse

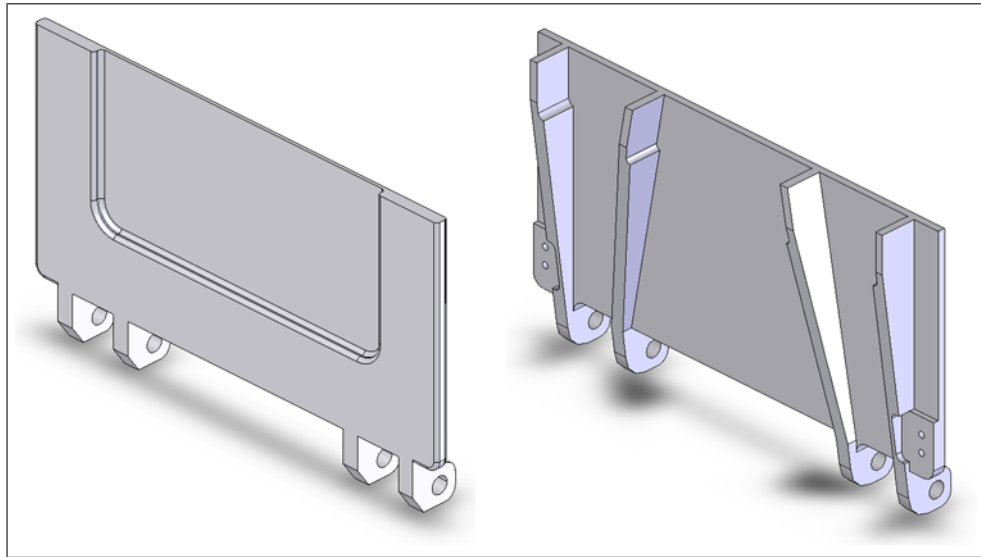


Figure 4.22: Cross sections of old (left) and new (right) P-POD doors.

from the inner hinges to the location where the mounting bolt is located, thus providing a robust load path.

These ribs increased the door stiffness by 400% allowing only 0.5 mm of deflection under maximum load. As before, the loads were considered static for this analysis. This is a significant improvement over the original design, which deflected up to 2.2 mm under the same loads.

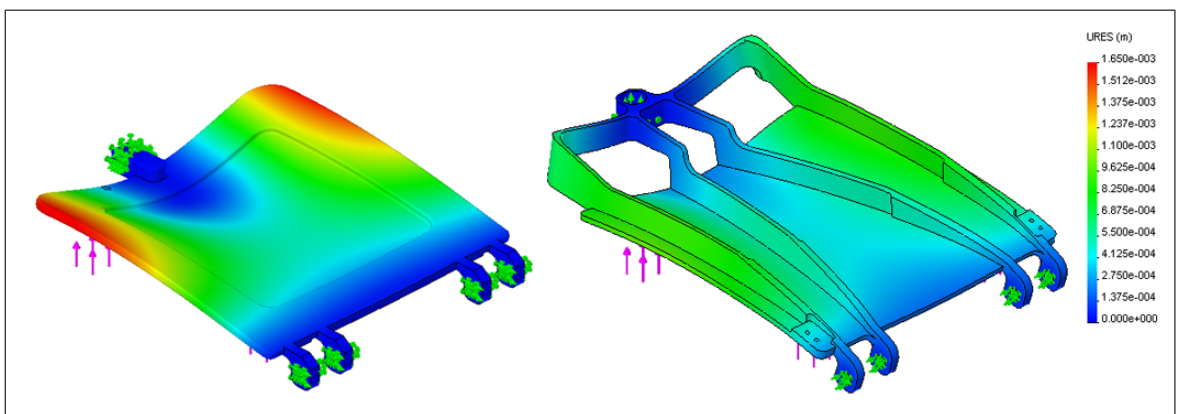


Figure 4.23: FEA of old (left) and new (right) P-POD doors under static loading.

4.6.3 Bolt Clearance During Release

Since the release bolt stays connected to the door during deployment, it is important to reduce the chances of the bolt interfering with CubeSats as they are ejected from the P-POD. Two solutions to this problem were considered, the first being the use of a bolt retractor. As this is a common problem when using separation nuts, spring loaded bolt retractors are available to capture bolts in a safe and reliable fashion.

In the case of the P-POD, the bolt retractor would have to be installed on the door. Adding a significant mass to the top of the door would severely effect the rotational inertia of the door, in turn increasing the time required to move the door out of the path of the CubeSats. Stronger torsion springs would be required to spring the door open in the required time.

Instead of redesigning the hinge of the door, a simpler and much more cost-effective solution was implemented. The length of engagement of the bolt in the Qwknut was known and predetermined by Starsys. By moving the whole release mechanism forward along the P-POD, it was possible to position the bolt such that interference is geometrically impossible.

A lot of attention was given to bolt position throughout the range of motion to minimize the risk of snagging in the mechanism and causing a possible deployment failure. In addition to keeping the bolt tip flush with the inner door surface to avoid damaging satellites, the position of the bolt minimizes the possibility of a snag in the mechanism. Placing the bolt and mechanism so far forward — actually in front of the front of the P-POD — allows the bolt to rotate out and away from the mechanism. If the Qwknut face were placed flush with the collar, the bolt tip would first slightly move up and then down and out as the door rotates away.

4.6.4 Ability to Open 270°

A final design element was the ability to open the door a full 270° from its closed position.

A rotation of 90° puts the door well out of the path of the CubeSats, further rotation helps alleviate collision risks. Designing the door ribs to angle down to the hinges prevents the ribs from colliding with the bottom panel of the P-POD when door is fully open. This interference proved to be a major annoyance on the prototype, but could cause inadvertent damage to the flight units.

4.7 Torsion Springs

The addition of stiffening elements in the door was necessary, but also increased the mass of the door. This additional mass was kept to a minimum to avoid significantly increasing launch costs. The additional mass also affected the rotation rate of the door. A quick kinematic analysis was performed to ensure that the existing torsion springs were adequate to move the door out of the CubeSats' path. Door position over time was predicted using the moment of inertia around the hinge from Pro/E, and the spring rate from the manufacturer specifications of the existing springs. In the unlikely event that the door is not fully out of the CubeSats path, the inside of the door is flat and smooth to minimize possible damage to the CubeSat.

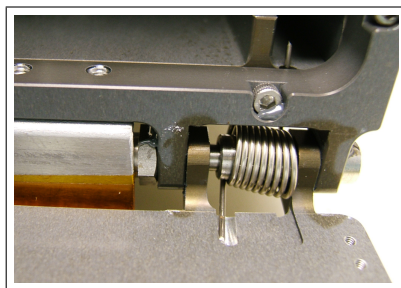


Figure 4.24: Close-up of P-POD door hinge.

4.8 Main Spring

The main spring in the P-POD was sized to meet ejection requirements imposed by the launch provider. The large number of payloads manifested on the mission required space-craft to be deployed one after another, often with only a second between deployments. The maximum velocity differential of 2 m/s is required to ensure that no collisions occur between separating objects. During the separation phase, the launch vehicle upper stage is accelerating in the direction of travel with the aft end forward.

This seemingly bizarre motion allows the upper stage to drop off payloads as it moves over a target location — a very appropriate feature for a rocket designed to deploy multiple nuclear warheads. Fortunately for small payloads, this design allows ISC Kosmotras to perform cluster launches with ease.

Also, the CubeSats were required to be fully ejected in less than one second from receipt of a separation signal. This is required to ensure that all the payloads are deployed before the upper stage attitude control system fuel tanks are depleted.

Additionally, the final mass of each CubeSat was unknown. The spring rate and size were designed to eject the CubeSats within the defined restraints and to account for the possibility of CubeSats being slightly underweight.

A Matlab model was created to simulate the deployment of CubeSats during the launch. The ejection of the CubeSats was modeled as a one dimensional, four degree of freedom system and took into account the effects of the main spring, kick springs at the rear of the P-POD, and separation springs between the CubeSats. The separation springs help increase the rate of separation between the CubeSats after deployment.

This model was used to size the main spring properties. The full simulation details and results are presented in Appendix D. A summary of the results is presented here.

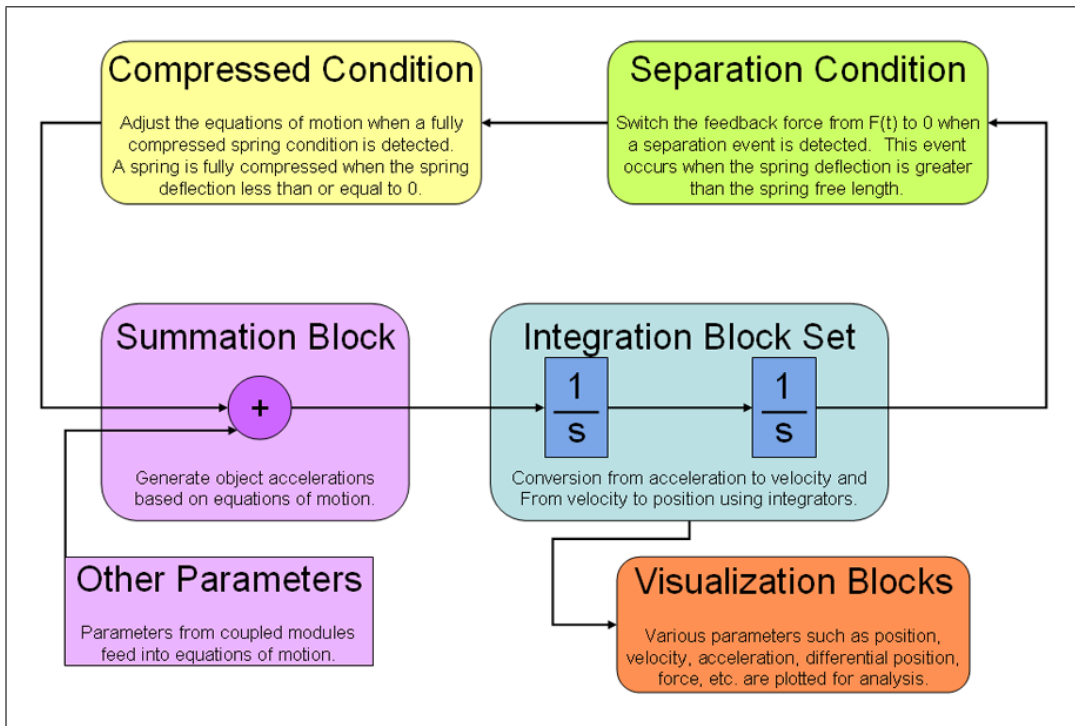


Figure 4.25: Deployment simulation block diagram.

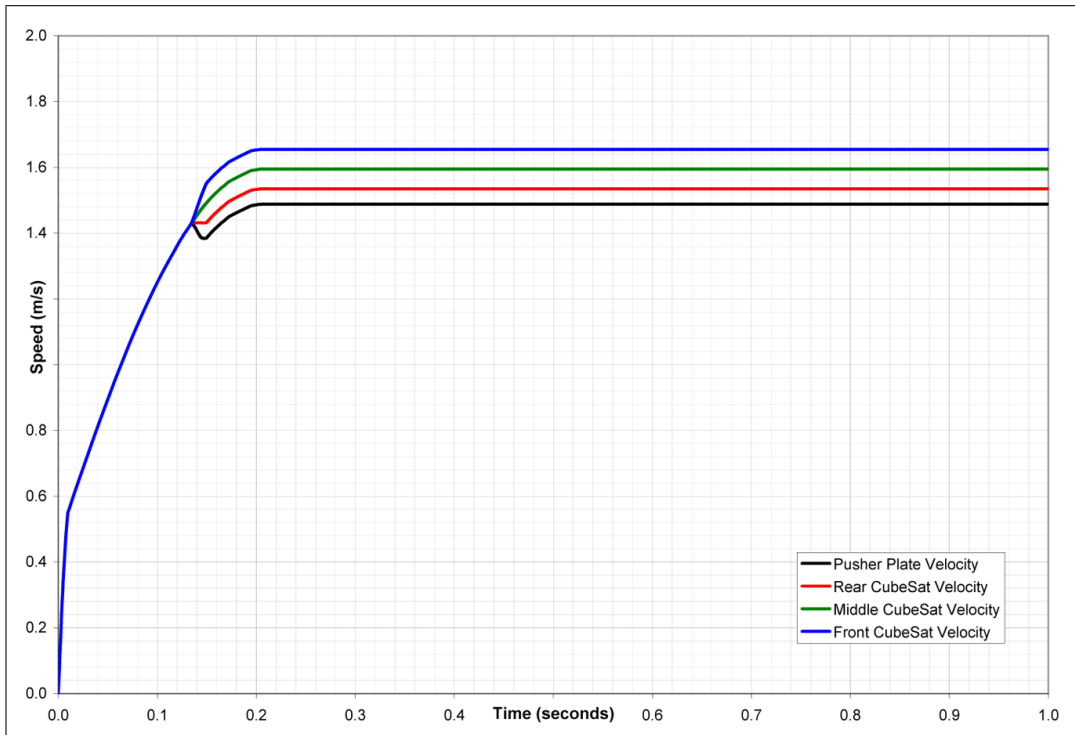


Figure 4.26: Results of P-POD deployment simulation.

An interesting note is that the spring ordered is slightly different than the ideally sized spring according to the model. The ideal coil diameter was too small in proportion to the other dimensions of the spring, and thus the spring was impossible to manufacture. By discussing the problem with the spring manufacturer a compromise was devised that was both manufacturable and would meet the specifications. The new spring, however, does not extend to the very front of the P-POD. This extension is favorable to ensure that the entire body of the P-POD has been cleared.

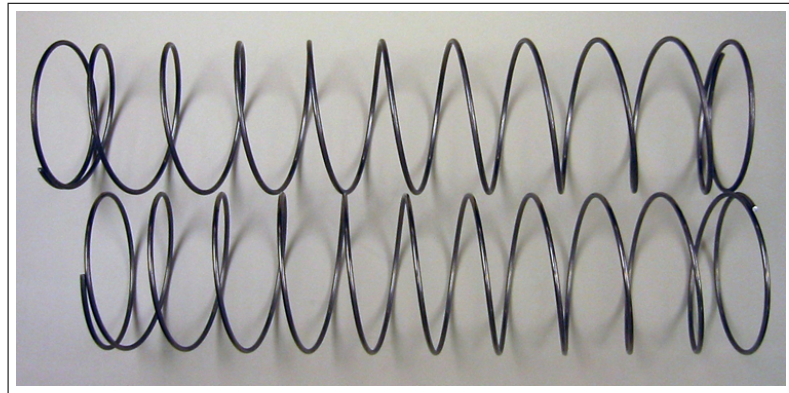


Figure 4.27: Difference between old (top) and new (bottom) P-POD main springs.

4.9 Kick Springs

The kick springs are short throw, high stiffness springs which provide an additional force which may help start the ejection process if any binding or interference occurs during launch. The kick springs are not preloaded, because they are not designed to act as structural members. The inside of a spring plunger is mostly hollow and the material is rather soft. Rather, the spring plungers are held in place by locking Heli-Coils.

These kick springs serve two purposes. First, they provide a relatively high initial force which may help overcome any interference issues created during launch (i.e. deployed antennas or warped structures). More importantly, they allow the integration team to

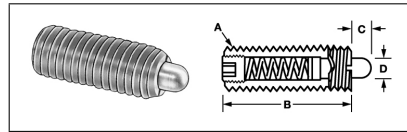


Figure 4.28: Diagram and internal view of a spring plunger.

adjust the inner envelope of the P-POD to account for CubeSat rail length tolerances.

The downside to using spring plungers is that they are difficult to use and are easily damaged (for reasons mentioned above). The requirement to use a locking mechanism instead of preload implies that a relatively large amount of torque must be placed on the spring plungers to install or adjust them. In fact, the initial holding torque of the locking Heli-Coils is greater than the maximum recommended torque specification of the spring plungers, even when using the high-torque, hex drive models.

	Initial Force		Heli-Coils	
				
			Unified Thread Size	
			Max Installation Torque (in·lb)	
2 (.086)-64	20 oz-in	3 oz-in	No.4	0.60
3 (.099)-56	32 oz-in	7 oz-in	No.5	1.25
4 (.112)-48	48 oz-in	10 oz-in	No.6	1.65
6 (.138)-40	6 lb-in	1.0 lb-in	No.8	2.15
8 (.164)-36	9 lb-in	1.5 lb-in	No.10	3.15
10 (.190)-32	13 lb-in	2.0 lb-in	1/4	6
1/4 (.2500)-28	30 lb-in	2.5 lb-in	5/16	11
5/16 (.3125)-24	60 lb-in			
3/8 (.3750)-24	80 lb-in			
7/16 (.4375)-20				
1/2 ''				

Spring Plungers

Optional Locking Element

Figure 4.29: Torque data, courtesy of Heli-Coil and Emhart.

Both Heli-Coils and spring plungers come in standard and locking varieties. The spring plunger documentation specifically states that locking Heli-Coils should not be used with locking spring plungers [13]. The NyLock locking elements in the spring plungers do

not provide enough holding force for our required vibration environment. Using non locking versions of both components is out of the question when the joint is not preloaded. Therefore, the chosen configuration included locking Heli-Coils and regular spring plungers.

Experimenting with the P-POD Mk. I had exposed the many difficulties and drawbacks to the current configuration. At this point, a lot of thought was put into redesigning the kick springs by either using larger spring plungers or moving to another type of spring mechanism. However, the design was left unchanged to avoid unnecessarily changing critical components of the P-POD which had already been flight qualified and thoroughly tested. In retrospect, different solutions to this problem should have been explored and implemented, as there are a number of major issues related to serviceability and reliability which arise from this configuration.

4.10 Back Panel

One of the modifications requested by Kosmotras early on was that the back of the P-POD be completely flat. This would allow the P-PODs be mounted to the launch vehicle with the back panels flat against the adapter. The original back panel had some pocketed sections for mass reduction on the outside while the inside was completely flat.

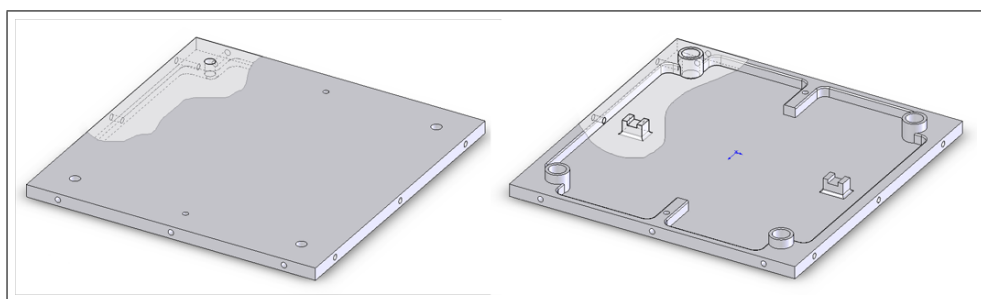


Figure 4.30: Old (left) and new (right) P-POD back panels.

Instead of completely redesigning this part, the back panel was merely flipped inside-out. The holes on the back panel lined up perfectly with the corresponding holes on the top, side, and bottom panels whether the pocketed sections faced in or out.

Some minor modifications were still made to the back panel. On the P-POD Mk. I, the main spring was held in place by a titanium strip wrapped around the first coil of the spring. The pocketed sections on what was now the inside of the back panel required additional standoffs to securely mount the spring. In addition, the threaded holes which support the kick springs described in Section 4.9 were made thicker to provide a longer thread engagement length.

As a result of these modifications, the top, side, and bottom panels and pusher plate all required slight changes. Shallow cuts were made in the rear portion of the rails on all four panels to allow clearance for the thicker kick spring supports.



Figure 4.31: Internal P-POD rails cut to accommodate kick springs.

Eventually, the launch vehicle adapter design was changed so that the P-PODs would be mounted through the bottom panel instead — a more robust mounting scheme — which eliminated the requirement for the back of the P-POD to be flat. The redesign was still implemented, however the spring plungers were not designed to be fully contained, and do protrude from the back of the P-POD when integrated.

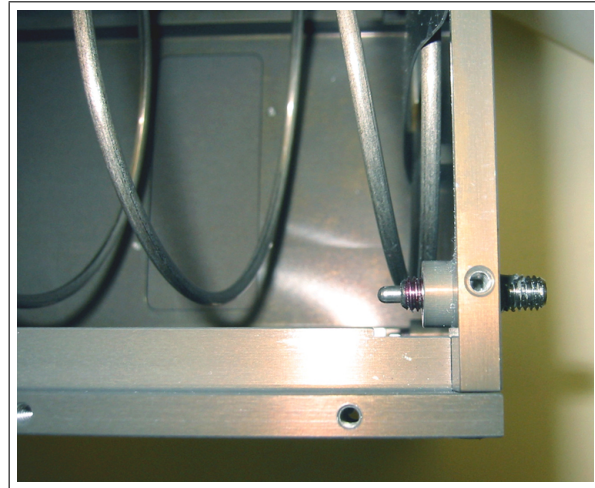


Figure 4.32: Side view of kick springs integrated into the P-POD.

4.11 Pusher Plate

Due to the height difference of the back panel, the pusher plate had to be shortened to maintain the correct interior P-POD envelope. The pusher plate was shortened by 6 mm, and all other dimensions were left the same.

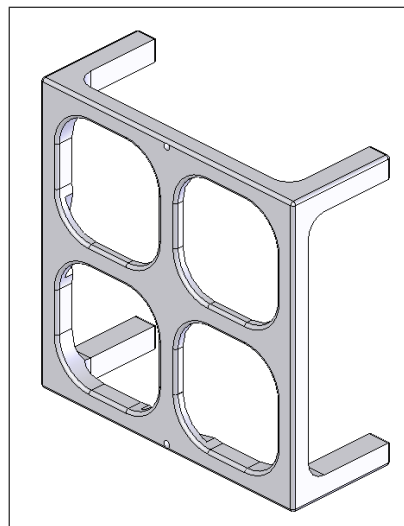


Figure 4.33: P-POD pusher plate.

The shorter length of the pusher plate made it more prone to getting stuck in the P-POD. A number of qualitative tests were performed to compare the probability of binding

with the shorter design. To perform the tests, the main spring assembly was compressed inside the P-POD by hand, then the obstruction was suddenly removed. After compressing the main spring assembly, the test engineer manually tried to bind the pusher plate against the P-POD rails by angling the pusher plate into one corner of the P-POD.

The test cannot really be used to predict reliability of the system, and should only be used as a comparison between design iterations. In reality, the pusher plate must work against the inertia of the CubeSats and is not capable of moving as it does in the test. Even with underweight CubeSats, there is no probable way for the pusher plate to bind up during release.

4.12 Telemetry System

During the 2003 Eurokot mission, there were difficulties contacting the three educational CubeSats in one of the P-PODs. There were concerns that a P-POD had malfunctioned. As time progressed, NORAD radar tracking data confirmed that all three CubeSats had been deployed.

Lessons learned from the first generation P-POD led to the addition of a telemetry system. One large drawback to first generation design was the lack of feedback upon deployment of the CubeSats. A telemetry system is important because it provides confirmation that the P-POD has functioned as designed and the CubeSats have been deployed. If a failure does occur, and one or more of the CubeSats cannot be contacted, the telemetry information is also useful in tracking down the potential cause of the failure.

The problem was approached by defining desired telemetry information, then identifying technologies to accomplish the objectives, and finally performing a trade study based on the complexity, risk, and benefits of each method.

The first decision made was to keep the telemetry system as simple as possible, as it would be yet another interface and would tie up additional launch vehicle resources. The telemetry system was designed to be an optional, add-on system for the same reason. To keep this interface simple, the signal sent back to the launch vehicle was defined as a simple on/off signal. No complicated information would be stored in the signal and the telemetry system would not require power from the launch vehicle.

4.12.1 Optical Sensors

The most thorough solution would signal when the physical satellites have left the P-POD. The challenge was to design a sensor into the P-POD that did not affect the CubeSats in any way. An optical sensor placed at the front of the P-POD would allow detection of this event much like the a doorbell when walking into a convenience store. An emitter placed on one side of the P-POD could project a beam onto a collector on the other side. When the CubeSats are in the P-POD, this beam would be broken.



Figure 4.34: A photodiode could be used to sense deployment.

This method had a number of drawbacks, and was quickly abandoned. The system required power to operate, as the emitter is constantly on. This power does not necessarily have to come from the launch vehicle, but either way, the system requires additional electronics and a number of new components.

Furthermore, projecting optical or infrared energy onto the CubeSats in the P-POD would have to be studied for compatibility with CubeSats on a case by case basis.

4.12.2 Hall Effect Sensors

A similar approach could be taken using magnetic sensors similar to those used in many home alarm systems. A magnet could be embedded in the pusher plate and a sensor placed at the front of the P-POD. This system does not necessarily require additional power, but does have its limitations as well.

Tripping the switch requires the magnet in the pusher plate to correctly align with the sensor. The pusher plate may not always stop in the same spot, or may not function as planned, providing a false negative. Also, many satellites have magnets for attitude control, or have components that respond adversely in the presence of strong magnetic fields. The sensor may not always be compatible.



Figure 4.35: A hall effect sensor could be triggered by a magnet in the pusher plate.

4.12.3 Limit Switch in Back of P-POD

A very easy method of sensing deployment is to add a simple mechanical switch to the rear of the P-POD. A stop on the pusher plate would depress the switch when the P-POD is fully integrated. This method is simple, does not require power, and is reliable. However, the signal is sent when the pusher plate starts moving; there is no guarantee that the CubeSats make it all the way out. The pusher plate's exact position is adjusted with the kick spring plungers. The switch would have to be adjustable as well.

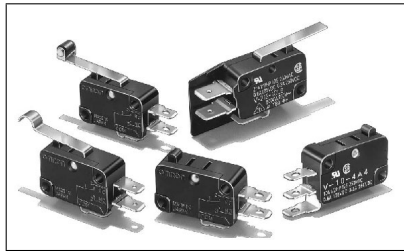


Figure 4.36: Various styles of mechanical limit switches.

4.12.4 Break Wire

Next, a break wire was considered. A thin electrical wire would be connected to the back of the P-POD as well as to the pusher plate, and would physically break when the pusher plate moves past a certain point, causing an open circuit. This method is extremely simple and requires the minimum number of components.

There are drawbacks though. Coiling the wire so that it does not affect the motion of the spring is challenging. The wire would have to be replaced every time the P-POD is actuated. Thus the flight hardware would need to be disassembled many times, and the flight break wire could never be tested. Finally, the wire potentially could fail to break sending a false negative signal.

4.12.5 Limit Switch on Door

It was decided that using limit switches was the most practical approach. More sophisticated systems could always be implemented on later revisions if desired. Instead of monitoring the pusher plate or satellites, a sensor was placed on the door. Since it is very unlikely that CubeSats will fail to eject if the door is completely open, the sensors were designed to detect when the door opened 90°.

The switches are manufactured by Saia -Burgess and were chosen for their size and form factor. These switches are not space qualified components, nor do they have extraordinary

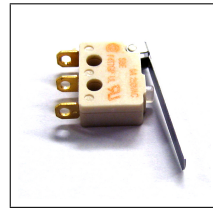


Figure 4.37: Saia-Burgess F4 series microswitch.

thermal or mechanical resilience properties. They do provide a simple, low cost solution and were verified to function well in the required environments through testing.

Two switches (for redundancy) were mounted to a corner of the P-POD door, and the contacts held closed by a guide rail attached to the collar. The door and collar were designed to allow mounting of the switches on either side of the P-POD or one on each side. The guide rails were sized to allow the switch levers to spring open once the door has opened a minimum of 90°.

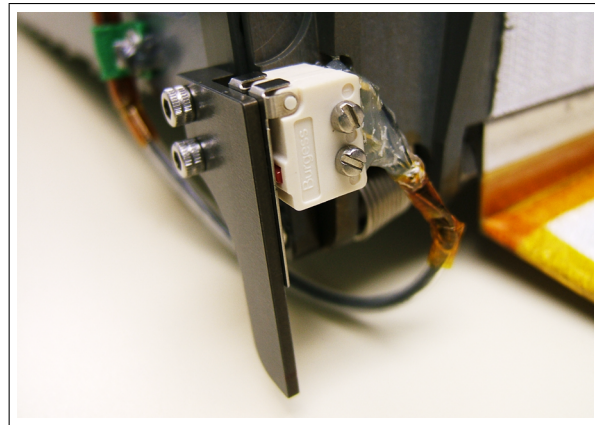


Figure 4.38: Telemetry switches and guide rail.

4.13 Stopper Bracket

Due to the large number of payloads manifested on the mission, real estate on the space head module was hard to come by. Kosmotras asked that the P-POD doors be limited to opening 105° from their closed position. This still allowed the minimum 90° required for

successful deployment, but not much margin.

A stopper bracket was designed to accomplish this task. The solution is not the most elegant, since it was an add-on after the P-POD Mk. II parts had already been received.

The simplest solution was to use a sheet metal bracket bolted to the collar. The light weight of the door and low torque of the torsion springs did not require a very strong bracket. Aluminum 5052 was chosen since it is a common sheet metal alloy, is readily available, and inexpensive.

Pieces of Nomex Velcro applied to the door and bracket served as a capture mechanism. Nomex is a space rated Velcro listed on the NASA approved materials list [22]. The final assembly was assembled on a prototype unit and tested to ensure functionality. The bracket was demonstrated to successfully stop and capture the door throughout a number of tests. The bracket does flex when the door strikes it, however, this deflection takes advantage of the natural damping in the aluminum to help slow the door to a stop.

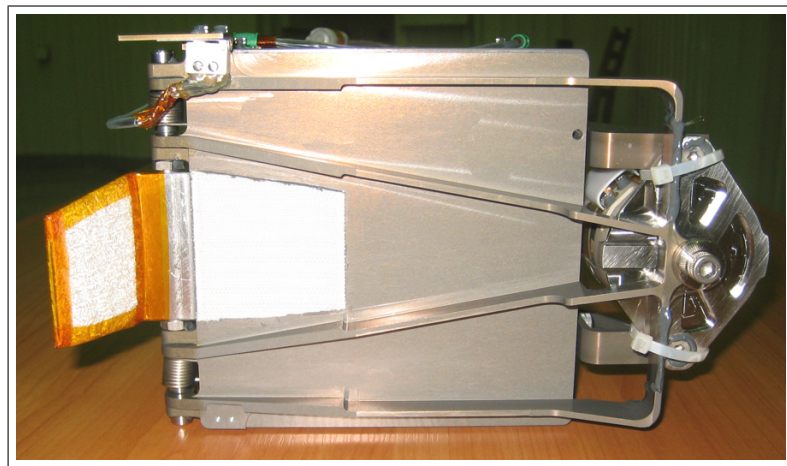


Figure 4.39: P-POD with stopper bracket attached.

4.14 View Ports

Another P-POD Mk. II feature was the addition of view ports on the side panels. Two small holes were cut in each side panel over the location where the spring plungers met up with the rear of the pusher plate. These view ports were meant to assist during integration by allowing the technicians to see the state of the spring plunger tip. This feature was added because it is very difficult to tell when the spring plunger tip is fully compressed when using locking Heli-Coils. The view ports were supposed to allow for easy visual inspection. However, the implementation was poor, and it was hard to see much of anything through them. In the CAD model, it was very easy to see the critical features, however, in real life, there simply is not enough ambient light to clearly see anything.

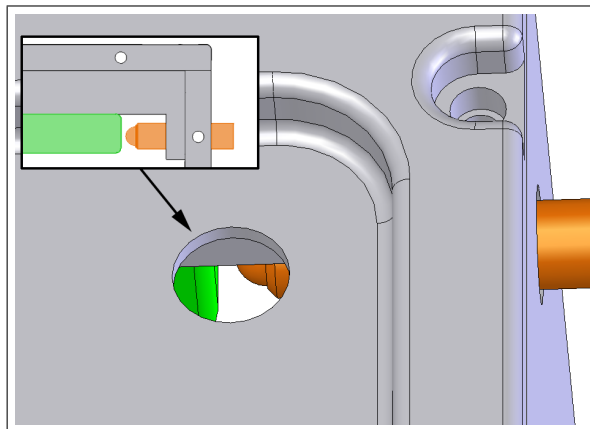


Figure 4.40: Theoretical view through P-POD view port.

Chapter 5

Prototype Testing

Testing was performed at virtually every level of development. Every piece of flight hardware underwent a series of tests. In addition, changes were qualified through testing before being implemented into the final design. This section will describe the qualification testing performed on the first fully assembled P-POD Mk. II, while testing on flight units is described in Section 7. Every test described in this section was performed on a single engineering unit.

5.1 Test Flow

The P-POD Mk. II test plan followed the testing objectives outlined in Section 2. Furthermore, the test plan included a barrage of analytical, functional, and environmental tests. The test flow focused mainly on vibration testing, since this would most likely cause a failure that could result in damage to the launch vehicle or primary payload.

5.2 Vibration Testing

The first test performed was a series of sine sweeps, with accelerometers in various locations of interest and at relatively low intensity. The P-POD was always integrated with CubeSat mass simulators to provide the correct mass and loading properties.

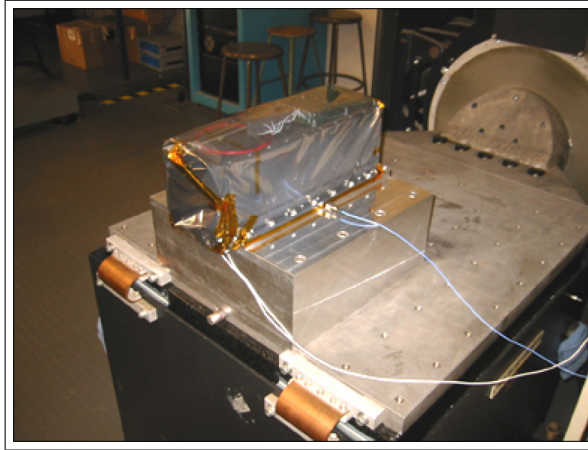


Figure 5.1: Vibration testing on the Cal Poly shake table.

Sine sweep tests are very useful in identifying natural frequencies and amplification factors at those frequencies. The main objective in this part of the testing was to compare real world natural frequency data with theoretical values obtained during FEA analysis. However, since natural frequency response data can also be deduced from random vibration test data, only a minimal amount of sine sweep testing was performed. Correlation between vibration data and finite element models is discussed in section 5.3

One major drawback to sine sweep tests is that they are not good at simulating real world vibration environments. By definition, a sine sweep test only excites one frequency at a time: something that, in a launch vehicle, typically only occurs at frequencies below 20 Hz [14]. Since the P-POD's fundamental frequencies are well above this range, random vibration testing was performed to study the effects of a realistic environment on the P-POD structure.

Random vibration utilizes a broadband input signal to excite many frequencies simultaneously. Not only does this better simulate the launch environment, but could also potentially identify unpredicted responses caused by interactions between excited frequencies. A random vibration profile is defined by the launch provider based on the characteristics of their vehicle and is provided to the customer. These profiles are represented by Acceleration Spectral Density (ASD) plots — commonly misnamed Power Spectral Density (PSD) plots — which depict the power input over a specified frequency range. These plots are always shown in log-log scale in the frequency domain [18].

Qualification of the P-POD consisted of two sets of random vibration tests. Testing was performed in all three axes (one axis at a time). Raytheon was generous enough to donate time and access to their testing facility in Goleta, CA for the qualification test. Although it required a rather lengthy drive, this allowed us to circumvent any calibration problems with the Cal Poly transducers and accelerometers and allowed us to learn a lot about vibration testing by having experts assist us in the process.

5.2.1 Dnepr Qualification

The first test performed was the qualification test for the Dnepr launch vehicle. This test would qualify the P-POD Mk. II design for the upcoming Dnepr launch. Per the Dnepr User's Guide, random vibration testing was to be performed at 150% of launch levels for 100% of the duration specified. In addition, each axis was to be tested sequentially with two different profiles, one for liftoff and one for flight [14].

5.2.2 NASA GEVS Qualification

Since the P-POD was designed to be compatible with many launch vehicles, additional testing was performed to ensure that the P-POD could survive the harsher launch envi-

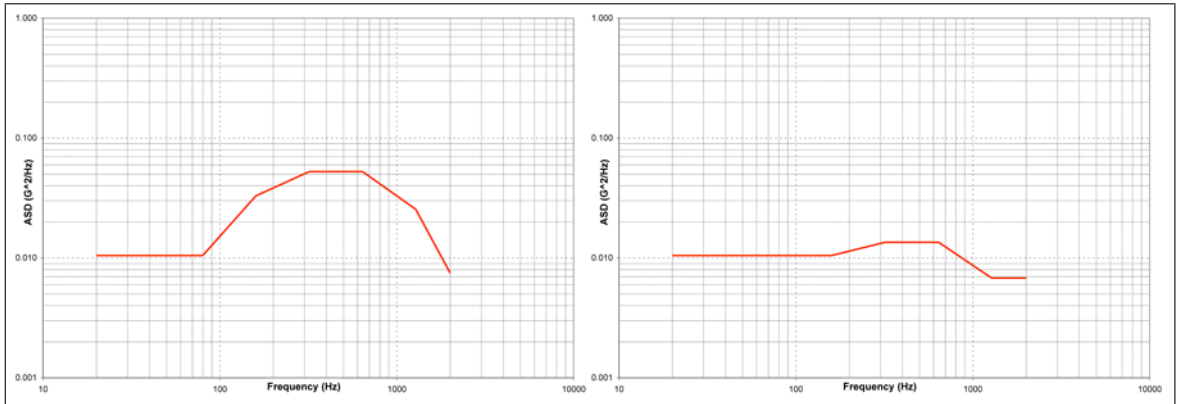


Figure 5.2: Dnepr two stage random vibration qualification profile.

ronments of a wide variety of launch vehicles. The worst-case random vibration profiles outlined in the NASA GEVS document were used in this case [19].

This profile envelopes a variety of launch vehicles typically used for NASA missions. This test is much more violent than the Dnepr qualification. GEVS specifications require 1 minute of testing per axis. However, to demonstrate the P-POD's durability and continue stringent testing practices set by the previous generation of CubeSat members, testing was performed for 10 minutes per axis, increasing cyclic loading by 1000%.

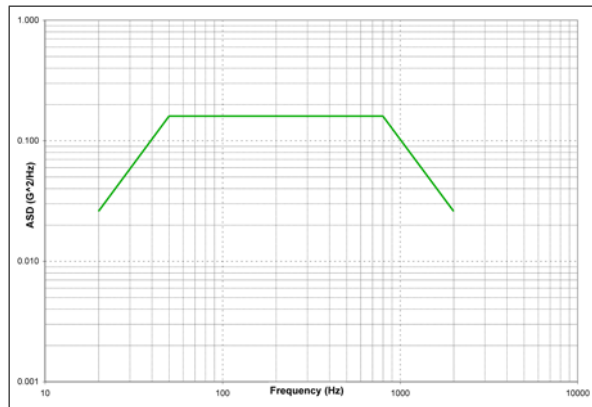


Figure 5.3: NASA GEVS random vibration qualification profile.

5.3 Finite Element Model Verification

The primary objective in testing the P-POD was to verify structural soundness and functionality of the P-POD after testing. A secondary objective was to verify the finite element models developed during redesign. The following discussion is an attempt to pair theoretical natural frequency predictions from finite element models with real vibration test data. Testing was conducted in all cases from 20 - 2000 Hz.

5.3.1 Finite Element Models

A number of models were used throughout the design process: mostly for static analysis. Three of these models were used specifically for modal analysis in order to predict the P-POD's dynamic response. Models were analyzed completely free as well as in a restrained case.

P-POD Frame

Finite element analysis was primarily performed on a model of the P-POD frame. Components in the model included the top panel, bottom panel, side panels, back panel and collar. The model was generated as one solid object to avoid joining parts in an assembly before analysis. Only structurally important features were included in the model and simplification of features were made whenever possible.

Previous analysis was only done with models of the P-POD frame without the panels [20, 15]. The primary reason for this is to exclude unimportant drumming modes of the thin panels themselves. Although these modes are not structural in nature, excluding the panels from the model has a noticeable effect on the results of the analysis. Therefore, the panels — with correct thickness — were included in the model.

P-POD Door

The major drawback to the P-POD frame model is its lack of representation of the P-POD's internal components or CubeSats. In fact, there are a number of natural frequencies that are probably caused by the CubeSats rattling around inside the P-POD. Axial rattling would surely be amplified around the natural frequencies of the door and back panel. Modal analysis of the back panel was included in the P-POD frame model, whereas the door was analyzed separately. Since the door is a relatively simple part in general, no simplifications were made to the model for analysis.

The CubeSats were not included in any of the analysis due to the difficulty in modeling them. First, the gap between the CubeSat rails and P-POD rails makes it very difficult to model the CubeSats' motion in the P-POD under vibration. In addition, the mass and stiffness properties can vary widely between CubeSats and a thorough analysis would be required to yield useful results. Experimental data, safety factors, and extensive testing were used to circumvent any problems that may be caused by imprecise knowledge of these characteristics.

Release Mechanism Subassembly

A third model was developed to simulate the Qwknut and mounting brackets. The model was drawn as one solid object, and was used to match natural frequencies of the subassembly with those of the door and P-POD frame. Although the Qwknut is extremely robust, its mechanism is sensitive and it was desirable to decouple natural frequencies of the subassembly and the rest of the P-POD as much as possible.

5.3.2 P-POD Frame FEA Results

A modal analysis of the P-POD frame model was conducted using a solid mesh and solving for all modes between 20 - 2000 Hz. This range of frequencies is adequate for most — if not all — currently available launch vehicles. Twenty five modes were predicted in this range of frequencies, with three distinctly unique mode shapes. Most of these modes are drumming modes associated with the thin panels. Only the structural modes are discussed here, which are considered to be normal modes of the P-POD [11].

“Shearing” Mode

At the first fundamental frequency, the P-POD panels experience torsional displacement along the Z axis. While the back panel provides support to resist this motion, deformation at the collar takes shape in a squishing of two opposing diagonal corners towards one another and extension of the other two opposing diagonal corners apart from one another. The mode shape can clearly be seen here in analysis results for an unconstrained P-POD.

When restrained along the bottom panel, this motion is better described as a shearing motion in the X direction. Since the Y axis is fixed along the bottom panel, the top panel similarly stays mostly parallel to the bottom. The resulting motion of the P-POD at its fundamental frequency is one of the front top section of the P-POD swaying horizontally. Therefore, this mode will be referred to as the P-POD’s “shearing” mode. Based on analysis, this mode shape accounts for the P-POD’s 1st, 3rd, 8th, 13th, 15th, 17th, 22nd, 23rd, and 24th modes.

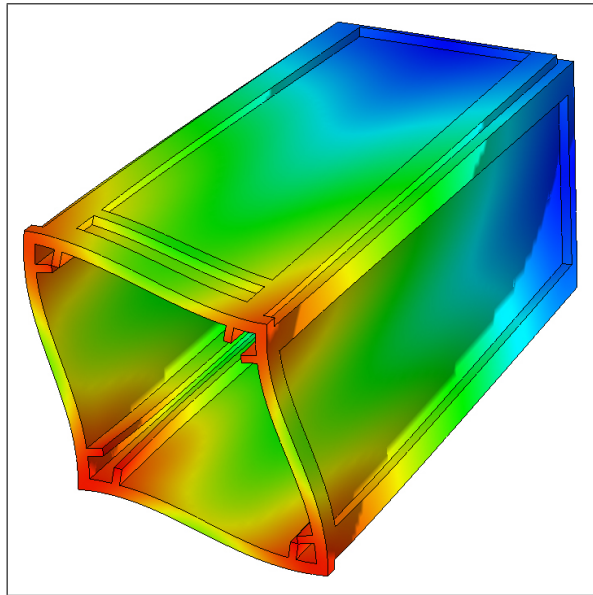


Figure 5.4: Fundamental shearing mode in an unrestrained case.

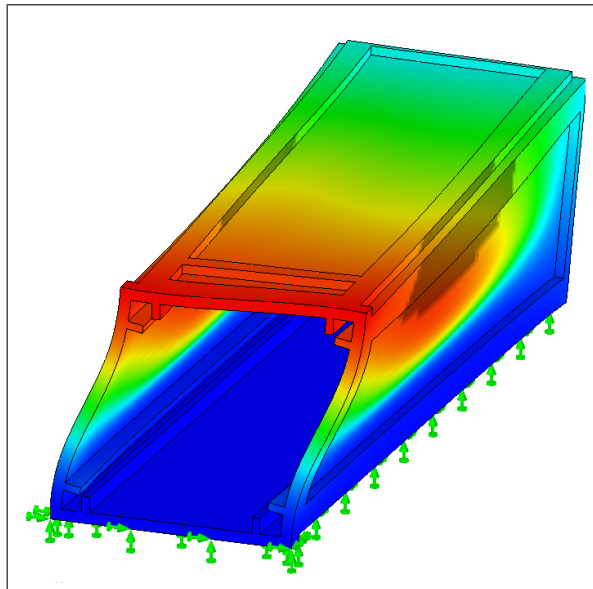


Figure 5.5: Fundamental shearing mode with bottom panel restrained.

n=2, m=1,2,... “Breathing” Mode

The second dominant mode shape is very similar to “breathing” modes experienced by thin containers and bottles [21]. In this mode, two opposing panels deflect outward while the other two opposing panels deflect inward. This mode shape exhibits two nodal diameters

n and one nodal circle m (or in this case nodal rectangle). Based on analysis, this mode shape can describe the P-POD's 2nd, 4th, 5th, 9th, 11th, 12th, 16th, 18th, and 21st modes, with m varying for various panel drumming mode harmonics.

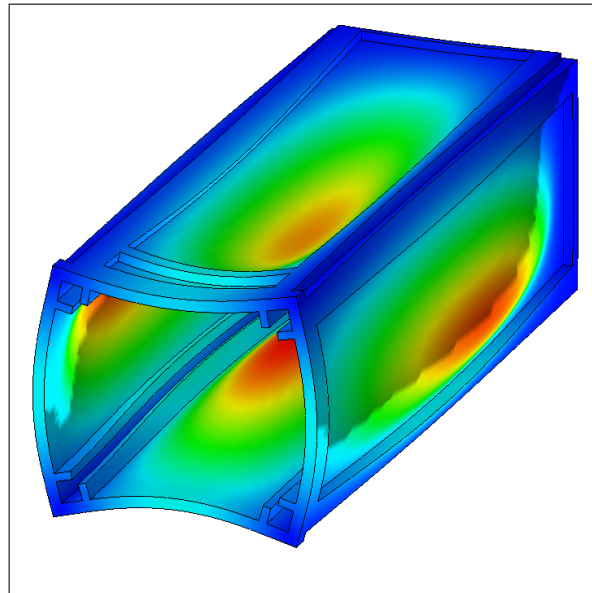


Figure 5.6: First breathing mode in an unrestrained case.

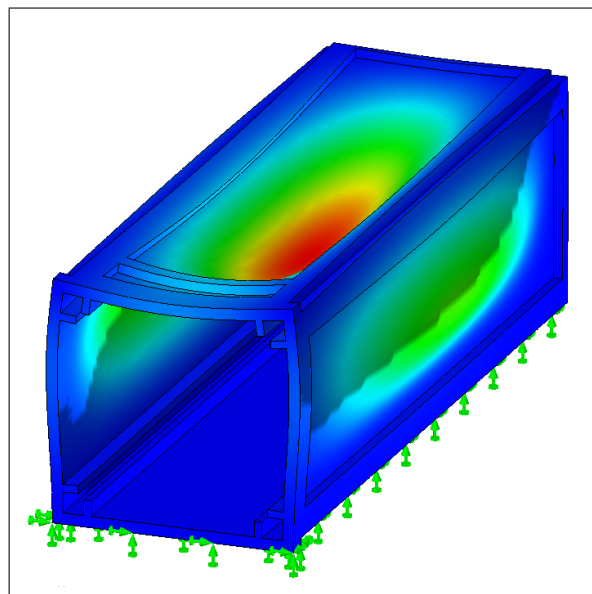


Figure 5.7: First breathing mode with bottom panel restrained.

The shape is very evident in analysis results for an unconstrained P-POD. After restraining the bottom panel of the P-POD, there is a drastic attenuation of shape. Still, this motion accurately describes the motion of the structural components of the P-POD.

n=4, m=3,4,... “Breathing” Mode

Similarly, the P-POD exhibits another breathing mode with four nodal diameters instead of two. In this mode shape, all four panels move inward and outward in unison. Again, the nodal rectangles are a function of drumming mode harmonics. This mode is not as prominent, only accounting for the 20th and 25th modes. An unrestrained P-POD analysis was not conducted for high enough frequencies to observe this mode’s natural shape. The mode shape is shown here for a restrained case with 3 nodal rectangles.

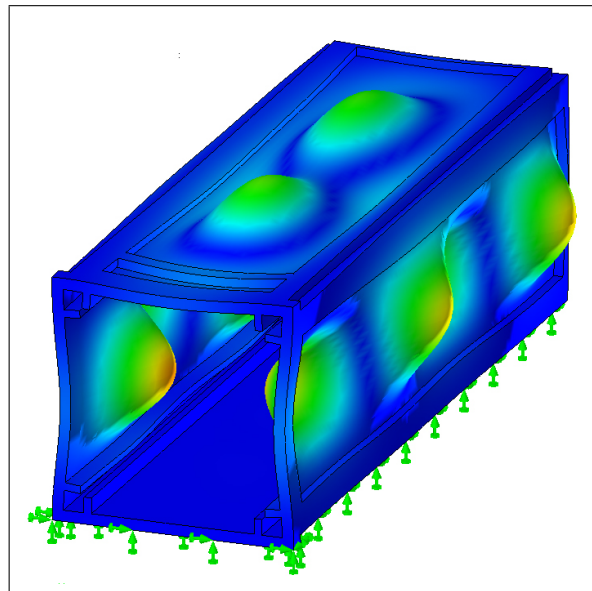


Figure 5.8: Second breathing mode with bottom panel restrained.

5.3.3 P-POD Door FEA Results

The redesigned P-POD door has five predicted natural frequencies below 2000 Hz, only two of which are fundamental modes. The first is a torsional mode around 613 Hz and

the second is a bending mode at 720 Hz. The bending mode is of great interest as the door will bow in and out at this frequency possibly allowing CubeSats to move in the Z direction.

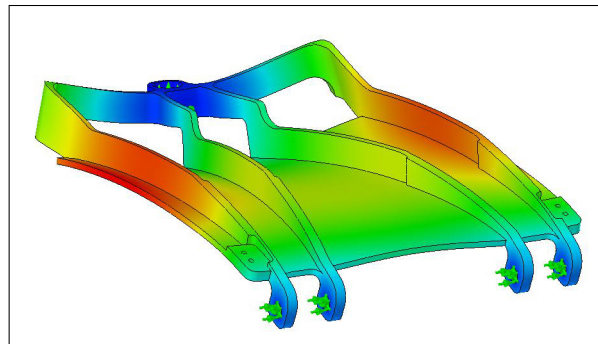


Figure 5.9: P-POD door fundamental bending mode.

5.3.4 Release Mechanism Subassembly Results

There are only two natural frequencies predicted for the release mechanism subassembly below 2000 Hz. Fortunately, neither mode is significant as maximum bending occurs in the mounting plate of the Qwknut in both cases. It is assumed that Starsys has conducted adequate analysis and testing to verify functionality under advertised conditions.

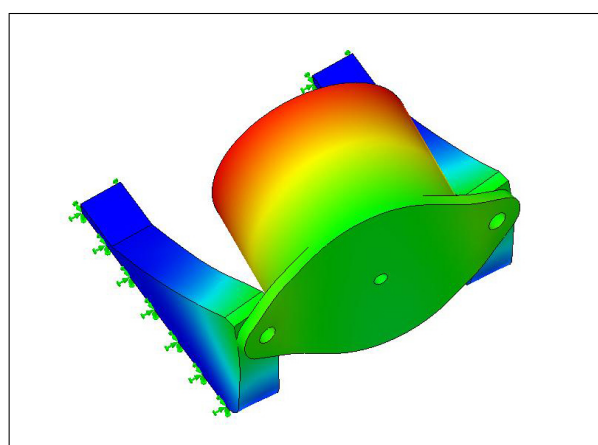


Figure 5.10: P-POD RMS second mode shape.

Nevertheless, this analysis was important in showing that the release mechanism subassembly is more or less decoupled from the rest of the P-POD. This alleviates concerns of the release mechanism subassembly being artificially excited by vibration in other components of the P-POD.

5.3.5 Comparison to Experimental Data

Data from a number of random vibration tests was collected and reduced in an attempt to identify the P-POD's natural frequencies experimentally. Frequency Response Functions (FRFs) were measured using accelerometers placed at various locations on the P-POD. The reduced data can be seen in Appendix F. The raw data was reduced by subjectively identifying peaks in the accelerometer PSD plots. These peaks were tagged and their frequency and amplitude were recorded. In addition, the level of the control channel at the same frequency was recorded so that a normalized amplification factor could be calculated for each data point. Test axis and measurement axis were also recorded to explore possible correlations between natural frequency and test or measurement direction.

Fundamental P-POD Structural Mode

The first observation is an obvious cluster of data points around 430 Hz. In fact, 8.2% of all data point fall between 400 - 420 Hz. Expanding the spectrum slightly shows that 15.3% of the data falls between 380 - 460 Hz. The data is highly heterogeneous among all three excitation and measurement directions, with a slightly higher concentration of data measured in the Z axis. Comparison to FEA results shows a very close correlation between this data and the theoretically predicted fundamental P-POD frame frequency of 430.96 Hz. Therefore, it is logical to conclude that there is a definite natural frequency in this range.

Lateral P-POD Structural Mode

Two more clusters of data occur around 600 Hz and 730 Hz. About 6% and 7% of the total data are collected around these two frequencies respectively, with most of the data being measured in the X and Y directions. Therefore, it can be said that the P-POD's first lateral natural frequencies fall within this range.

CubeSat Rattling Mode

About 8% of the test data is clustered between 140 - 200 Hz. Almost all the data is measured in the X and Y directions and zero data points in this range are excited by vibration in the Z direction. In addition, the data is amazingly consistent among tests and CubeSat payloads, however it does not show up in any of the analytical predictions. One final piece of information holds the key to this puzzle: most of the data in this range was measured by accelerometers attached to CubeSats inside the P-POD. Since none of the CubeSats or CubeSat mass models placed inside the P-POD have such low natural frequencies, it is possible that the data at this frequency range correlates to the movement of CubeSats inside the P-POD. This motion is thought to be the rattling of the CubeSats in the lateral directions caused by the gap between the outside of the CubeSat rails and inside of the P-POD rails [20]. Fortunately, this mode is not very prominent when instrumenting the outside of the P-POD.

CubeSat Axial Mode

Another cluster of data points is centered around 280 - 320 Hz. Again, analytical methods do not predict this mode, yet 11% of the data falls within this region. Upon closer inspection, it becomes clear that most of the data points in this range were measured in the Z direction, especially on the door. Although neither the door or back panel exhibit

natural frequencies in this range, it seems that this mode is caused by inertial differences between the CubeSats and the P-POD structure. This natural frequency is most likely caused by the mass of the CubeSats reacting with the door and back panel flexing — like leaf springs — along with the main spring, kick springs, and separation springs inside the P-POD.

Much of this data comes from instrumented CubeSats, however, unlike the CubeSat rattling mode, vibration at this frequency is easily recorded on the outside of the P-POD (at least on the door).

Higher Frequencies

A number of natural frequencies appear around 950 Hz, 1100 Hz, 1250 Hz, 1500 Hz, 1750 Hz, and 1950 Hz. Most of these are predicted rather accurately from the finite element models. These modes are mostly small displacement drumming modes and should have negligible impact on the P-POD's structural soundness. In addition, these natural frequencies are well outside the range that most launch providers care about.

As a side note, it should be mentioned that the Cal Poly Mechanical Engineering vibration table has a natural frequency of about 1000 Hz [20, 15, 4]. For tests run at Cal Poly, the abundance of data and large amplifications in this range should be closely examined.

5.4 Thermal and Vacuum Testing

Industry convention groups thermal tests into four categories: thermal cycling, thermal vacuum, thermal balance, and burn-in [10]. Another important factor to consider is the tendency for materials to outgas. A thermal “bakeout” procedure is used to release volatile substances — naturally found in most materials — prior to integration of hardware onto

the launch vehicle [19]. Thermal testing on the P-POD was straightforward for a number of reasons.

- No electronic components
- Compliance with NASA outgassing requirements [22]
- Small amounts of plastics, epoxies, etc.
- P-PODs only have to survive launch, not orbit

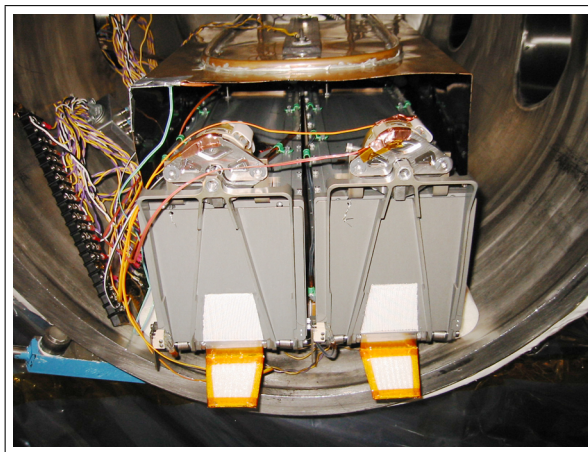


Figure 5.11: P-PODs being prepared for thermal vacuum testing.

The main objectives were to ensure functionality of the mechanism in vacuum and in cold temperatures and measure outgassing properties of P-POD materials. Kosmotras only required a bakeout of hardware to qualify the P-PODs for flight. A single test profile combining a number of thermal testing elements was generated to meet Dnepr outgassing requirements while cycling through temperatures. This procedure was performed under “hi-vac” pressures of around 5×10^{-5} torr.

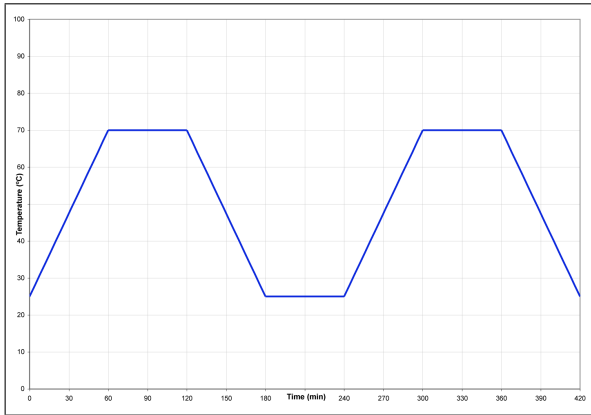


Figure 5.12: Thermal vacuum bakeout profile.

5.5 Functional

Functional testing was performed concurrently with environmental testing to verify the P-POD's operability after being subjected to harsh environments. Additional functional tests were performed to understand the operational characteristics of the P-POD mechanisms and to improve confidence in the system and its reliability.

5.5.1 Geometry

A tremendous benefit to building a prototype P-POD Mk. II was being able to experiment with it. The ability to have hardware in hand is often overlooked but very beneficial. Significant time was spent understanding how the components fit together, and how the mechanisms operated. The geometry and tolerances between the door, release bolt, and Qwknut were analyzed to understand how all the components moved during deployment.

5.5.2 Deployment

The most obvious purpose for these tests was to verify successful and reliable operation of the P-POD in a variety of environments. Over 40 deployment tests have been performed on the P-POD engineering unit; many following an environmental test.

One interesting deployment test was a misalignment test. In this test, force was artificially applied to the release bolt head to simulate stresses caused by misalignment between the release bolt and release mechanism. Deployment was performed while pushing on the bolt head in the $-X$ direction with a force meter. Tests were performed successively with 0, 45, 90, 130, and 180 Newtons applied.

A deployment test was performed in vacuum to verify P-POD functionality under thermal vacuum environments. The test began with a 3 axis NASA GEVS vibration qualification test at 1 minute per axis (see Section 5.2.2). The P-POD was inspected and immediately transported to the thermal vacuum chamber. Next, the chamber was ramped up to 70°C where the P-POD soaked for 30 minutes. Temperature was then ramping back down to -10°C , followed by another 30 minute soak. A deployment test was performed at the cold soak temperature via electrical pass throughs and an external power supply. The P-POD deployed successfully and a post-test inspection showed no signs of damage. No deployments were conducted at high temperature as this condition is favorable for operation of the release mechanism.

In addition to the tests discussed above, deployment tests were performed on the P-POD engineering and flight units prior to and following any form of environmental testing. Many more — less documented — deployment tests were conducted to check various aspects of performance and functionality during the early stages of development.

5.6 Problems with the Qwknut

Of course, tests don't always go as planned. One major problem emerged during the first ever vibration test of the redesigned P-POD — a NASA GEVS test (see Section 5.2.2).

After performing the test, the P-POD engineering unit was brought back to the MSTL

for inspection and deployment. The inspection showed no signs of damage, however the P-POD failed to deploy. This situation was quite disconcerting, as the first test ever of the P-POD Mk. II had resulted in failure. To make matters worse, one of the Qwknut circuits was permanently damaged as a result of attempting to troubleshoot the problem. Analysis after the fact identified a number of potential design problems with the P-POD and revealed inadequacies in both Cal Poly's understanding of the Qwknut mechanism and with Qwknut documentation provided by Starsys. The investigation, redesign, and subsequent retesting of the P-POD are explored in the Section 6.

Chapter 6

Post Failure Design Iteration

The failure immediately mobilized efforts to find and correct any flaws in the P-POD design. As any failure involving a Qwknut reflects poorly on Starsys, they provided full support in diagnosing and correcting any problems. A thorough analysis of the failure was performed by a collaborative team with the following objectives in mind.

1. Determine what went wrong during the test.
2. Determine why the failure occurred.
3. Use knowledge gained to identify other potential problems.
4. Investigate solutions to the identified problems.

6.1 Detailed Analysis of the Problem

6.1.1 How Curiosity Killed the Qwknut

After a successful post-test inspection, the Qwknut circuit was actuated per standard Cal Poly deployment procedures. Health of the Qwknut circuits was checked, and an actuation signal was sent, but the Qwknut only made a clicking sound and did not deploy

the bolt. Following the unsuccessful deployment attempt, the circuits were checked again and appeared to be in good health.

After discussing the situation amongst the team, a second deployment test was performed. Since the power supply is operated by hand, it was thought that the failure could be due to toggling the power too quickly. It was later verified that it is not possible to generate too short of a pulse — under 100 milliseconds — by hand with the equipment used. Power was left on for about one second, but the Qwknut reacted exactly as it did during the previous test.

A third deployment attempt was made with a larger power supply. The power supply used in the first two tests only sources about one fifth the power specified in the Qwknut User's Manual. This supply is preferred because it is of higher quality and can be controlled more precisely. A bigger power supply was available, but the controls are rough at best. A deployment test was performed using the bigger power supply and the same procedures as before. The results were the same.

At this point, testing should have stopped and Starsys should have been consulted. Frustrated, the team decided to try one last test. For this test, the power supply was turned on and left on. This procedure is not recommended, however it was used because of a safety feature in the Qwknut test circuits. In theory, the mechanism would not accept more power than needed for deployment. The Qwknut did not deploy however. Instead, a bright orange flash, followed by a plume of smoke emanated from the back of the Qwknut. The bright flash and smoke were actually signs of the SMA wire burning up inside the Qwknut. By applying too much power, the SMA wire became too hot, and failed thermally.

As a side note, though it is standard practice to alternate actuation between primary and redundant circuits to evenly wear down the mechanism, every deployment attempt

during this test was made using the primary circuit. With another day of testing planned, it was desirable to leave one of the Qwknut circuits in good condition.

6.1.2 Test versus Flight Circuits

Damage to the SMA wire was rooted in the electrical circuitry of the Qwknut. Each Qwknut has two redundant circuits; the interface to each of these circuits is comprised of a signal line and a signal return line. In addition to these “flight” circuits, the Qwknut also provides one extra wire per circuit for testing purposes. The “test” circuits add a mechanical limit switch in series with the SMA wire. The limit switches automatically cut power to the SMA wire after activation. During a launch, the vehicle bus provides a pulsed deployment signal to the mechanism and the test circuit is unnecessary. The test circuits are extremely useful for testing, however, as they eliminate the need for a controlled pulse.

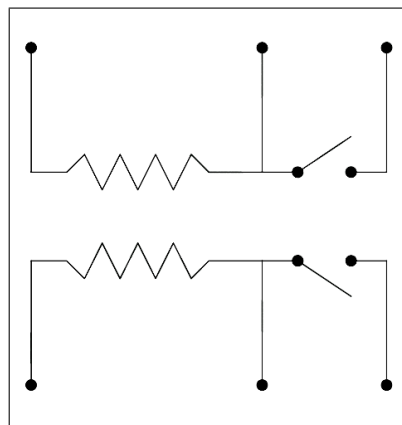


Figure 6.1: Schematic of Qwknut circuits.

This feature has a serious drawback: the physical mechanism must successfully deploy in order for the switches to do their job. If the mechanism is bound up, it is possible to damage the SMA wire by sending too much energy to the circuit. This is in fact what happened during the last deployment test. Since the signal was not pulsed, power was applied for too long a period of time.

As it turns out, this failure was a result of lack of information. The functionality of the test circuits was not properly documented in the Qwknut User's Guide. In hindsight, the functionality and limitations of the test circuits are obvious. However, without a good understanding of the system, it was very easy to make incorrect assumptions about its capabilities.

6.1.3 Shear Stress

After the Cal Poly team had a chance to inspect and document the failure, the entire P-POD was shipped to Starsys for inspection and refurbishment of the Qwknut. With the hardware at their facility, Starsys engineers were able to look at the P-POD as a system to pinpoint the failure and work with Cal Poly to ensure that the P-POD was compatible with the Qwknut.

After weeks of investigation and discussion, the main cause of the problem was found to be improper accommodation for shear loads in the mechanism. The Qwknut (and most separation nuts in general) are designed to handle axial loads very well, but are not meant to sustain any shear loads whatsoever. It is believed that since the door was not restrained in the X axis, the bolt was allowed to displace slightly during vibration.



Figure 6.2: Two side views of the Qwknut and release bolt.

This misalignment created a binding condition between the bolt and the inside of the mechanism. When the actuation signal was sent, the bolt was physically restrained and could not release. As a result, the limit switches were never actuated and the circuit was

not disconnected.

6.1.4 Low Grade Fasteners

Starsys also showed concern about the release bolt being used. Although the bolt was installed per their specifications, Starsys suggested the use of a higher grade National Aerospace Standard (NAS-1351) bolt instead of the Military Specification (MIL-16996) that had been chosen. The change had no impact on the rest of the system, and was implemented. Although cost was not an issue in this case (there is only one bolt per P-POD), it is easy to see the cost impact that fasteners can have on large systems.

Table 6.1: Common fastener grades and prices (McMaster Carr, 2007).

Regular Bolt	\$ 0.13 ea.
MIL Spec Bolt	\$ 0.44 ea.
NAS Spec Bolt	\$ 2.01 ea.

6.1.5 Qwknut Misalignment

Starsys also had some concern about the fasteners used to attach the Qwknut to the mounting brackets. The brackets were originally designed to use 8-36 fasteners, however the Qwknuts were designed for use with 10-32 fasteners. The larger diameter holes in the Qwknut paired with the undersized mounting screws created a rather loose tolerance that could lead to misalignment of the mechanism.

In addition, there was a good amount of slop between the brackets and top panel, which could also contribute to this misalignment. Some slop was purposefully added to the bolt hole in the door to compensate for possible tolerance issues with the brackets, top panel, Qwknut, and door, however it was agreed upon that the design did not adequately address tolerance issues.

6.2 Rework of Parts

The problems described above offered some interesting challenges. Since the P-POD components had already been manufactured, it was important to keep any modifications to a minimum. Due to the large quantity of the order, the preferred approach was to modify pre-existing parts rather than remanufacture new parts.

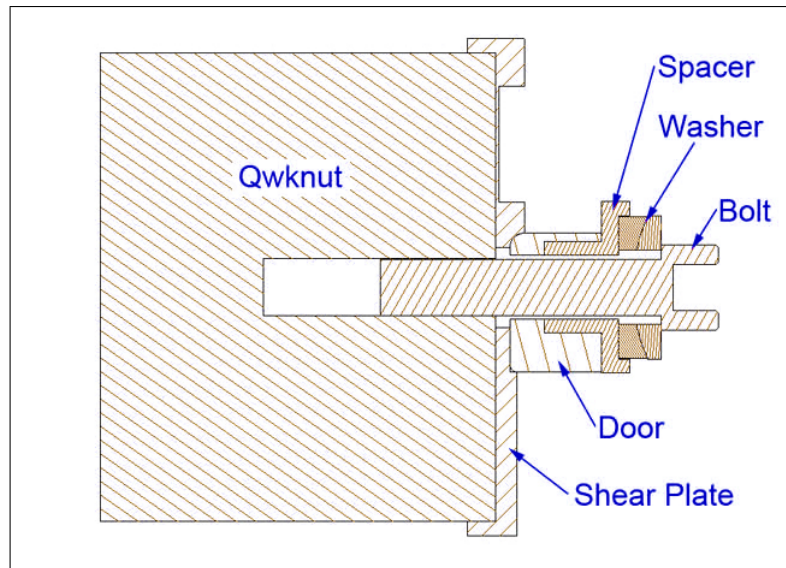


Figure 6.3: Cross section of the reworked release mechanism assembly.

6.2.1 Shear Plate

It was clear that the P-POD needed a mechanism to counteract shear forces between the door and the Qwknut, and relieve the mechanism of such forces. The chosen solution was to add a thin plate between the Qwknut and door. This “shear plate” would incorporate certain features to absorb the shear forces in the X and Y axes. A common way of dealing with shear forces in a mechanism is to incorporate a cup/cone system somewhere in the design. A number of cup/cone implementations were considered, each with its benefits and drawbacks. The shear plate was designed to mate up with the ribs of the door. This design maximized contact area and made use of pre-existing features.

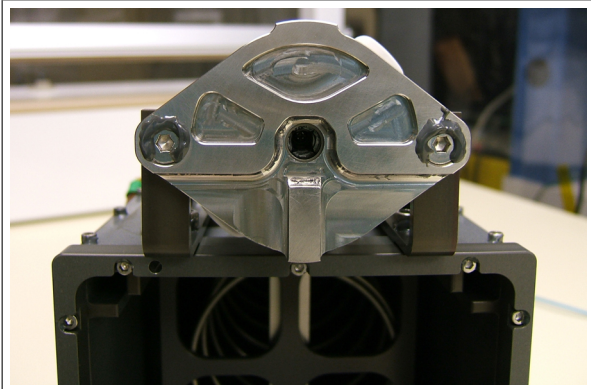


Figure 6.4: P-POD Mk. II shear plate.

Due to the complicated features, a lot of time was spent making sure that the door would match up exactly with the shear plate. All contact surfaces were rounded to eliminate any potential for binding. The requirement for the door to be modified meant that there would be bare aluminum surfaces in contact with the shear plate. To prevent cold welding, the shear plate was made of A304 grade stainless steel. Although stainless steel is heavier than other considered materials like titanium, it is less expensive and is also cheaper to machine. The shear plate added a total of 45 grams to the system. Thermal expansion differences between steel and aluminum were deemed negligible based on P-POD thermal requirements.

In retrospect, this method was probably the least ideal way of counteracting shear. The mating features were complicated and required extreme precision, increasing the probability of failure. In addition, most shear relief features in aerospace systems prefer a cone shape rather than a rounded shape as these are easier to manufacture with the high levels of precision required. Although there were concerns with removing a lot of material from the door, a coaxial implementation probably would have been the most effective method.

6.2.2 Bracket Locator Pins

The mounting brackets were shifted back slightly to accommodate additional thickness of the shear plate. This was accomplished by slotting the mounting holes in the brackets. In addition, locator pins were incorporated to precisely align the brackets against the top panel. The stainless steel pins were friction fit into the top panel and slip fit to the brackets.

6.2.3 Mounting Screw Sizing

The brackets were also modified to incorporate size 10 fasteners to mount the Qwknut. This was accomplished with the somewhat questionable procedure of re-tapping the existing holes in the front of the brackets. This was possible due to the larger diameter of the new holes, however did result in approximately 15% loss in thread diameter. The re-tapped holes have been thoroughly tested with no signs of damage or fatigue. Finally, flat screws and countersunk holes in the shear plate assisted in aligning the subassembly during installation.

6.2.4 Spherical Washers

As a final precaution, spherical washers were used in the joint to prevent shear caused by bolt misalignment. Spherical washers are two mating washers stacked on top of one another. The bottom washer is concave in shape while the top washer is a corresponding convex shape. This geometry allows the bolt to sit at a slight angle in slightly misaligned joints. These additional degrees of freedom prevent the bolt from being overconstrained and counteract binding effects caused by misalignment.



Figure 6.5: Picture of release bolt and spherical washer set.

6.3 Requalification

After the modifications were made, a new prototype P-POD was built using modified parts and the refurbished Qwknut. As would be expected, the modified P-POD was subjected to an exhaustive testing regime to validate the design. Fortunately, the redesigned P-POD did not experience any subsequent failures.

6.3.1 NASA X Axis Qualification

During the failure investigation, it was determined that vibration in the X axis most likely caused the failure. The first test in the requalification process was to see if the modified P-POD would survive a shake in the X axis. There was no reason to subject the system to additional vibration if it was not even going to survive this test. The area surrounding the Qwknut was thoroughly instrumented to document the environment in the subassembly.

A 10 minute random vibration test was performed to NASA GEVS qualification levels. The P-POD successfully deployed after the vibration test.

6.3.2 Full NASA Qualification

The next step was to perform the same test in all three axes. Another NASA GEVS random vibration test was conducted — as described in Section 5.2 — at 10 minutes per axis. Once again, the P-POD successfully deployed after the test.

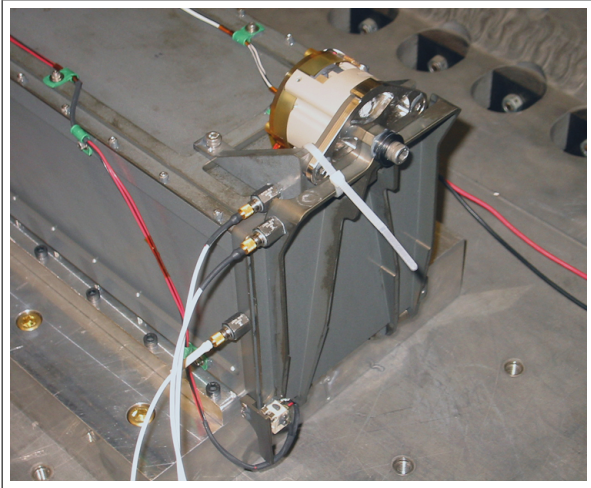


Figure 6.6: Strategically placed accelerometers during a vibration test.

6.3.3 Vibration and Thermal Vacuum

After proving that the P-POD could survive the vibration environment, we decided to conduct a more thorough test of the system. A third test was performed consisting of vibration and thermal-vacuum portions. The P-POD was subjected to a 3 axis NASA GEVS random vibration qualification for 1 minute per axis (the minimum requirement per NASA GEVS).

The P-POD was inspected after the vibration test and immediately transported to the thermal vacuum chamber. The P-POD was subjected to thermal cycling and was successfully deployed at -10° C. This test is more fully described in Section 5.5.2.

6.3.4 Dnepr Vibration Qualification

To finish requalification, a random vibration test was performed to Dnepr Qualification levels. This test was more of a formality, as the NASA GEVS levels are much higher than the Dnepr levels. However, the test was performed to certify testing of the P-PODs to Kosmotras' specifications. Needless to say, the P-POD was unscathed and deployed successfully after the shake.

Chapter 7

The “Dnepr Launch 1” Mission

Although this paper deals mostly with the development and validation of the P-POD Mk. II, one tremendous benefit to the CubeSat Program is being able to see one’s work go beyond just development. The constant attention towards designing for compatibility makes it easy to forget that this entire effort was based around a specific launch opportunity.

Coordinating the launch opportunity presented many challenges — technical and non-technical. Some of the non-technical challenges include interacting with a Russian launch provider, coordinating eleven universities, dealing with launch delays, compliance with ITAR regulations, and paperwork of various types. Simon Lee’s thesis [17] on the administrative aspects of the Dnepr launch should be used as a complement to the technical issues discussed in this paper.

As for technical challenges: there were plenty to deal with even after the development phase of the P-POD was complete. Ensuring uniformity in manufacturing, assembly, and testing was key to a standardized launch process. In addition, interface issues both between the P-POD and launch vehicle, as well as between the CubeSats and P-POD seemed never-ending. This section outlines the processes and techniques employed by the Cal Poly team to achieve these goals.

7.1 Assembly and Qualification

Development and practice of good procedures was a key element in the preparation of the six P-PODs needed for the mission (five flight units and one spare unit). A detailed assembly and testing plan had been developed during the prototype testing phase of development.

Standardized procedures simplified the process and helped bring new technicians up to speed quickly. P-PODs were assembled simultaneously in a period of about one week. The hardware was assembled with no long gaps in schedule to assure consistency in the assembly process.

Similarly, testing was conducted within a matter of days of one another. Each P-POD underwent an environmental qualification process involving a random vibration test and thermal bakeout procedure. Vibration testing was conducted at the Raytheon vibration testing facility in Goleta, CA. A vibration fixture was used to test two P-PODs simultaneously. This approach reduced testing time as each session took an entire day. The test profile was 150% of the Dnepr levels for liftoff and flight for 100% of the duration, as shown in Figure 5.2.

Special mass models were made to simulate CubeSat mass while protecting the P-POD inner rails from unnecessary wear and tear. These mass models were made of solid blocks of Delrin and were sized to match the dimensions of triple CubeSats. No analysis was done to verify similarity between the mass models and actual CubeSats, since structural properties vary widely between CubeSats.

The thermal bakeout procedure was conducted at the Cal Poly CubeSat thermal vacuum facility. Again, two P-PODs were baked out simultaneously. The test profile was identical to that shown in Figure 5.12. Thermal bakeout was performed with the P-PODs



Figure 7.1: CubeSat triple mass model used for P-POD qualification.

empty to save time and avoid outgassing from the triple mass model.

Inspection of various P-POD components as well as functional tests were performed throughout the assembly and qualification process to ensure functionality of the P-POD flight units. Often times, identical tests were performed before and after every environmental test so that problem causes could be pinpointed in the event of a test failure. All six P-PODs passed the qualification process with no anomalies to report. At the end of the process, careful inspection and documentation was performed for each P-POD to record each unit's history and minor differences between units.

7.2 P-POD / Launch Vehicle Fit Check

A fit check was conducted between Kosmotras and all the launch customers. The fit check took place in February 2005 at the Yuzhnoe State Design Office (YSDO) in the Ukraine. The objectives of the fit check were threefold:

1. Ensure compatibility between P-POD and LVI mechanical interfaces.
2. Test compatibility of P-POD electrical systems with the LV computer.
3. Perform a vibration and shock test of the SHM with payload mass simulators.



Figure 7.2: Mass simulator for the P-POD Mk. II.

During the fit check, four P-POD mass models and one P-POD engineering unit were integrated with the LVI adapter that Kosmotras had manufactured. In addition, two sets of electrical simulators and an actual Qwknut were provided to Kosmotras for testing of electrical systems. Finally, Kosmotras conducted a number of environmental tests to ensure that the SHM and all the payloads would survive launch.

7.3 CubeSat / P-POD Fit Check

A fit check between Cal Poly and the CubeSat developers took place in the MSTL during the 1st Annual CubeSat Developers' Workshop in April 2004. The main objective was to check on the status of all the satellites and check for any mechanical interface problems between the CubeSats and the P-POD. The fit check served as a good chance for developers in the same P-POD to meet, learn about each others CubeSats, and voice any concerns with their neighbors designs. The main highlight of the fit check was a mock integration between the P-POD prototype unit and dimensional models of the CubeSats themselves. These models ranged from basic CubeSat structures to fully integrated engineering units. The only requirement was an accurate representation of the outer dimensions of the CubeSat.

The fit check was a big success, and developers left with a sense of direction and clear

objectives. A number of interference issues were found during the fit check, which resulted in increased contact between those developers and Cal Poly to ensure that the problems were addressed.

7.4 Integration

All 14 CubeSats were integrated into their five respective P-PODs in April of 2005. Integration had been planned and scheduled over and over again as Cal Poly personnel tried to balance the readiness of developers with the delays in launch schedule. In fact, this game of Russian roulette was played for almost one year between the original integration and when the P-PODs were sealed up and ready for flight. Far from ideal, this situation was a byproduct of trying to keep things as stagnant as possible while still responsibly addressing CubeSat safety and launch readiness issues.



Figure 7.3: P-PODs being integrated with CubeSats at Cal Poly.

The approach taken by the Cal Poly team was rather democratic, and everyone in the respective P-PODs had a say in how that P-POD was handled between integration and launch. Although Cal Poly maintained final authority on decisions (to ensure P-POD safety), the Cal Poly team tried to reach a consensus amongst developers whenever possible. Integration of the P-PODs was finally completed for the last time in May 2005.

7.5 Acceptance

Part of the challenge with integration was the requirement of acceptance testing flight hardware. In addition to qualification tests, every piece of hardware (CubeSats and P-PODs) were acceptance tested to ensure workmanship and provide a final screening before delivery. Acceptance testing was the first time that the actual flight P-PODs and flight CubeSats would be tested together. The test was designed to identify any potential problems resulting from interaction between the specific CubeSats and P-PODs.



Figure 7.4: P-POD bagged for cleanliness, ready for testing.

Kosmotras only required a random vibration test of the integrated flight P-PODs to qualify them for flight. Testing was conducted using the same Dnepr profiles, but at 100% of the levels for 100% of the duration. The P-PODs were inspected before and after the acceptance test to ensure health and functionality. Also, CubeSat developers were allowed to run diagnostics on their CubeSats before and after the test. A visual inspection of the CubeSats was performed through the diagnostic ports to screen for obvious test failures. This method, although rudimentary, actually caught a number of potentially hazardous failures.

The baseline integration plan required P-PODs to stay closed after acceptance testing. The idea was to verify that integration had been performed correctly and the release

mechanism was properly set. As it turns out, every single P-POD had to be opened for one reason or another. This was disconcerting and the Cal Poly team was extremely reluctant to de-integrate P-PODs. The matter was always scrutinized, but ultimately resulted in de-integration in every case.

In fact, the only P-POD that followed the original plan was the spare P-POD. Early on, it had been decided that the spare P-POD would undergo exactly the same procedures as the other flight units, whether it be testing, transportation, or handling. The plan was to deploy and inspect the spare P-POD at the launch integration facility to verify functionality after shipping and storage, and allow inspection of a P-POD having undergone the aforementioned conditions.

7.6 Launch Swapping

Due to chronic launch delays, the integrated P-PODs ended up sitting on the shelf for nearly a year before a launch date finally materialized. With a launch approaching, the lab was motivated and excited. There was only one problem: the upcoming launch was the second of two launched being coordinated between Cal Poly and Kosmotras. The Cal Poly team was placed in the awkward position of having 14 completed CubeSats sitting on the shelf, and seven other CubeSats — in three P-PODs — rushing to finish their satellites in time for a launch. After thorough discussions with Kosmotras and participating developers, a very difficult decision was made to try and swap P-PODs between launches. Logistical planning and filing of paperwork was all that was required. It is important to note that no changes to any of the hardware were necessary. And so, only months before launch, the entire CubeSat manifest was altered.

Two important factors made this switch possible. First, most CubeSat developers

were much more interested in launch date than being placed in a specific orbit. Also, the second launch had been planned to accommodate more P-PODs than were being flown. Therefore, the adapters and interfaces for additional P-PODs were already in place. These factors were of course in addition to standardization and flexibility built into the P-POD design.

7.7 Launch Campaign

In July 2006 — exactly three years after contacting Kosmotras — three Cal Poly students and the Cal Poly Empowered Official began the long and arduous journey to an unfamiliar part of the world. The hardware and equipment were to follow a different path, and had already made the voyage to the launch site in the small, mysterious town of Baikonur, Kazakhstan. A small data logger included in the package would be the only indication of the precious cargo's shipping accommodations.



Figure 7.5: P-PODs awaiting integration at Baikonur Cosmodrome.

The itinerary took the Cal Poly team to Moscow then Baikonur, where other satellite teams were already making preparations. Between the display of Soviet rockets peppered throughout the city, the armed soldiers on base, and an integration facility reminiscent of a James Bond movie set, it was easy to lose sight of reality in this place.

After the euphoria wore off, the Cal Poly team began thorough inspection and documentation of the P-PODs. When everything had been checked, double-checked, and rechecked, custody of the P-PODs was finally placed in the hands of ISC Kosmotras. One could only watch as the Russian technicians installed each P-POD in the Dnepr upper stage one after another. Just as 14 CubeSats had joined with five P-PODs only months before, the five P-PODs had now been fused into something greater than themselves. Suddenly, the sleepless nights, the personal sacrifice, the endless arguments were all gone, overshadowed by a blindingly clear sense of purpose. Not a cleanroom in the world could keep the students' fingerprints off these satellites.



Figure 7.6: Installation of P-PODs onto the SHM.

Darkness finally set in as the spacecraft were encapsulated in the rocket fairing. The anxiety was felt by CubeSat developers worldwide, as everyone waited for the moment when these satellites would rise above the horizon, declaring their existence with only a series of faint, electro-magnetic cries.

The following days were busy ones for Kosmotras as they integrated the rocket and SHM, and made final preparations for launch. Those “days of rest” for the integration team were surprisingly short, and before anyone could blink, another trip to the airport revealed a handful of students and faculty from various participating universities fortunate

enough to make the trip out. These were not customers, but friends, and those who were unacquainted did not stay that way for long.

Finally the launch date had arrived. After an entire day of mental preparation, the mood was still one of utter disbelief as the bus pulled in to the modest bunker that was the observation post. The scene was completely dark, save for a two dimly lit towers off in the distance. It was only a matter of time now.



Figure 7.7: Silo launch of the Dnepr launch vehicle.

As the countdown began, updates were streamed back to Cal Poly and a number of other universities via video over the web and with satellite phone. Before anyone knew it, a bright flash on the horizon, a thundering roar, and it was off. The crowd watched the trail of fire as the rocket flew overhead. As the first stage motors shut down, everyone waited in deafening silence for the second stage motor to ignite. And then, there it was, nothing but silence. “No update,” the launch director kept repeating. After several minutes, the gut wrenching anxiety had turned into an overwhelming sense of denial, but nothing more. But wait, there was another flash! This time not in the sky, but against the opposing horizon, and finally, confirmation that the Dnepr rocket had in fact crashed into the desert sand. The sorrow was almost competitive at that point, and the bus ride back never ending.

Months after the crash, the problem was finally traced back to a 1/4 second malfunction



Figure 7.8: Dnepr vehicle crash site.

in one of the first stage hydraulic motors (see Appendix G), causing the rocket to veer off course and the flight computer to terminate flight. After all that hard work and emotion, the fate of these satellites had been determined by a few bytes of code running on a computer; the decision was mechanical, automated, indifferent.

The aftermath left many questions as to the effects of this launch on the future of the CubeSat Program. In many peoples' minds, this launch was the quintessential university mission. Each one of the 18 satellites on the launch had student involvement. In a funny display of perseverance, the integration team, upon their return, was greeted with a lab too busy to think about the failed launch. Some schools were effected more than others, but the community — if anything — was only stronger because of it. The new generation of students was too motivated and energetic to be affected, and those who had grown wiser with experience were slowly making their way into industry.

Chapter 8

Conclusion

Although the five P-PODs and their CubeSat payloads never made it into orbit, many basic objectives of the mission were completed. The P-POD design was iterated and a number of critical improvements were made. Most fundamentally, the P-POD Mk. II was shown to be compatible with the Dnepr launch vehicle systems. In addition, based on initial conversations with launch providers, the P-POD Mk. II design has demonstrated versatility in meeting the requirements of a wide variety of launch vehicles. Numerous second generation P-PODs have been thoroughly tested and the design has been qualified for the harshest of launch environments. Additionally, the P-POD played an integral part in creating a launch opportunity for the 14 CubeSats, served as a viable means of transporting satellites to the launch site, and a practical way of adding small payloads to space missions. The enclosed design of the P-POD made it easier to obtain export approval, and the standardized design allowed payloads to be swapped at a moment's notice.

Finally, the P-POD has served as a great educational enabler, not only for the students working on the P-POD and coordination of this launch, but for all the students involved in the various participating CubeSat projects. Through the CubeSat Program and the

P-POD, students were able to participate in the entire life cycle of a space mission, and will enter industry with real world experience under their belts.

8.1 Future Recommendations

In an effort to meet objectives of reliability, simplicity, and others cited at the beginning of this paper, a number of compromises were made. In addition, a lot of knowledge was gained by going through the development process. The following is a list of possible improvements to the P-POD: either additional features that are a logical step in the evolution of the P-POD design, or problem areas discovered as a result of the development process that should be addressed.

8.1.1 Design

Mounting Screw Sizing

The mounting screws may be oversized for some applications, resulting in thread damage to the P-POD panel instead of bolt failure. Fastener diameter should be reevaluated and probably reduced. This topic is covered in depth in Appendix C.

Spring Plungers

The spring plungers used in the back panel are soft and fragile. The actual problem is the tiny drive size chosen by the manufacturer. The allen socket in the spring plunger is extremely easy to damage. Larger spring plungers or a different style may help.

Locking Heli-Colils

The locking Heli-Coils in the back panel require significant practice to service reliably. While unexperienced students will not likely be working with flight hardware, this design is

prone to inconsistency and requires more finesse than following of procedures. Checknuts, locknuts, adhesives, lubricants, and Heli-Coil made of other materials should be considered.

Better Telemetry Sensors

The telemetry system on the P-POD Mk. II is simple and effective, and was a good first pass at including this functionality. However, the current system adds width and height to the P-POD, and switch levers are easily damaged by accidental mishandling. As discussed in Section 4.12, an ideal system would provide feedback on actual CubeSat deployment, not just door opening.

Better View Ports

The view ports — as implemented — are completely worthless. Either larger or more strategically placed view ports should be used. The functionality is very useful, but the implementation is poor.

Release Mechanism Mounting

A number of modifications were made to the release mechanism mounting brackets (see Section 6). The design should be iterated with these improvements designed into the bracket instead of added on.

Shear Relief

The shear relief mechanism in the release mechanism bracket and door should be redesigned. The current method is complicated and prone to tolerance problems. A simpler, more elegant approach should be taken.

Spring Length

Due to non-linear stiffness characteristics of helical springs at the beginning and end of their stroke, it is actually standard practice to use only the middle 80% of a compression spring's travel [16]. This improvement will make the linear spring models in the current simulation — $F = -kx$ — more accurate.

Pusher Plate Stop

The previous improvement will require a lengthening of the main spring. This will force the pusher plate to hang out of the P-POD frame in its free state. By incorporating a stop somewhere in the new design, the pusher plate will stay inside the P-POD frame.

Release Mechanism Reevaluation

At the time of this writing, Qwknut pricing has increased approximately threefold. The updated pricing structure cannot be supported with current budgets. It is suggested that a replacement mechanism — or mechanisms — be selected to replace the Qwknut, at least for the short term.

Bigger Access Ports

The current access ports in the bottom panel are rather small and arbitrarily defined. CubeSat developers would undoubtedly benefit from larger access ports, and possibly ports on multiple panels. The additional access ports would also be of great benefit when inspecting the CubeSats for failures after testing.

Collar Dimensions

The current P-POD collar is slightly wider than the rest of the P-POD frame. This was left unchanged between the P-POD Mk. I and Mk. II, however it would be nice to have the collar flush with the rest of the panels for ease of mounting.

8.1.2 Analysis

Frequency Response Analysis

Only modal studies have been conducted on P-POD finite element models. Frequency response analysis is the next important step in being able to predict the P-POD's behavior under vibration.

Low Frequency Vibration Modes

A number of relatively low frequency vibration modes showed up in testing (see Section 5.3.1). There is currently no definitive explanation for these modes, only assumptions. The dynamic response of the P-POD Mk. II should be carefully evaluated (at least at these frequencies) to provide a concrete explanation.

Spin Rate Due to Ejection From P-POD

This question of P-POD induced spin rates comes up time and time again. At the very least, a simple simulation can provide some insight into the ejection characteristics of CubeSats with various properties.

Friction Between Rails

The effect of friction (between P-POD and CubeSat rails) on ejection dynamics is unclear. The gap between rails, varying properties of CubeSats, and microgravity environment

make this a difficult problem. Best of luck!

8.1.3 Testing

Sine Sweep

Although there is a lot of random vibration data for the P-POD Mk. II, not many sine sweep tests were conducted. Additional sine sweep tests may help with finite element model verification.

Thermal Propagation

It may be beneficial to characterize the thermal propagation properties of the P-POD panels in order to provide a thermal environment for CubeSat customers.

Faraday Cage — EMI Protection — Verification

The P-POD Mk. II is designed to be a faraday cage, and should provide shielding of RF signals. However, this has never been tested.

Contamination Hazard Analysis

There has always been this desire to see what happens to the P-POD if something were to go terribly wrong inside. Unfortunately, the opportunity never presented itself, however as CubeSats continue to advance, it will be important to address contamination control aspects despite CubeSat disintegration, pressure vessel explosions, propellant and battery fires, etc. Lucky you...

8.1.4 Long Term Improvements

Kinematic Restraints for CubeSats

The P-POD currently has no structural restraints for its CubeSat payloads. This has been seen as a benefit as complicated interfaces leave a lot of room for error, especially in university projects. However, the current rattling of CubeSats is also undesirable as it increases loads on the CubeSats, the P-PODs, and makes it very difficult to analyze P-POD dynamics under vibration.

Force Sensors

Setting of release mechanisms on large spacecraft and launch vehicle systems is often performed with load cells attached to the release bolts to ensure proper preload. This is an expensive option and is not very practical for university programs. However various low cost pressure sensors and load cells are beginning to be available that may inspire creative solutions for monitoring release bolt preload as well as spring plunger preload.

Thermal Shielding Option

Thermal blankets or coatings could easily be added to a P-POD upon customer request. This option may become significant for missions where a P-POD is mounted to a spacecraft instead of a launch vehicle, not only for the payload, but for the P-POD mechanisms as well.

Bibliography

- [1] “Bolted Joint Diagrams with External Forces Applied”, 2007.
[<http://www.boltscience.com/pages/basics5.htm>](http://www.boltscience.com/pages/basics5.htm).
- [2] “Fastener and Screw / Bolt Design, Formula and Calculation”, 2007.
[<http://www.engineersedge.com/fastener...thread...menu.shtml>](http://www.engineersedge.com/fastener...thread...menu.shtml).
- [3] Richard T. Barrett. *Fastener Design Manual*. NASA Lewis Research Center, 1990.
- [4] Veronica Bashbush. “Characterization of the Internal and External Environments of the CubeSat P-POD and Test Pod”. Master’s thesis, California Polytechnic State University, 2003.
- [5] Laurence J. Bement. *A Manual for Pyrotechnic Design, Development, and Qualification*. NASA Langley Research Center, 1995.
- [6] The CubeSat Program. *CubeSat Design Specification Rev. 9*, 2005.
- [7] James Cutler and Greg Hutchins. “OPAL: Smaller, Simpler, and Just Plain Luckier”. In *14th Annual AIAA/USU Conference on Small Satellites*, August 2000.
- [8] Emhart Teknologies. *Tensile Strength of Threaded Insert Assembly*. Technical Bulletin 68-2.
- [9] Emhart Teknologies. *Heli-Coil Insert Systems*, 2003.

- [10] David G. Gilmore, editor. *Spacecraft Thermal Control Handbook*. The Aerospace Corporation, 2002.
- [11] Cyril M. Harris. *Shock and Vibration Handbook*, volume 2. McGraw-Hill Book Company, 1961.
- [12] Hank Heidt and Jordi Puig-Suari. “CubeSat: A New Generation of Picosatellites for Education and Industry Low Cost Space Experimentation”. In *15th Annual AIAA/USU Conference on Small Satellites*, August 2001.
- [13] Vlier Inc. “Spring Plunger Selection Criteria”, 2000.
[<http://207.234.151.179/product...index/sld/sel...01...what.html>](http://207.234.151.179/product...index/sld/sel...01...what.html).
- [14] International Space Company Kosmotras. *Dnepr Space Launch System User’s Guide*, 2001.
- [15] Nicholas Johansen. “Qualification testing of the Cubesat Poly Pico-satellite Orbital Deployer”. Master’s thesis, California Polytechnic State University, 2003.
- [16] Robert C. Juvinall. *Fundamentals of Machine Component Design*. John Wiley & Sons, 2000.
- [17] Simon Lee. “Cal Poly Coordination of Multiple CubeSats on the DNEPR Launch Vehicle”. Master’s thesis, California Polytechnic State University, 2006.
- [18] Jim Loughlin. “FEMCI Book”. NASA Goddard Space Flight Center.
[<http://femci.gsfc.nasa.gov/femcibook.html>](http://femci.gsfc.nasa.gov/femcibook.html).
- [19] J. Scott Milne and Robert C. Baumann. *General Environmental Verification Specification*. NASA Goddard Space Flight Center, 1996.

- [20] Isaac Nason. “Development of the CubeSat P-POD Deployment System. Master’s thesis, California Polytechnic State University, 2002.
- [21] Dan Russell. “Vibrational Modes of a Beer Bottle”, 2006.
[<http://www.kettering.edu/~drussell/Demos/BeerBottle/beerbottle.html>](http://www.kettering.edu/~drussell/Demos/BeerBottle/beerbottle.html).
- [22] Mike Sampson. “NASA Parts Selection List”, 2002.
[<http://npp.nasa.gov/npsl/index.htm>](http://npp.nasa.gov/npsl/index.htm).
- [23] Wikimedia Foundation Inc. Dnepr rocket, 2006.
[<http://en.wikipedia.org/wiki/Dnepr...rocket>](http://en.wikipedia.org/wiki/Dnepr...rocket).

Appendix A

Aluminum 7075-T73 Properties

MatWeb Data Sheet

Aluminum 7075-T73; 7075-T735x

Date: 1/26/2007 12:38:44 AM

KeyWords:

AA7075-T73; AA7075-T735, UNS A97075; ISO AlZn5.5MgCu; Aluminium 7075-T73; Aluminium 7075-T735x

SubCat: Aluminum Alloy, Nonferrous Metal, 7000 Series Aluminum Alloy, Metal

Material Notes:

General 7075 characteristics and uses (from Alcoa): Very high strength material used for highly stressed structural parts. The T7351 temper offers improved stress-corrosion cracking resistance.

Uses: Aircraft fittings, gears and shafts, fuse parts, meter shafts and gears, missile parts, regulating valve parts, worm gears, keys, aircraft, aerospace and defense applications.

Data points with the AA note have been provided by the Aluminum Association, Inc. and are NOT FOR DESIGN.

Component	Value	Min	Max
Aluminum, Al		87.1	91.4
Chromium, Cr		0.18	0.28
Copper, Cu		1.2	2
Iron, Fe			0.5
Magnesium, Mg		2.1	2.9
Manganese, Mn			0.3
		0.05	
		0.15	
Silicon, Si			0.4
Titanium, Ti			0.2
Zinc, Zn		5.1	6.1

Properties	Value	Min	Max	Comment
Physical				
Density, g/cc	2.81	--	--	AA; Typical
Mechanical				
Hardness, Brinell	135	--	--	500 kg load with 10 mm ball. Calculated value.
Hardness, Knoop	120	--	--	Converted from Brinell Hardness Value
Hardness, Rockwell A	50.5	--	--	Converted from Brinell Hardness Value
Hardness, Rockwell B	82	--	--	Converted from Brinell Hardness Value
Hardness, Vickers	155	--	--	Converted from Brinell Hardness Value
Tensile Strength, Ultimate, MPa	505	--	--	
Tensile Strength, Yield, MPa	435	--	--	
Elongation at Break, %	13	--	--	In 5 cm; Sample 1.6 mm thick Average of Tension and Compression. In Aluminum alloys, the compressive modulus is typically 2% greater than the tensile modulus
Modulus of Elasticity, GPa	72			
Poissons Ratio	0.33	--	--	
Fatigue Strength, MPa	150	--	--	500,000,000 Cycles
Fracture Toughness, MPa-m ^{1/2}	32	--	--	Plate. K(IC) in L-T Direction
Fracture Toughness, MPa-m ^{1/2}	20	--	--	Plate. K(IC) in SL direction
Fracture Toughness, MPa-m ^{1/2}	20	--	--	Plate. K(IC) in T-L direction
Machinability, %	70	--	--	0-100 Scale of Aluminum Alloys
Shear Modulus, GPa	26.9	--	--	
Shear Strength, MPa	300	--	--	Calculated value.
Electrical				
Electrical Resistivity, ohm-cm	4.30E-06	--	--	
Thermal				
CTE, linear 68°F, µm/m-°C	23.6	--	--	AA; Typical; Average over 68-212°F range.
CTE, linear 250°C, µm/m-°C	25.2	--	--	Average over the range 20-300°C
Specific Heat Capacity, J/g-°C	0.96	--	--	
Thermal Conductivity, W/m-K	155	--	--	AA; Typical range based on typical composition for wrought products 1/4 inch thickness or greater.
Melting Point, °C	--	477	635	Homogenization may raise eutectic melting temperature 20-40°F but usually does not eliminate eutectic melting.
Solidus, °C	477	--	--	AA; Typical
Liquidus, °C	635	--	--	AA; Typical
Processing				
Annealing Temperature, °C	413	--	--	
Solution Temperature, °C	--	466	482	
Aging Temperature, °C	107	--	--	two stage treatment - second stage 325 to 350°F

Appendix B

Design Load Definition

The mounting bolts were designed by first defining the environment in which the P-POD would operate. Since the rails of the P-POD allow the bolt pattern to be easily defined for each mission, and since the number of fasteners can be increased for more violent launch environments, mechanical interface requirements were first defined for the Dnepr launch environment.

Table B.1: Dnepr LV maximum structural load factors.

Maximum Load	Level	Occurs During
Longitudinal Acceleration	$7.8 \pm 0.5 \text{ G}$	2nd stage burn
Lateral Acceleration	$-1.0 \pm 0.7 \text{ G}$	SHM transportation
Random Vibration	6.5 G_{RMS}	Liftoff

The orientation of the P-POD is defined with the P-POD Z axis aligned with the launch vehicle longitudinal direction. An overall design load is defined based on the requirements for defining structural loads in the NASA GEVS document. Equation B.1 defines the combined load factor N_i in relation to steady state load factor S_i , low frequency dynamic load factor L_i , and high frequency random vibration load factor R_i [19].

$$N_i = S_i \pm \sqrt{L_i^2 + R_i^2} \quad (\text{B.1})$$

The combined load factors are then calculated for each axis in relation to the P-POD coordinate system.

$$N_x = N_y = -7.5, \quad N_z = 14.3$$

The final design load factor is then calculated by taking the root sum square of all three axes. This conservative approach defines the design load factor as the maximum load that can be present at the interface under worst case static and dynamic loading in all three axes simultaneously.

$$N = \sqrt{N_x^2 + N_y^2 + N_z^2} \quad (\text{B.2})$$

$$N = 17.8$$

A design force (in Newtons) is then computed by limiting the mass of the fully integrated P-POD system to 6 kg and by defining a safety factor of 2. The resulting design force is approximately 2093 newtons.

$$F_D = G_{\oplus} NM(SF) \quad (\text{B.3})$$

Appendix C

Fastener Design Methodology

C.1 Fastener Specifications

The launch vehicle interface, mounting bolts, and mounting bolt torque specs were all to be defined by the launch provider. For the purposes of the redesign, it was assumed that standard metric screws between grades 8.8 and 12.9 would be used to secure the P-PODs to the launch vehicle interface. This assumption provided a range of tensile and shear strengths to design the interface around. The properties below are ultimate tensile strength, yield strength in tension, proof load in tension, and proof load in shear.

Table C.1: Strength of metric grade fasteners.

	Grade 8.8	Grade 12.9
S_u	830 MPa	1220 MPa
S_y	660 MPa	1100 MPa
S_p	600 MPa	970 MPa
S_{sp}	348 MPa	562 MPa

Since stainless steel is much weaker in shear than in tension, shear loading on the bolts is the first case considered. Also, the coefficient of friction between the P-POD and launch vehicle interface was assumed to be zero (as is customary for worst case consideration of mating surfaces under vibration). Thus the benefits of friction in the system are ignored, making this a very conservative design approach.

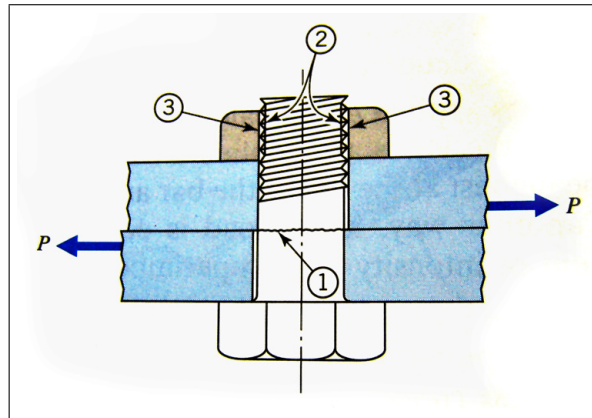


Figure C.1: Common failure points for bolted joints [16].

Another decision that was already made was the use of Heli-Coils at any bolt location where adjustments may need to be made or any joint where a failure would be catastrophic to the mission. Heli-Coil inserts are precision formed screw thread coils of stainless steel wire with a diamond shaped cross section [9]. The most important benefit to these threaded inserts is that they are replaceable. The ability to replace damaged threads without disassembling the P-POD is extremely beneficial and could easily save a mission in case of unexpected failures. Heli-Coil also claims that the threaded inserts evenly distribute loads against the entire threaded section (improving fatigue resistance) as opposed to tapped holes where the first few threads support nearly the entire load of the joint [9].

C.2 Shear Strength

The minimum shear strength of the bolts is assumed to be $S_{sy} = 0.58S_y$ based on the distortion energy theory for ductile materials [16]. At this point, the minor bolt diameters are calculated.

$$S_{sp} = \frac{F}{A}, \quad \text{or more applicably,} \quad A = \frac{F_D}{S_{sp}} \quad (\text{C.1})$$

By substituting the design load and proof stress defined above, the minimum required area is $1 \times 10^{-6} \text{ m}^2$. The fasteners must have a minor diameter of at least 1.13 mm to satisfy the requirements. The nearest acceptable fastener is of size M2 with a minor diameter of 1.62 mm.

C.3 Combined Shear and Tension

Since the P-POD interface will experience loading in the multiple directions simultaneously, it is important to consider the effects of loading in shear and tension simultaneously. The most conservative approach is to use a linear model to compare actual tensile and shear loads to allowable tensile and shear loads [3].

$$R_T + R_S \leq 1 \quad (\text{C.2})$$

Where R_T is the ratio of actual tensile load to allowable tensile load and R_S is the ratio of actual shear load to allowable shear load. The design load F_D takes into account forces acting in all directions simultaneously, and is not an accurate value to use in this analysis. To yield more realistic numbers, the loads were split into those acting on the mounting bolts in shear, and those acting in tension. The resulting equation becomes:

$$\frac{G_{\oplus}N_yM(SF)}{S_pA_t} + \frac{G_{\oplus}\sqrt{N_x^2 + N_z^2}M(SF)}{0.58S_pA_t} \leq 1$$

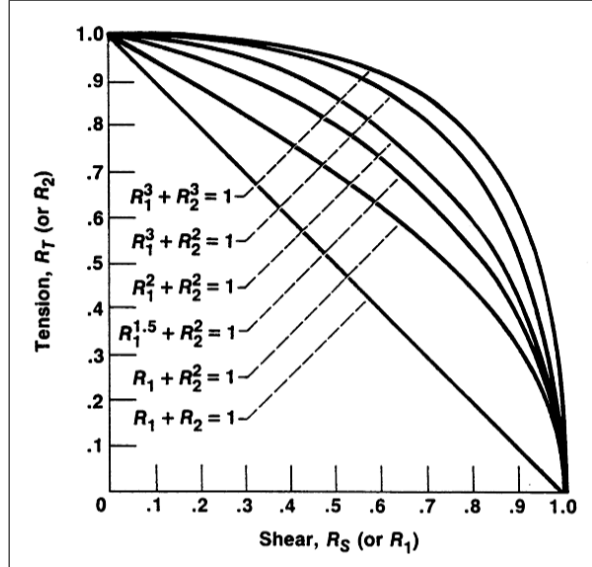


Figure C.2: Design curves for combined (tension and shear) loading [3].

Rearranging the equation, filling in values for N , M , and SF from above, and using the minimum value of 600 MPa for S_p , yields a minimum bolt root area A_t of 7.5×10^{-6} m². The smallest size fastener meeting this requirement is an M4 screw.

C.4 Preload

Next, it is important to consider the preload requirements for the bolted joint, and ensure that M4 screws are sufficient. Proper preload is important to prevent gapping — separation of clamped surfaces. It is common to preload fasteners to 90% of their proof load [3]. This practice usually creates much more preload than required, however, high preload has a number of important benefits.

- An increase in friction forces between surfaces helps counteract shear loading.

- High preload offers increased resistance to vibration, as relative motion between components is the primary reason for bolts backing out during vibration.
- Large preloads will minimize the possibility of gapping — where the fasteners support the full load of the joint.

The final benefit is somewhat counterintuitive and is just as much a factor of component stiffness as preload. To demonstrate the effects of stiffness and preload, a loading diagram is constructed from the following equations [1].

$$F_b = F_i + \frac{K_b}{K_b + K_j} F_e \quad (\text{C.3})$$

$$F_j = F_i - \frac{K_j}{K_b + K_j} F_e \quad (\text{C.4})$$

This method treats the bolted joint as a statically indeterminate problem [16]. We don't have to worry too much about the clamped aluminum surfaces failing under compression, so the goal is to minimize the loads experienced by the fasteners. The following bolt and joint stiffness are used.

Table C.2: Modulus of elasticity for aluminum and steel.

K_b	225 GPa	Slightly higher than the average for stainless steels.
K_j	72 GPa	LVI stiffness assumed to be comparable to AL7075-T73.

This diagram shows the loads experienced by the fasteners and the joint as an external load is applied. The slopes for K_b and K_j on the left side of the graph are determined by the stiffness ratios. The right side of the graph indicates gapping of the joint since the load supported by the joint F_j goes to zero. The slope of the fastener load F_b changes accordingly as the fasteners are now supporting the full load of the joint. With this chart, it is easy to see the effects of changing preload or stiffness.

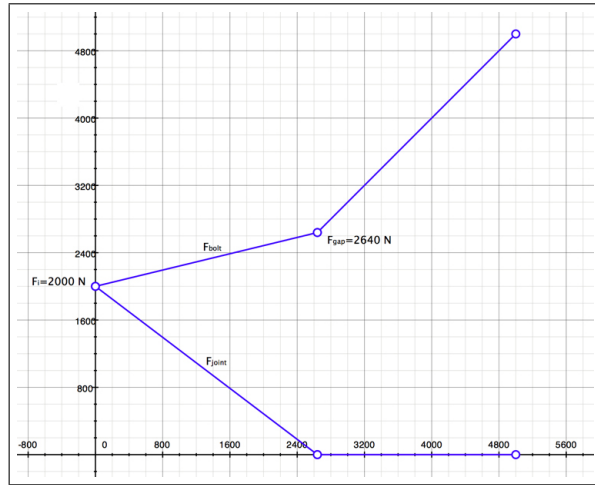


Figure C.3: Loading diagram for P-POD interface joints.

The minimum preload necessary $F_{i,min}$ is calculated by setting $F_j = 0$ in Equation C.4.

The minimum preload required to prevent gapping in the joint is about 1600 Newtons.

For added safety, we round up to $F_{i,min} = 2000$ Newtons. Based on the slopes, the fasteners support 24% of the external load, whereas the clamped surfaces support 76% of the external load. The load based on the equations is $F_{b,max} = F_i + 500$ Newtons. The ideal preload can be calculated using the following equation [16, 3].

$$F_{i,ideal} = 0.9A_tS_p \quad (\text{C.5})$$

For an M4 fastener under the defined loads, $F_{i,ideal} = 4700$ Newtons.

C.5 Tensile Strength

With this additional load defined, it is now important to verify that the selected fasteners are still strong enough for the system. This requires a quick check of tensile strength.

$$S_p = \frac{F_{b,max}}{A} \quad (\text{C.6})$$

Solving for area using $F_{i,min}$ yields a minor diameter requirement of 2.3 mm, which is

satisfied by using M3 fasteners. Solving the same equation using $F_{i,ideal}$ requires a minor diameter of 3.32 mm, satisfied by M4 or larger fasteners. Therefore, the M4 fasteners selected are adequate.

C.6 Thread Stripping: Fastener to Heli-Coil

The next failure mode considered was stripping of treads in the bolted joint. This failure can occur between bolt and Heli-Coil, as well as between the Heli-Coil and P-POD panel. Shear failure of the fastener threads against the Heli-Coil were considered first.

As a general rule of thumb, the preferred failure mode for bolted joints is for the bolt to fail in tension. The main benefit of designing the joint to fail in such a way is that it is much easier to replace a bolt rather than fix a threaded hole. In addition, bolt failures are visibly obvious whereas thread failures may go unnoticed. Common engineering practice states that in order to guarantee this type of failure, the shear area of the threads A_{ss} should be at least double that of the bolt tensile area A_t [2]. According to ISO 898-1, those parameters are defined as:

$$A_t = \frac{\pi}{4}(D - 0.938194p)^2 \quad (\text{C.7})$$

$$A_{ss} = \frac{1}{2}\pi A_t(D - 0.64952p)L_e \quad (\text{C.8})$$

where D is nominal screw diameter, p is thread pitch, and L_e is minimum required engagement length required to prevent stripping. L_e can then be found by substituting Equation C.7 into Equation C.8.

$$L_e = \frac{2A_t}{0.5\pi(D - 0.64952p)} \frac{1}{J} \quad (\text{C.9})$$

$$\text{where } J = \frac{S_{u,fastener}}{S_{u,Heli-Coil}} \quad \text{when } J < 1$$

Heli-Coils have a greater ultimate tensile strength (200ksi) than even the strongest bolts (grade 12.9) that the system is designed for. This adjustment factor has no effect on the required engagement length.

For an M4 screw, this equation yields a minimum thread engagement length of 3.15 mm, or less than one diameter (1D). Heli-Coils can be bought in 1D, 1.5D, and 2D lengths — 4 mm, 6 mm, and 8 mm respectively in this case.

C.7 Thread Stripping: Heli-Coil to P-POD

A technical bulletin published by Emhart allows the designer to choose the correct bolt size and Heli-Coil length based on the strengths of the bolt and parent material, as well as the load which the joint must sustain [8]. The document only provides this information for standard bolts. A UNF 8-36 screw was used for this analysis, as its dimensional properties are almost identical to that of an M4x0.7 screw.

By looking at the appropriate chart, it becomes clear that a Heli-Coil of 1D will provide the required load capacity. One should also notice that aluminum 7075-T73 is so strong, that a 1D Heli-Coil is sufficient for fastener grades up to 12.9 and fastener sizes up to 1/4-28 (the largest that can be installed in the P-POD panels). Since the mounting rails on the P-POD are 6 mm thick, there is no harm in using a 1.5D Heli-Coil instead.

C.8 Final Fastener Selection

At this point, a decision was made to use M6x1 fasteners to interface the P-POD to the launch vehicle. The larger screws have a number of benefits. Larger screws are easier to handle, as are the tools required to install them. The larger screws can sustain larger loads, and yield a higher safety factor — known as “derating” of components.

The Heli-Coil sizing charts for a 1/4-28 screw were consulted to verify that a 1D Heli-Coil would be sufficient. Bearing stresses on the P-POD mounting surface were not analyzed as there is still plenty of material surrounding the threaded holes.

That being said, this decision was made with limited knowledge, and a more robust design probably would have resulted if the smaller screws were used instead. Since the M4 screws are strong enough to support the loads, it would have been wiser to increase the thread engagement length rather than the screw diameter (1.5D for M4x0.7 rather than 1D for M6x1). The rationale behind this recommendation is to prevent damage to the P-POD panel threads at all cost. If greater load capacity is required, it is a better engineering practice to increase the number of fasteners used rather than the size of the fasteners.

C.9 Torque Specification

ISC Kosmotras claimed responsibility for the P-POD launch vehicle interface and mounting bolts. They chose a torque specification of $40 \pm 4 \text{ kg}_f\cdot\text{cm}$. In standard units, this translates to a nominal torque of 35 lb_f·in. Kosmotras allows for $\pm 10\%$ error, while most U.S. sources assume accuracies around $\pm 25\%$ when using a torque wrench [14, 3]. The following analysis is purely academic and serves as a verification of the calculations performed by ISC Kosmotras.

There is a great deal of literature regarding the derivation of torque values and their accuracies. Among other things, the amount of friction between the threads has a great deal of influence on the amount of torque required to generate a certain preload. Without going into detail here, a simple equation can be used to produce a torque specification [3].

$$T = KF_id \tag{C.10}$$

K is the torque coefficient, F_i is the preload, and d is the bolt diameter. Many sources use a torque coefficient of 0.2 in this equation, however NASA states that a value of 0.15 is more realistic for steel on steel — as in this case [3]. The diameter, of course, is 0.006 meters.

With known torque, the preload is calculated to be between 4000 and 4900 Newtons. This is well above the minimum requirement defined in Appendix C.4. For curiosity's sake, the torque required to reach an ideal preload is calculated to be about 95 kg_f· cm.

Appendix D

P-POD Deployment Simulation

Deployment of CubeSats from the P-POD was modeled using Matlab and Simulink. Equations of motion were derived for three CubeSats and the pusher plate attached to the main spring. The simulation is a four degree of freedom model describing linear motion of the masses in one axis. No damping of any kind is incorporated into the model. Similarly, friction is ignored due to the difficulty in predicting friction forces between CubeSat and P-POD rails in microgravity. Spring forces are based on ideal springs with linear elasticity.

Accurate values are used for all springs. CubeSats and the pusher plate are treated as rigid bodies of zero length. Therefore, the results predict relative (as opposed to absolute) position. To make the simulation easier, the pusher plate motion is ignored once it reaches the front of the P-POD. The simulation plots show the pusher plate being ejected from the P-POD along with the CubeSats. This is not the case, as the pusher plate is attached to the main spring. In any case, the motion of the pusher plate after the CubeSats have been ejected is inconsequential.

D.1 Deployment Simulation Block Diagram

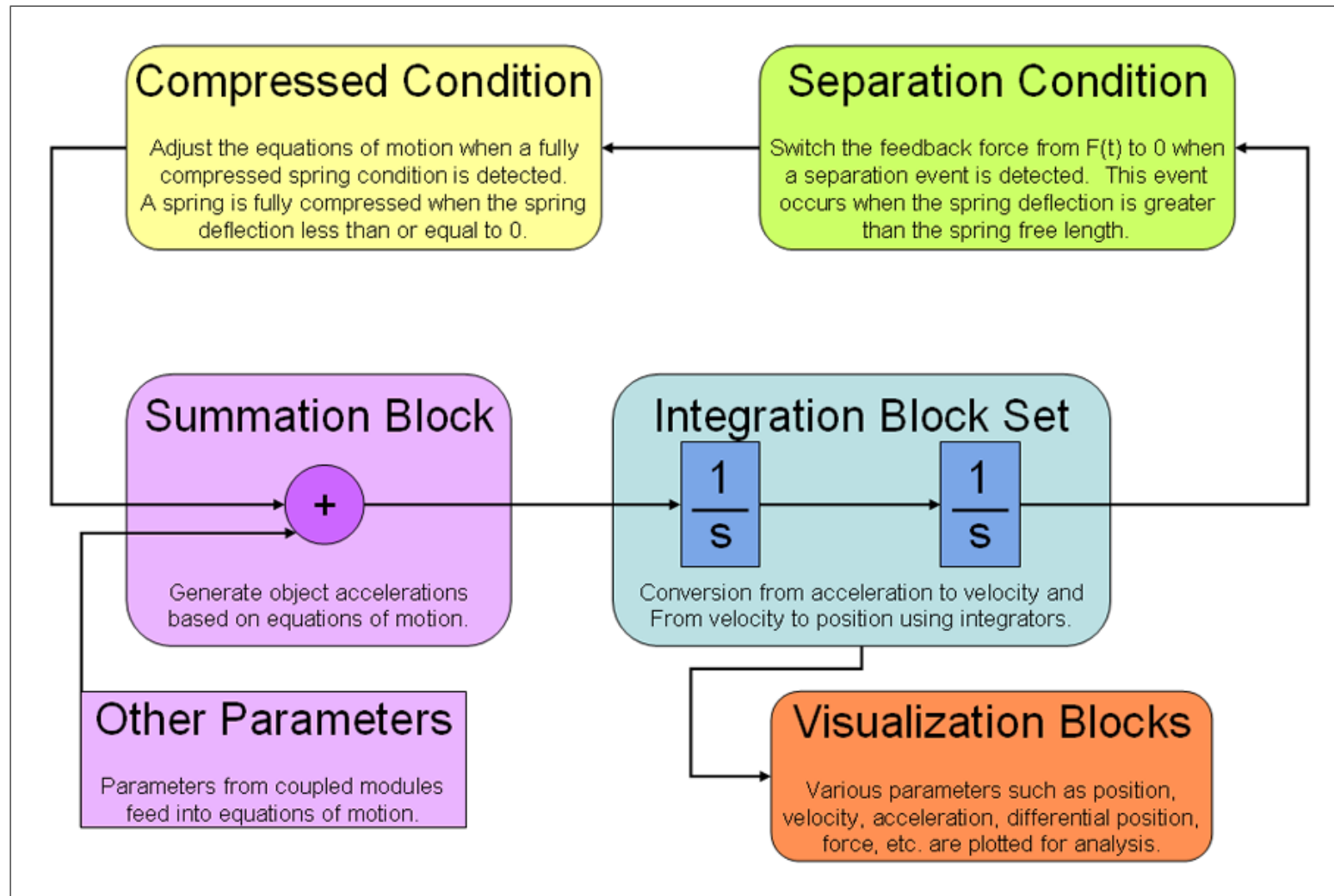


Figure D.1: Block diagram of deployment simulation components.

D.2 Deployment Simulation Integration Blocks

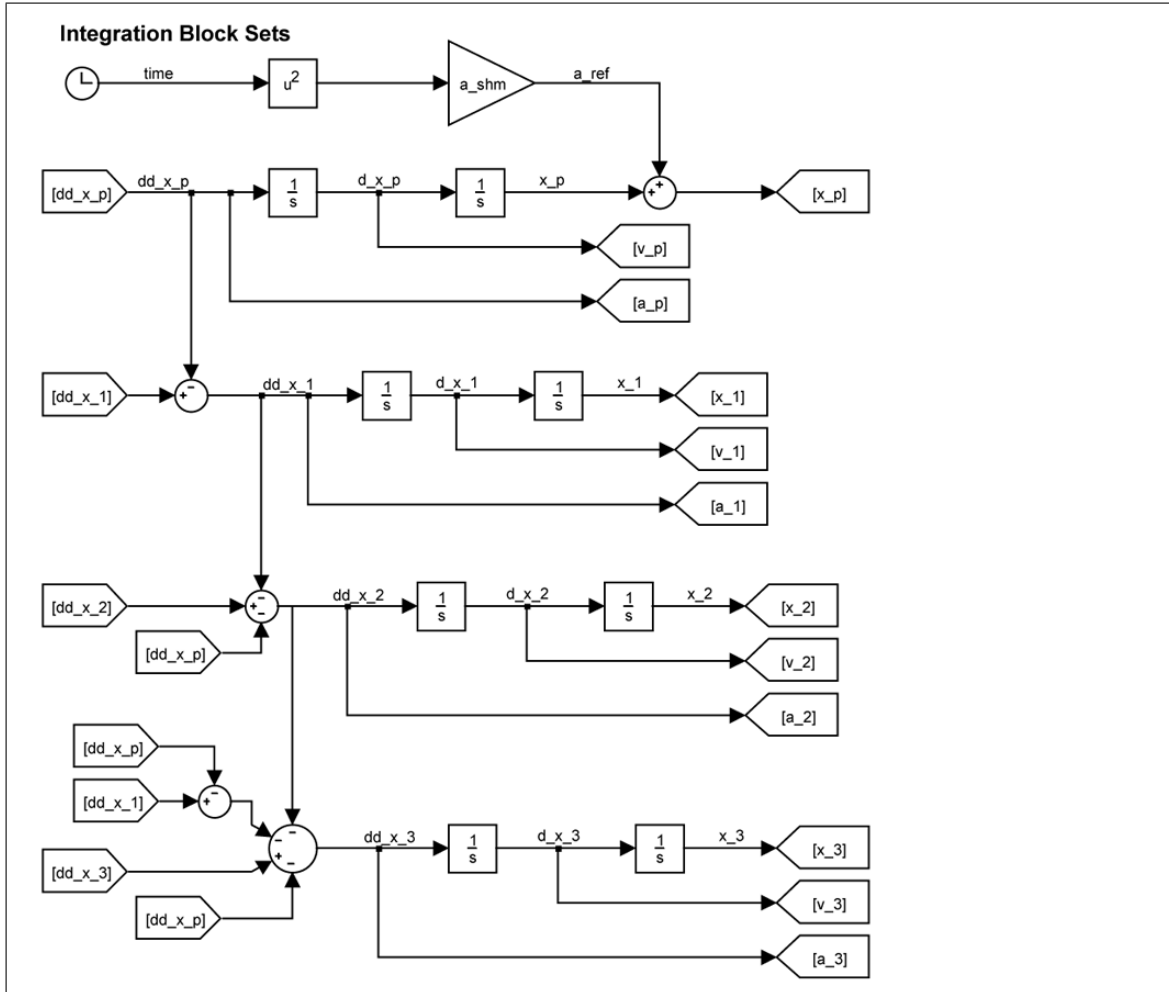


Figure D.2: Integration section of deployment simulation.

D.3 Simulation Parameter Code

```
% Parameters for CubeSat Deployment Simulation

clear

% === REFERENCE FRAME =====
% Acceleration of the reference frame in relation
% to the injection plane. This assumes linear
% motion, and is only accurate for short time
% frames. An example is the acceleration of the
% Dnepr space head module in the forward direction
% while deploying satellites aft.

a_ref = 0.25;    % Acceleration of shm in G's
a_shm = (1/2) * a_ref * 9.81;

% === MASSES =====
% Mass of deployment components in kilograms (kg).
% CubeSat numbering starts from the rear
% of the P-POD.

m_p = 0.1;      % Pusher Plate
m_1 = 1.0;      % CubeSat #1
m_2 = 1.0;      % CubeSat #2
m_3 = 1.0;      % CubeSat #3

% =====

% === SPRING CONSTANTS =====
% Spring stiffness in Newtons per meter (N/m).
% CubeSat numbering starts from the rear
% of the P-POD.

k_k = 11493;    % Kick Spring Plungers
k_m = 97;        % Main Spring
k_1 = 3369;      % CubeSat #1 Spring Plungers
k_2 = 3369;      % CubeSat #2 Spring Plungers
k_3 = 3369;      % CubeSat #3 Spring Plungers

% =====
```

```
% === SPRING FREE LENGTHS =====
% Extended lengths of springs in meters (m).
% Extended lengths can be the spring free lengths
% for normal springs, however for spring plungers
% free length does not equal extended length
% since the springs are still partially
% compressed when the tips are extended.
% CubeSat numbering starts from the rear
% of the P-POD.
```

```
EL_k = 0.00318; % Kick Spring Plungers
EL_m = 0.292;   % Main Spring
EL_1 = 0.00132; % CubeSat #1 Spring Plungers
EL_2 = 0.00132; % CubeSat #2 Spring Plungers
EL_3 = 0.00132; % CubeSat #3 Spring Plungers
% =====
```

```
% === SPRING PRESET LENGTHS =====
% This is the preset deflection in a spring
% plunger or similar system. This accounts for
% the nominal compression when the spring tips
% are fully extended. Units in (m).
% CubeSat numbering starts from the rear
% of the P-POD.
```

```
PL_k = 0.00112; % Kick Spring Preset
PL_1 = 0.00066; % CubeSat #1 Spring Preset
PL_2 = 0.00066; % CubeSat #2 Spring Preset
PL_3 = 0.00066; % CubeSat #3 Spring Preset
```

```
% =====
```

```
% === MAX FORCE =====
% Maximum force that can be exerted by the
% separation springs in kilograms.
% CubeSat numbering starts from the rear
% of the P-POD.
% 2 spring plungers fully compressed.
```

```
F_1_max = 2*k_1*(EL_1+PL_1);    % CubeSat #1
F_2_max = 2*k_2*(EL_2+PL_2);    % CubeSat #2
F_3_max = 2*k_3*(EL_3+PL_3);    % CubeSat #3
% =====
```

D.4 Deployment Simulation Separated Case Blocks

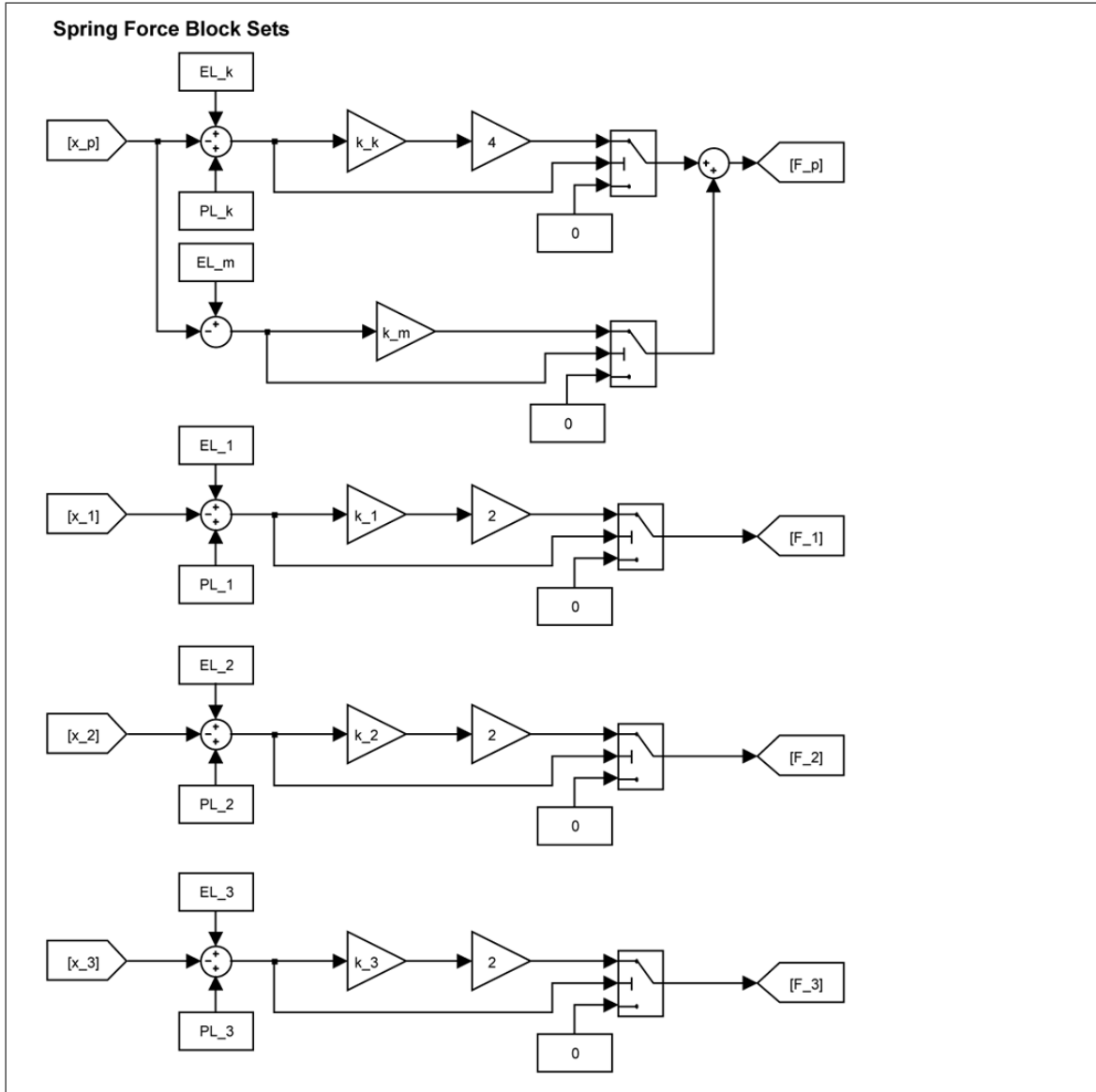


Figure D.3: Section of simulation to accommodate full extension of springs.

D.5 Deployment Simulation Compressed Case Blocks

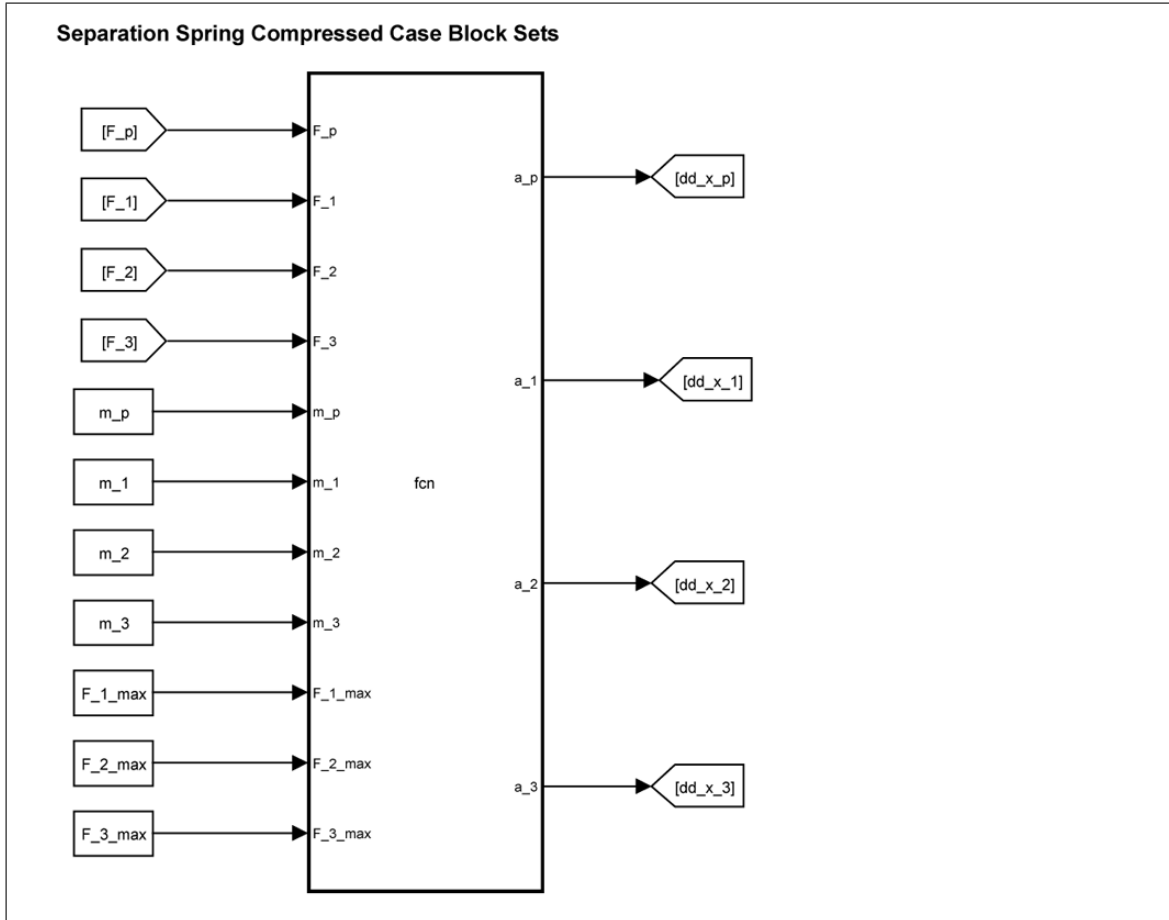


Figure D.4: Section of simulation to accommodate full compression of springs.

D.6 Compressed Case Code

```
% Function to deal with full compression of spring
% plungers between CubeSats. Nested if statements
% redefine equations of motion for all 3 CubeSats
% and the pusher plate on the fly in each iteration
% of the code.

function [a_p, a_1, a_2, a_3] = fcn(F_p, F_1, F_2, F_3,
m_p, m_1, m_2, m_3, F_1_max, F_2_max, F_3_max)

if F_p >= F_1
    if F_1 >= F_2
        if F_2 >= F_3
            a_p = (F_p/(m_p+m_1+m_2+m_3));
            a_1 = (F_p/(m_p+m_1+m_2+m_3));
            a_2 = (F_p/(m_p+m_1+m_2+m_3));
            a_3 = (F_p/(m_p+m_1+m_2+m_3));
        else %F_2 < F_3
            a_p = ((F_p-F_3)/(m_p+m_1+m_2));
            a_1 = ((F_p-F_3)/(m_p+m_1+m_2));
            a_2 = ((F_p-F_3)/(m_p+m_1+m_2));
            a_3 = (F_3/m_3);
        end
    else %F_1 < F_2
        if F_2 >= F_3
            a_p = ((F_p-F_2)/(m_p+m_1));
            a_1 = ((F_p-F_2)/(m_p+m_1));
            a_2 = (F_2/(m_2+m_3));
            a_3 = (F_2/(m_2+m_3));
        else %F_2 < F_3
            a_p = ((F_p-F_2)/(m_p+m_1));
            a_1 = ((F_p-F_2)/(m_p+m_1));
            a_2 = ((F_2-F_3)/(m_2));
            a_3 = (F_3/m_3);
        end
    end
else %F_p < F_1
    if F_1 >= F_2
        if F_2 >= F_3
            a_p = ((F_p-F_1)/m_p);
            a_1 = (F_1/(m_1+m_2+m_3));
            a_2 = (F_1/(m_1+m_2+m_3));
            a_3 = (F_1/(m_1+m_2+m_3));
        else %F_2 < F_3
            a_p = ((F_p-F_1)/m_p);
            a_1 = ((F_1-F_3)/(m_1+m_2));
            a_2 = ((F_1-F_3)/(m_1+m_2));
            a_3 = (F_3/m_3);
        end
    else %F_1 < F_2
        if F_2 >= F_3
            a_p = ((F_p-F_1)/m_p);
            a_1 = (F_1-F_2)/m_1;
            a_2 = (F_2/(m_2+m_3));
            a_3 = (F_2/(m_2+m_3));
        else %F_2 < F_3
            a_p = ((F_p-F_1)/m_p);
            a_1 = (F_1-F_2)/m_1;
            a_2 = (F_2-F_3)/m_2;
            a_3 = (F_3/m_3);
        end
    end
end
end
end
```

D.7 Deployment Simulation Visualization Blocks

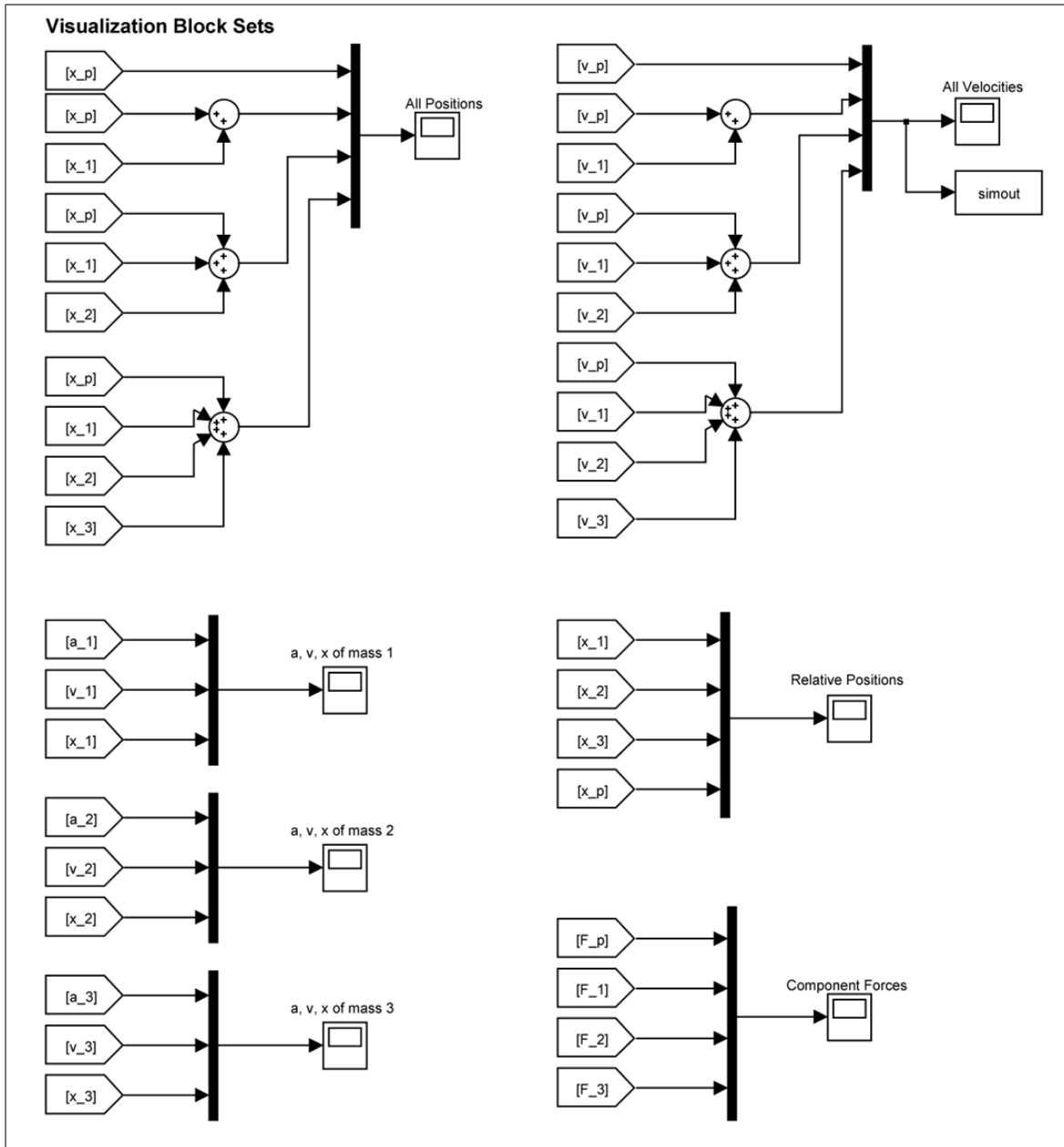


Figure D.5: Various visualization options for simulation results.

D.8 Position Plot for Nominal Case

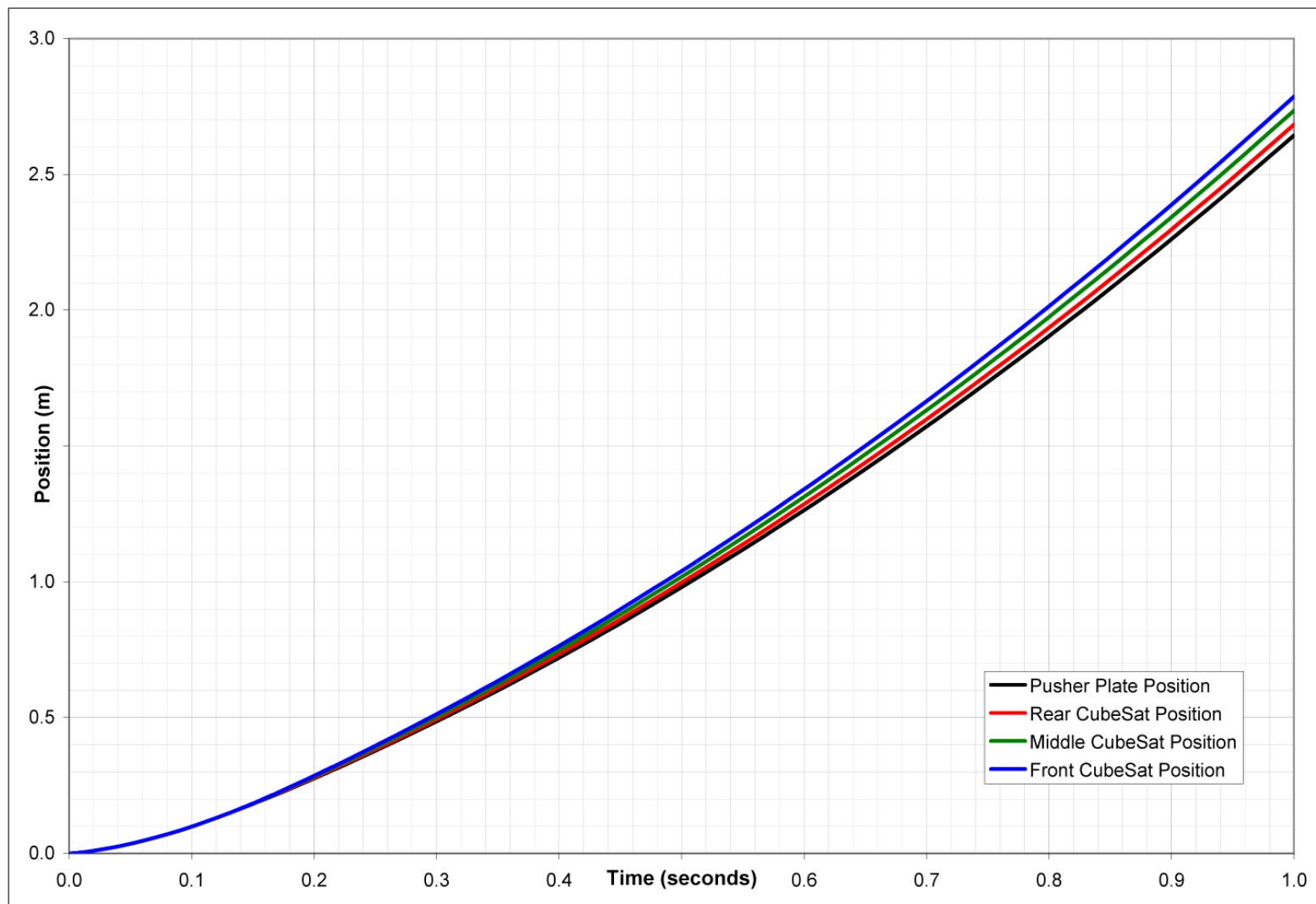


Figure D.6: Position vs. Time for nominal weight CubeSats ($m = 1.0 \text{ kg}$).

D.9 Velocity Plot for Nominal Case

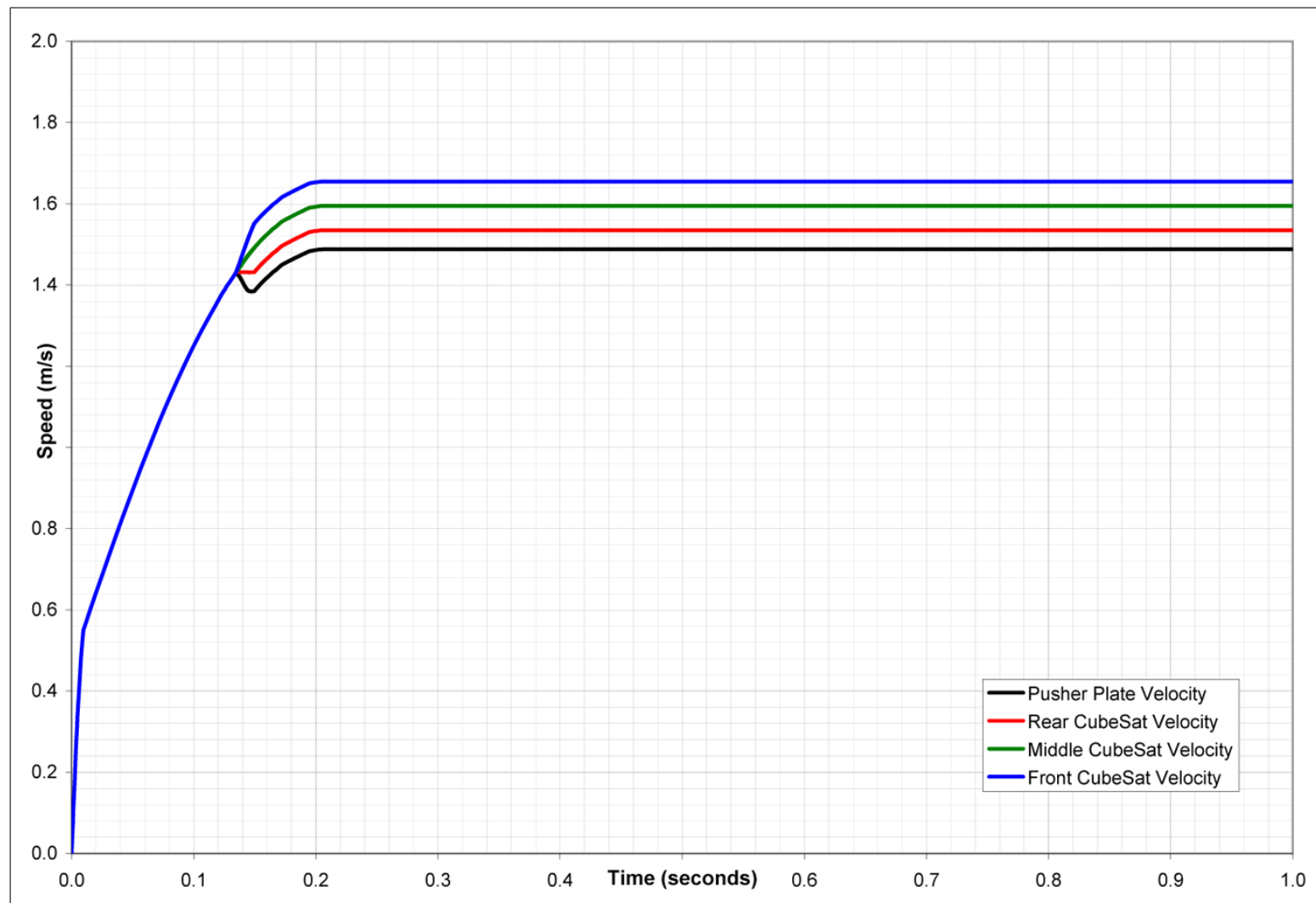


Figure D.7: Velocity vs. Time for nominal weight Cubesats ($m = 1.0 \text{ kg}$).

D.10 Velocity Plot for Light Case

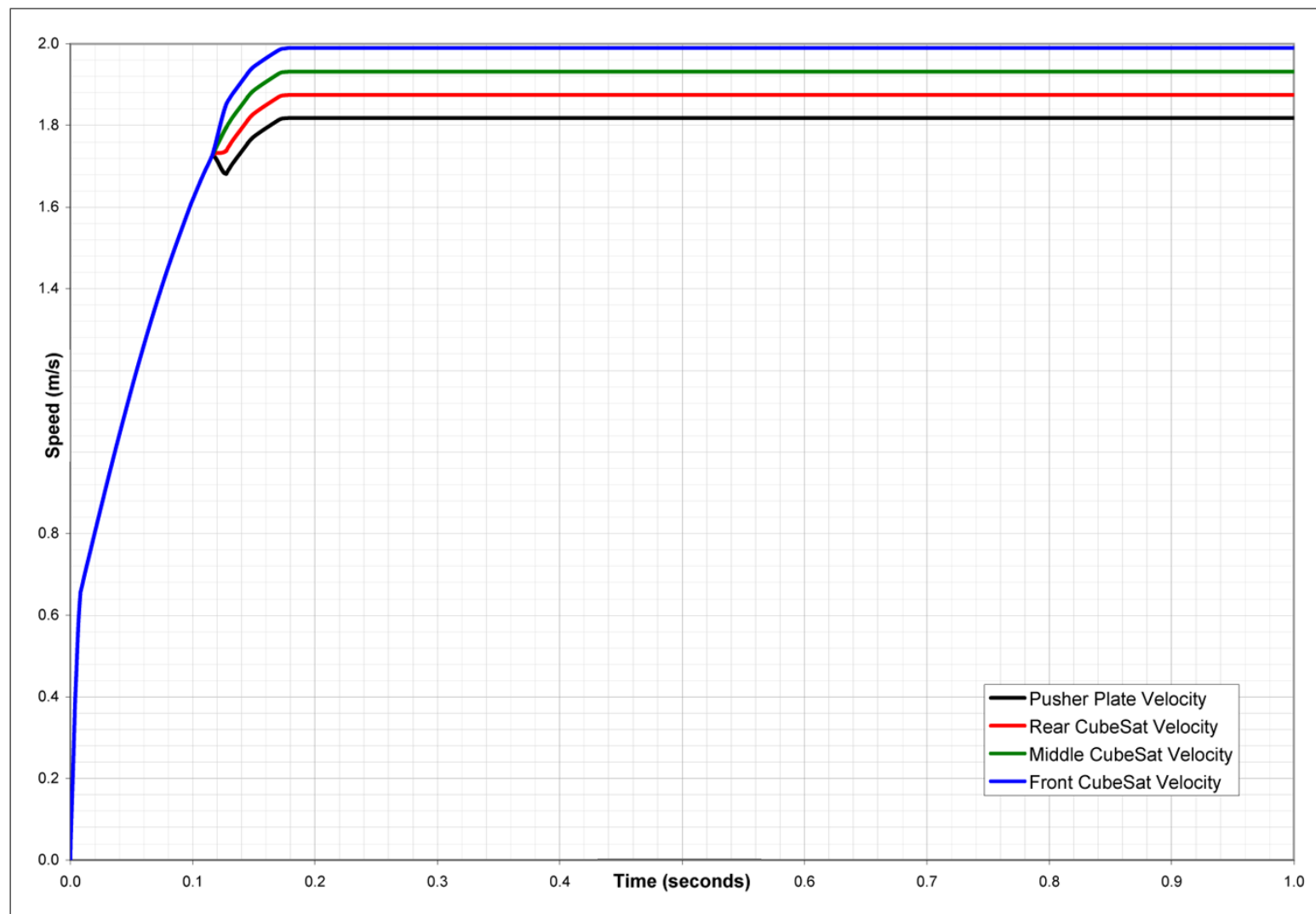


Figure D.8: Velocity vs. Time for underweight CubeSats ($m = 0.7$ kg).

D.11 Velocity Plot for Heavy Case

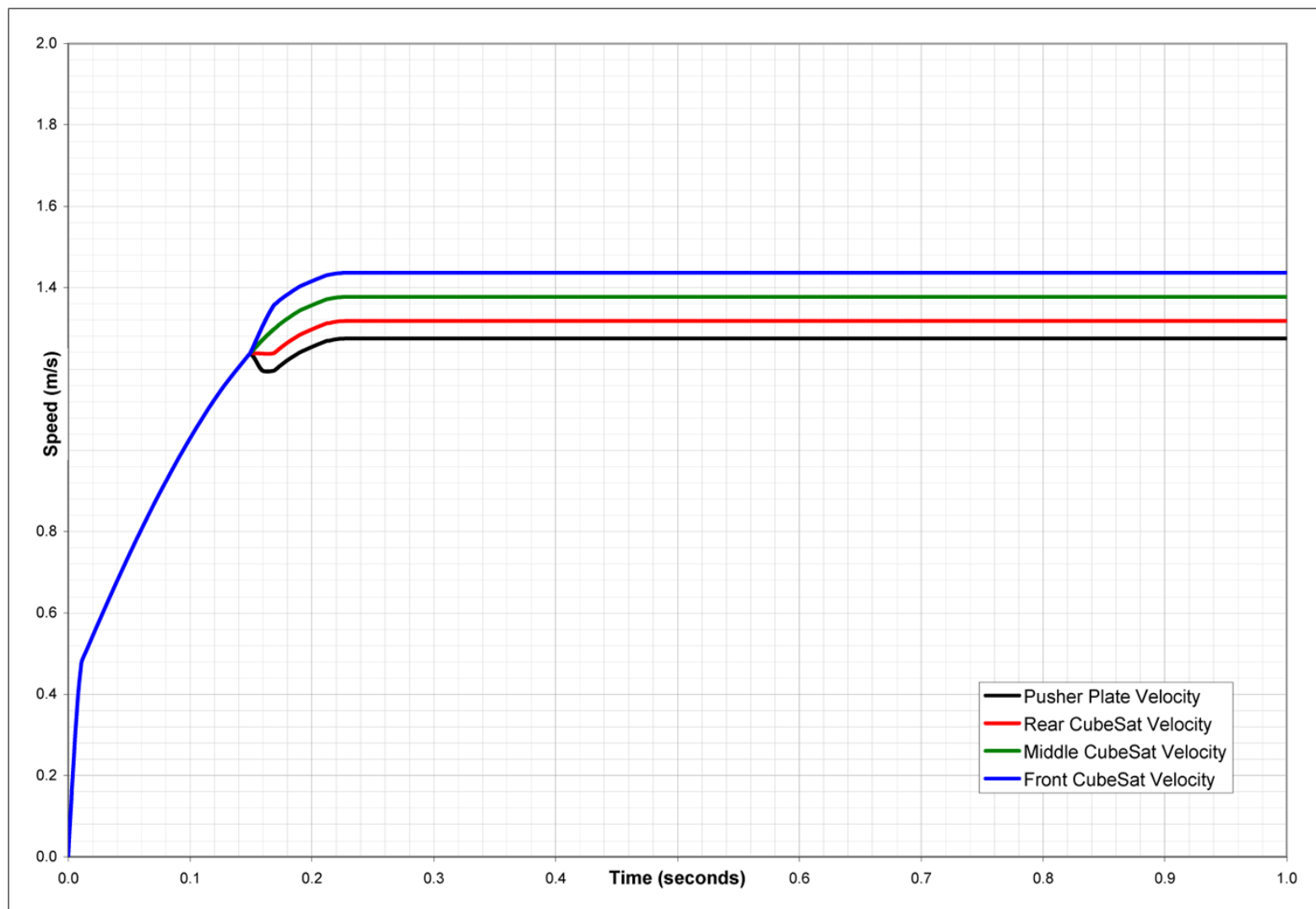


Figure D.9: Velocity vs. Time for overweight CubeSats ($m = 1.3$ kg).

Appendix E

Finite Element Analysis Results

This appendix provides details about finite element models used for prediction of natural frequencies of the P-POD Mk. II and comparison to vibration test data. Finite element models are discussed in Section 5.3.1 as are the conclusions drawn from this analysis. Three models were used as part of the analysis. A table of FEA properties and pictures of all the mode shapes are provided for each model.

E.1 Restrained Models

Results in this section were calculated based on models which were restrained in a manner that simulates the real world. Green triangles indicate restraints in the pictures below. “Fixed” type restraints (zero translation or rotation) were used in all cases except at the P-POD door hinges where “hinge” type restraints (zero translation, zero rotation along Y and Z axes) were used.

E.1.1 P-POD Frame

Table E.1: Finite element analysis properties for restrained P-POD frame.

FEA Package	COSMOSWorks
Material	7075-T73
Mesher Type	Solid Mesh
Mesher Used	Standard
Automatic Transition	Off
Smooth Surface	Off
Jacobian Check	None
Element Size	0.32905 in
Tolerance	0.016453 in
Mesh Quality	High
Number of Elements	23771
Number of Nodes	47170
Solver Quality	High
Solver Type	FFEPlus
Mass	1.63942 kg
Volume	0.000583424 m ³

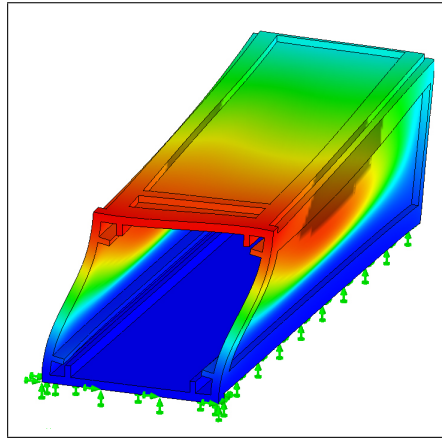


Figure E.1: P-POD Frame Restrained, 1st mode, 430.96 Hz.

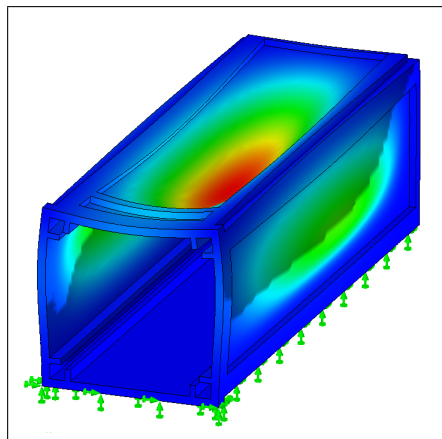


Figure E.2: P-POD Frame Restrained, 2nd mode, 582.92 Hz.

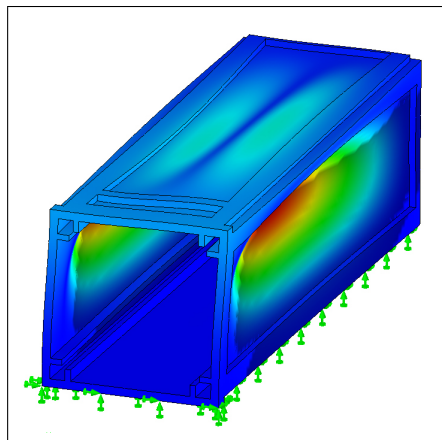


Figure E.3: P-POD Frame Restrained, 3rd mode, 760.6 Hz.

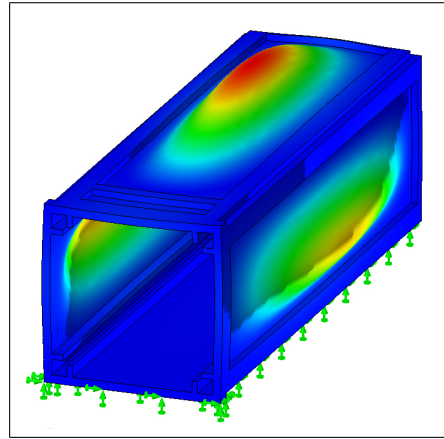


Figure E.4: P-POD Frame Restrained, 4th mode, 858.39 Hz.

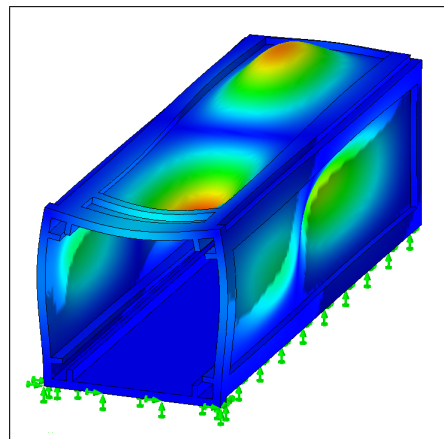


Figure E.5: P-POD Frame Restrained, 5th mode, 887.64 Hz.

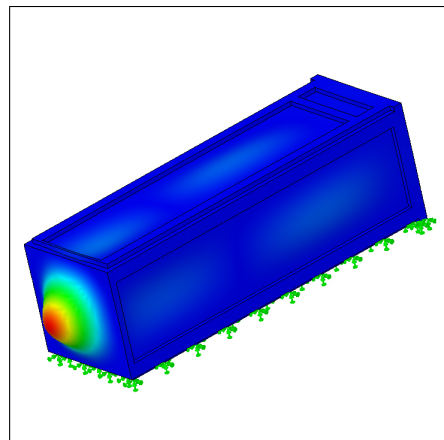


Figure E.6: P-POD Frame Restrained, 6th mode, 934.36 Hz.

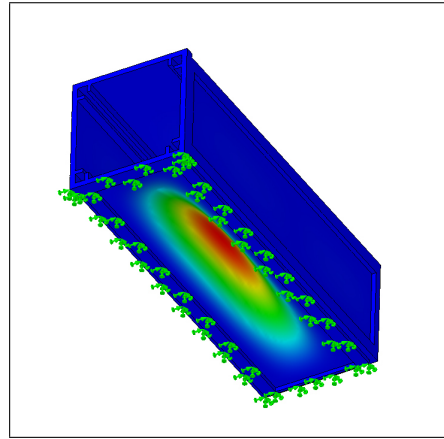


Figure E.7: P-POD Frame Restrained, 7th mode, 947.29 Hz.

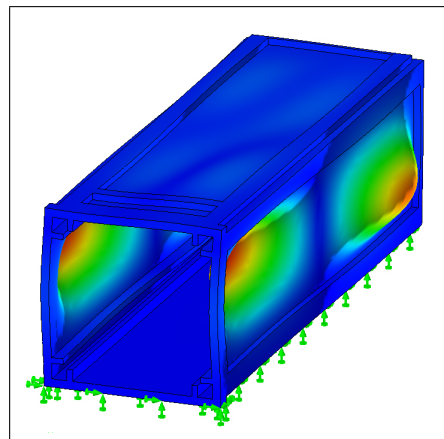


Figure E.8: P-POD Frame Restrained, 8th mode, 962.98 Hz.

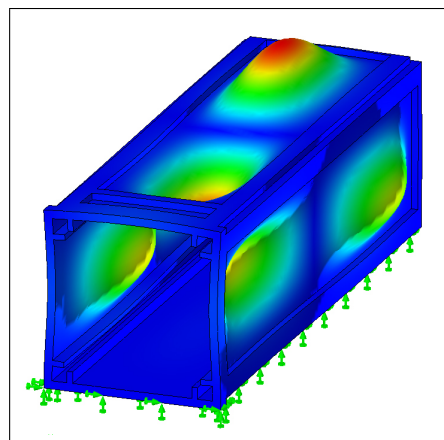


Figure E.9: P-POD Frame Restrained, 9th mode, 1011.3 Hz.

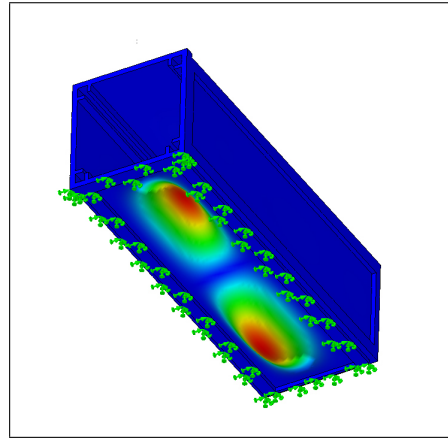


Figure E.10: P-POD Frame Restrained, 10th mode, 1064.7 Hz.

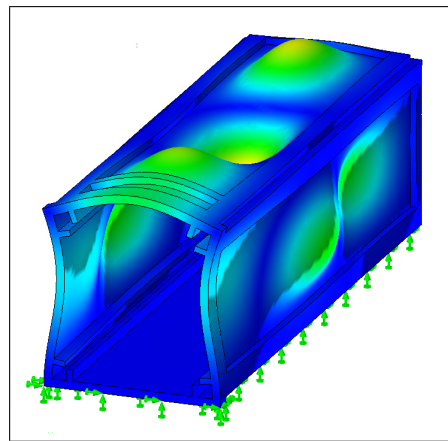


Figure E.11: P-POD Frame Restrained, 11th mode, 1109.8 Hz.

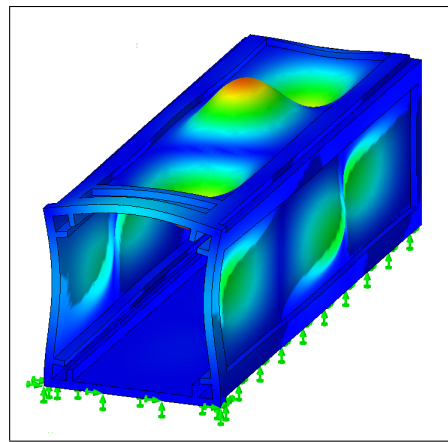


Figure E.12: P-POD Frame Restrained, 12th mode, 1220.2 Hz.

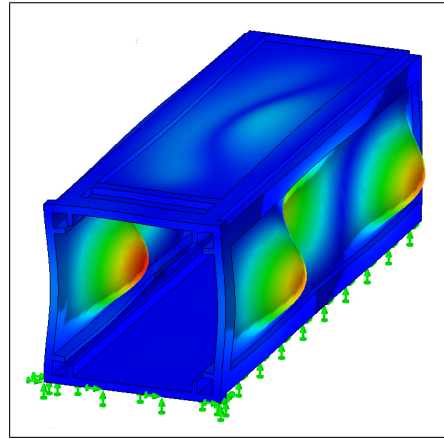


Figure E.13: P-POD Frame Restrained, 13th mode, 1229.9 Hz.

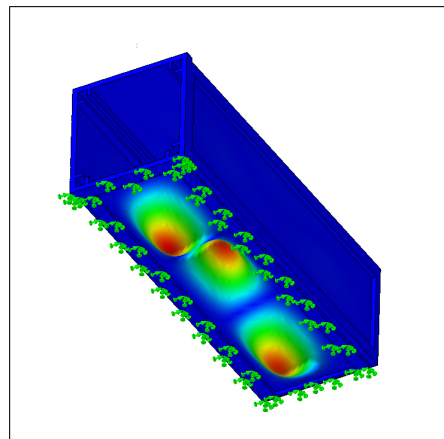


Figure E.14: P-POD Frame Restrained, 14th mode, 1255.5 Hz.

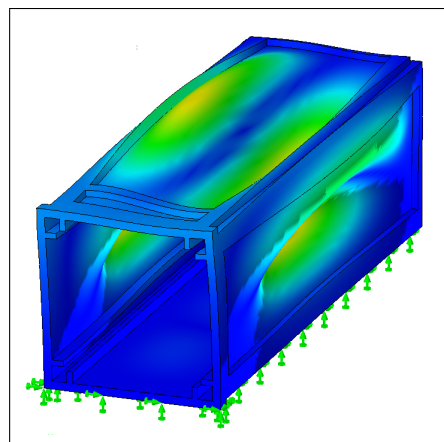


Figure E.15: P-POD Frame Restrained, 15th mode, 1262.9 Hz.

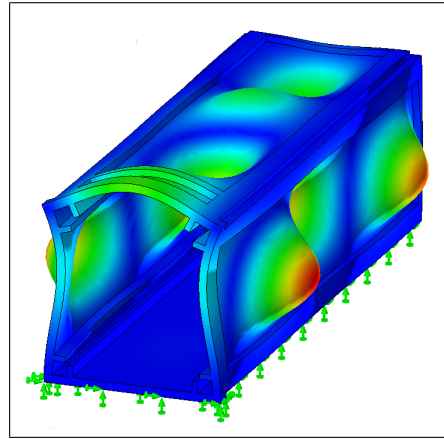


Figure E.16: P-POD Frame Restrained, 16th mode, 1283.6 Hz.

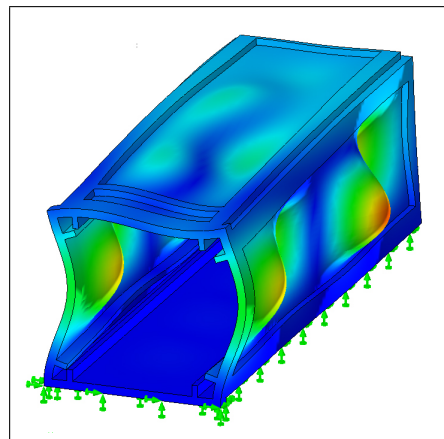


Figure E.17: P-POD Frame Restrained, 17th mode, 1472.6 Hz.

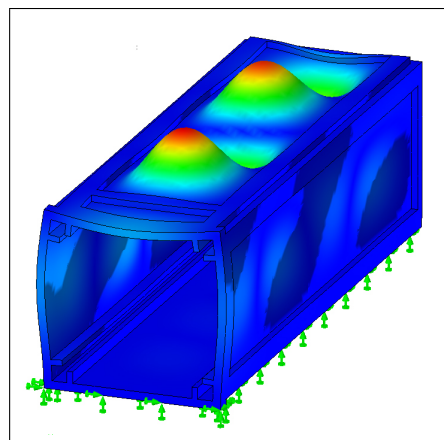


Figure E.18: P-POD Frame Restrained, 18th mode, 1479.1 Hz.

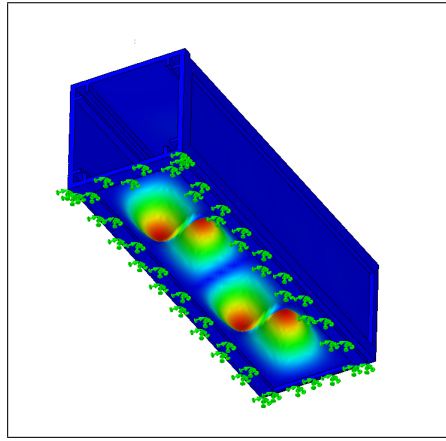


Figure E.19: P-POD Frame Restrained, 19th mode, 1518.7 Hz.

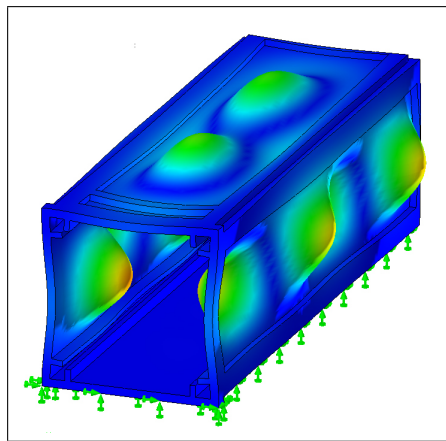


Figure E.20: P-POD Frame Restrained, 20th mode, 1533.1 Hz.

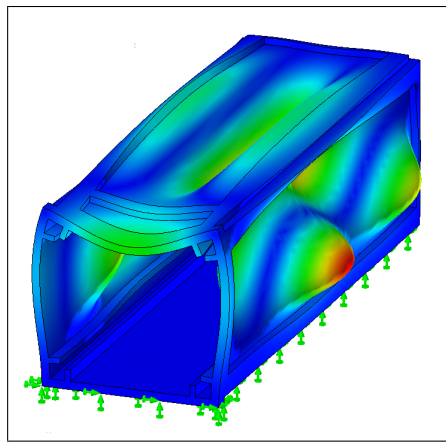


Figure E.21: P-POD Frame Restrained, 21st mode, 1611.3 Hz.

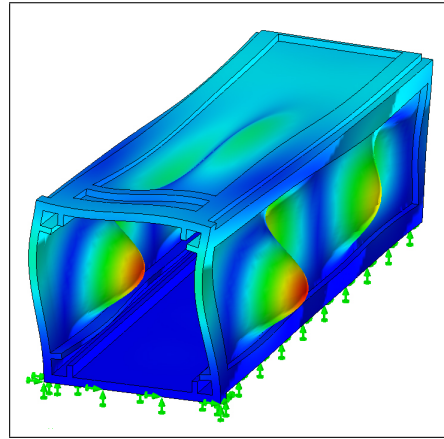


Figure E.22: P-POD Frame Restrained, 22nd mode, 1646 Hz.

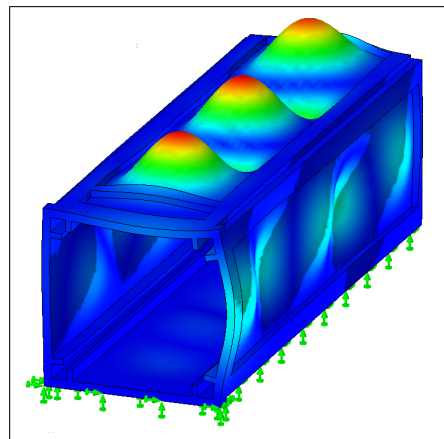


Figure E.23: P-POD Frame Restrained, 23rd mode, 1797.8 Hz.

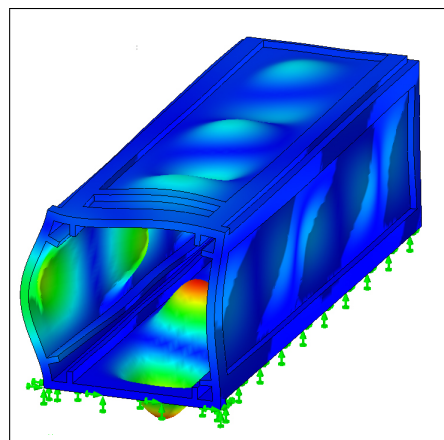


Figure E.24: P-POD Frame Restrained, 24th mode, 1863.9 Hz.

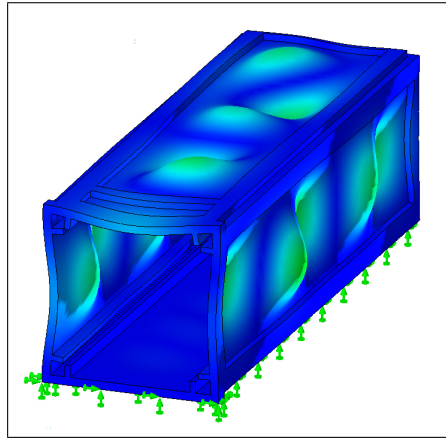


Figure E.25: P-POD Frame Restrained, 25th mode, 1938.9 Hz.

E.1.2 P-POD Door

Table E.2: Finite element analysis properties for restrained P-POD door.

FEA Package	COSMOSWorks
Material	7075-T73
Mesher Type	Solid Mesh
Mesher Used	Standard
Automatic Transition	On
Smooth Surface	On
Jacobian Check	4 Points
Element Size	0.14904 in
Tolerance	0.0074518 in
Mesh Quality	High
Number of Elements	24152
Number of Nodes	44866
Solver Quality	High
Solver Type	FFEPlus
Mass	0.152285 kg
Volume	5.41939 e -5 m ³

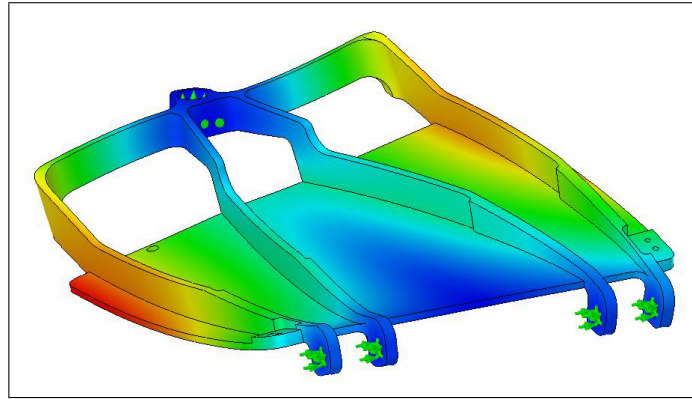


Figure E.26: P-POD Door Restrained, 1st mode, 613.04 Hz.

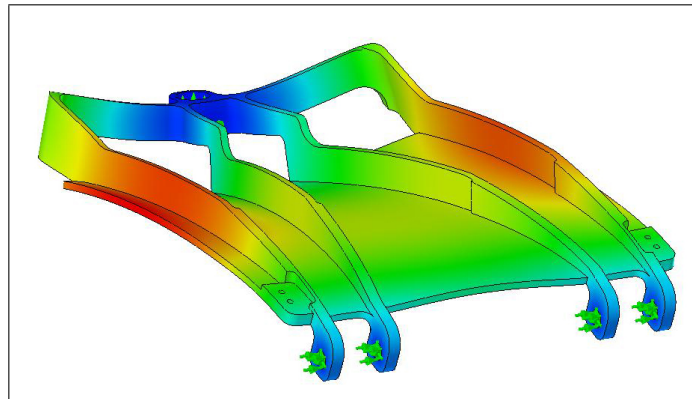


Figure E.27: P-POD Door Restrained, 2nd mode, 719.63 Hz.

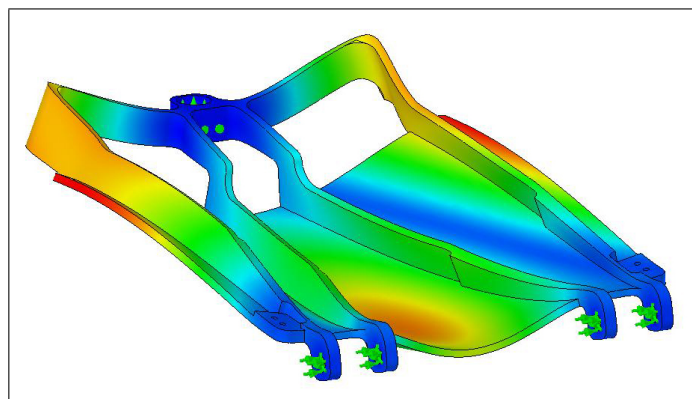


Figure E.28: P-POD Door Restrained, 3rd mode, 1137.3 Hz.

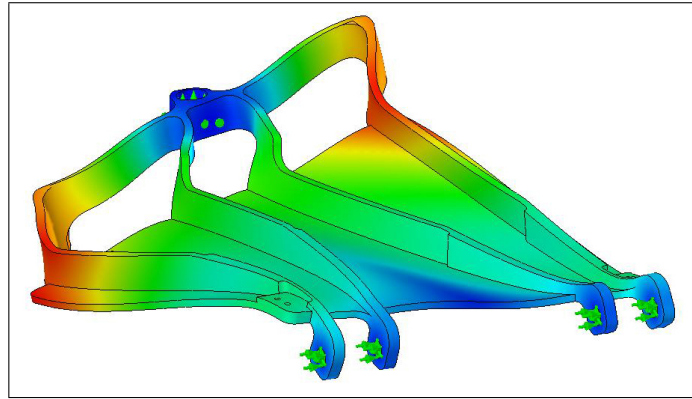


Figure E.29: P-POD Door Restrained, 4th mode, 1343.4 Hz.

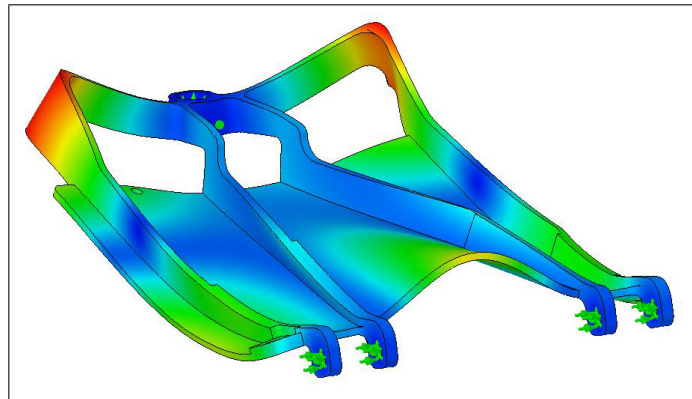


Figure E.30: P-POD Door Restrained, 5th mode, 1954.4 Hz.

E.1.3 P-POD Release Mechanism Subassembly (RMS)

Table E.3: Finite element analysis properties for restrained P-POD RMS.

FEA Package	COSMOSWorks
Material	7075-T73
Mesher Type	Solid Mesh
Mesher Used	Standard
Automatic Transition	Off
Smooth Surface	On
Jacobian Check	4 Points
Element Size	.18664 in
Tolerance	0.0093318 in
Mesh Quality	High
Number of Elements	11729
Number of Nodes	18383
Solver Quality	High
Solver Type	FFEPlus
Mass	0.199089 kg
Volume	1.06437 e -4 m ³

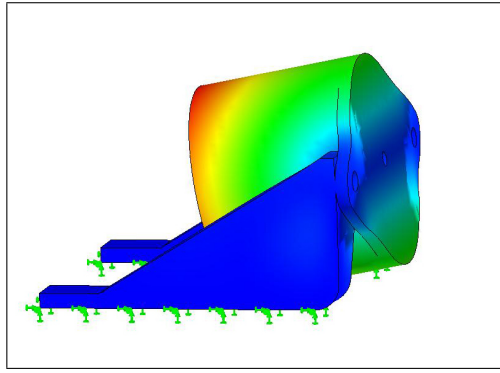


Figure E.31: P-POD RMS Restrained, 1st mode, 951.78 Hz.

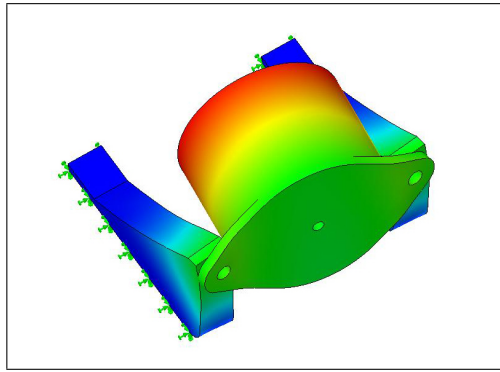


Figure E.32: P-POD RMS Restrained, 2nd mode, 1255.8 Hz.

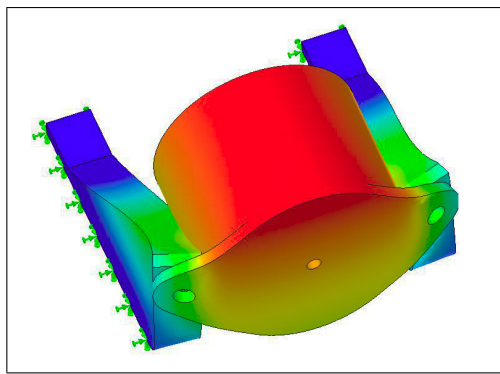


Figure E.33: P-POD RMS Restrained, 3rd mode, 1975.5 Hz.

Appendix F

Vibration Test Data

Both sine sweep and random vibration tests were performed on the P-POD Mk. II. Most of the tests consisted of random vibration tests following the NASA GEVS and Dnepr LV profiles [19, 14]. These test profiles are also discussed in Section 5.2. Accelerometers were placed in predefined locations as shown in Figure F.1

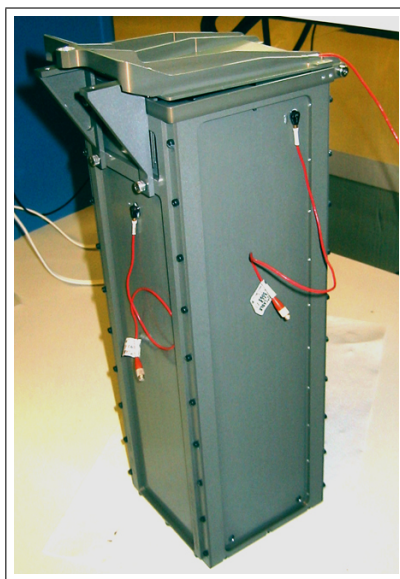


Figure F.1: VIbration test accelerometer locations.

F.1 Random Vibration Profiles

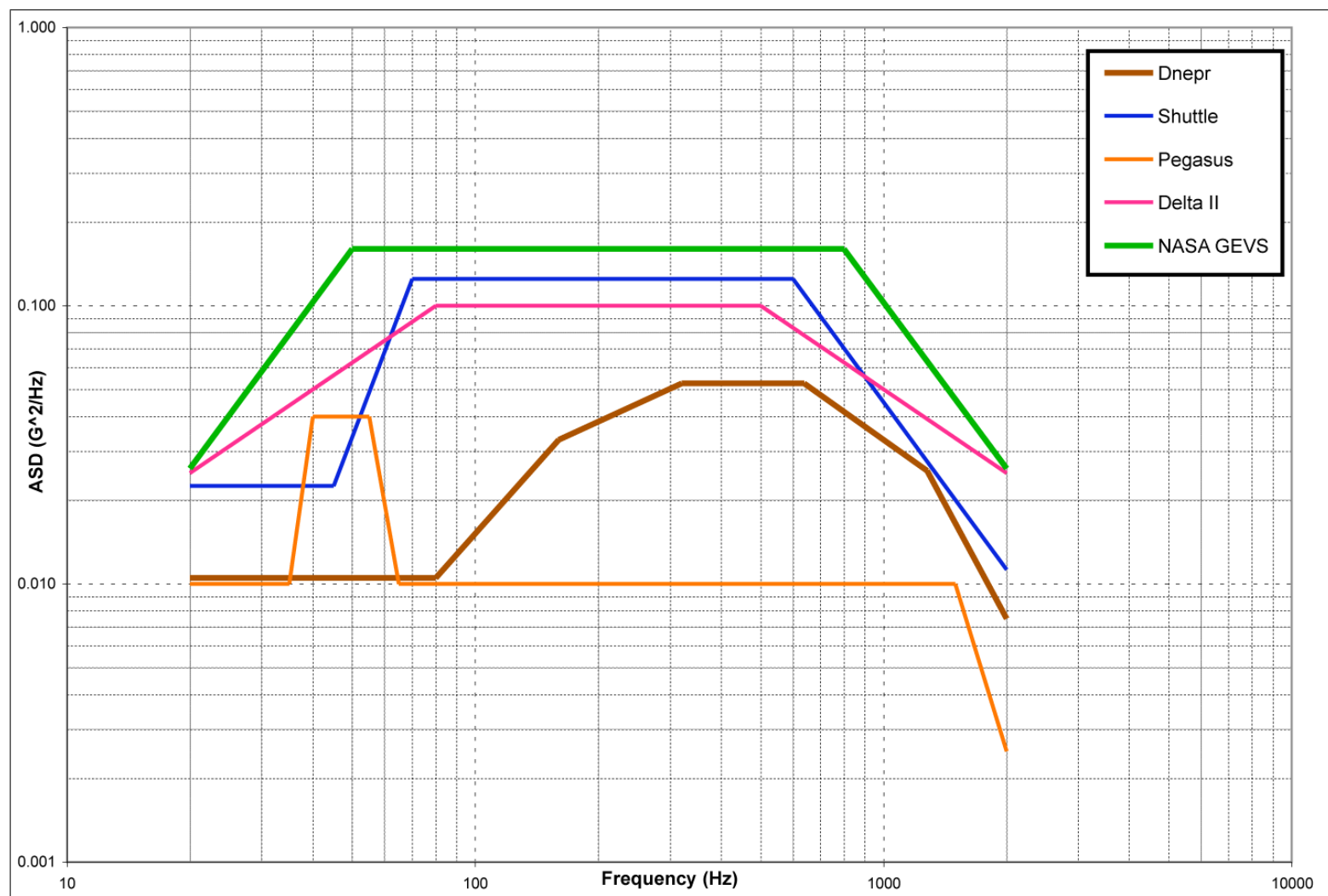


Figure F.2: Composite plot of various random vibration profiles.

F.2 Sample Vibration Data



Figure F.3: Sample plot of P-POD sine sweep test data.

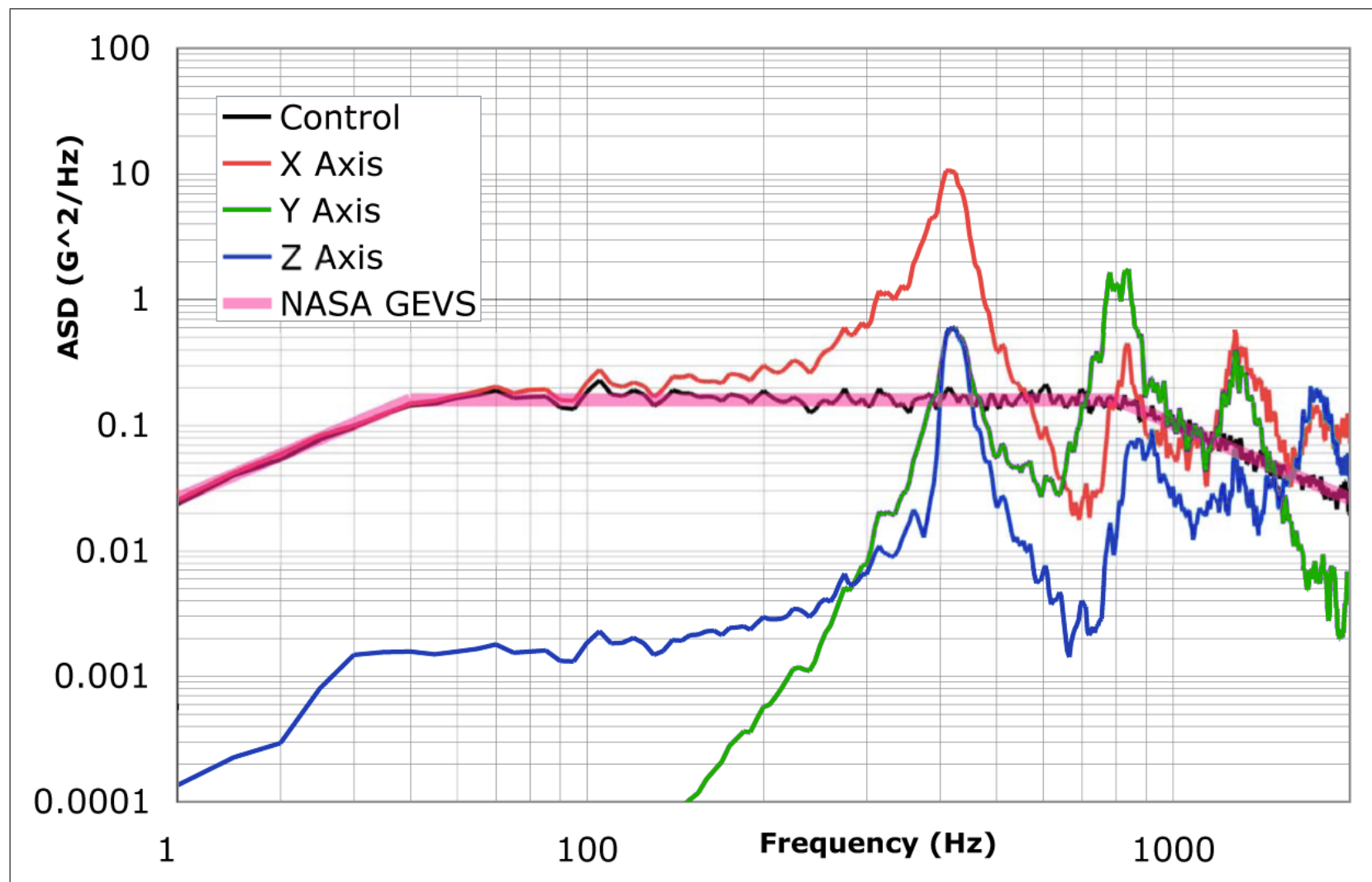


Figure F.4: Sample PSD plot of P-POD random vibration test data.

F.3 Reduced Natural Frequency Data

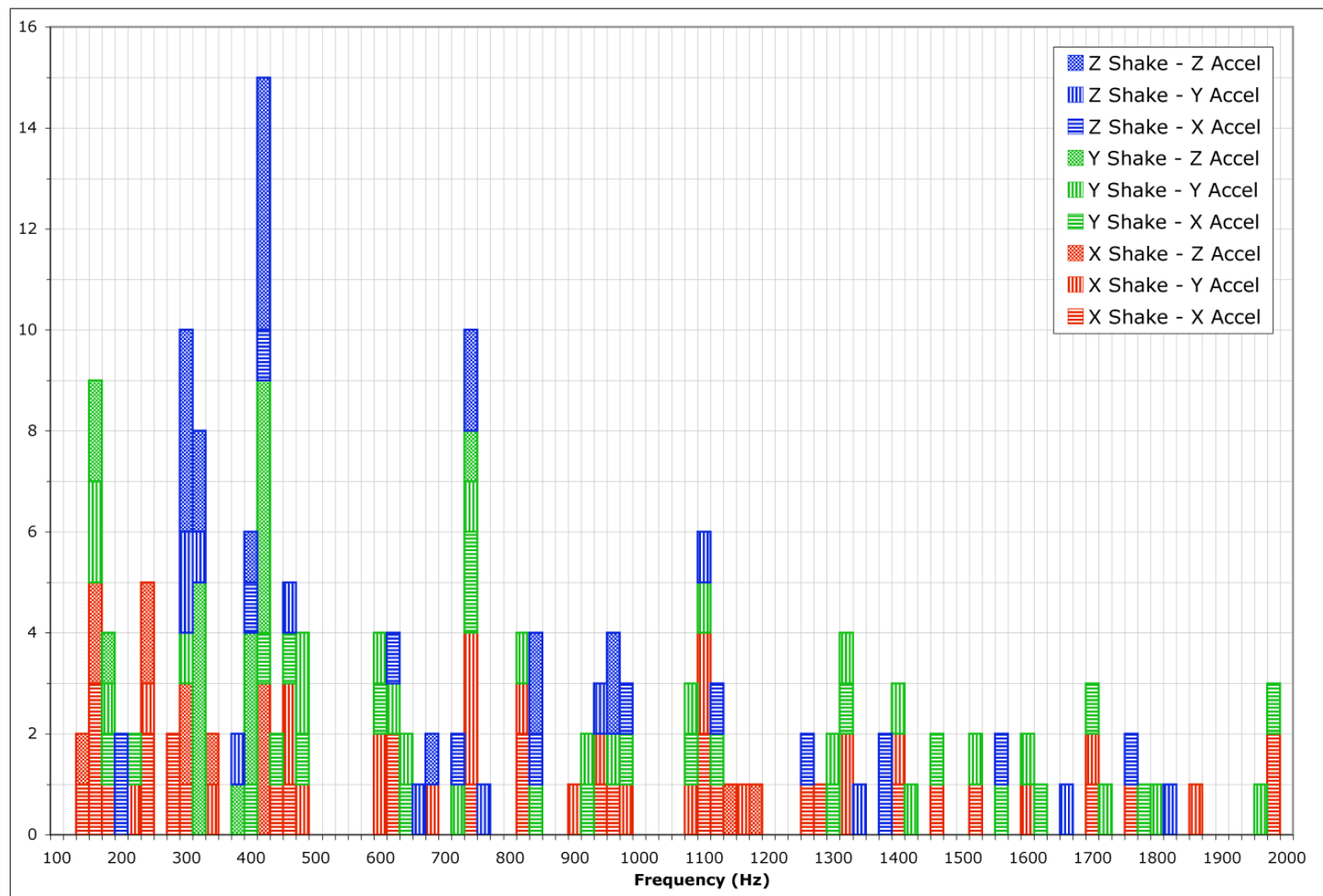


Figure F.5: Histogram of vibration accelerometer data.

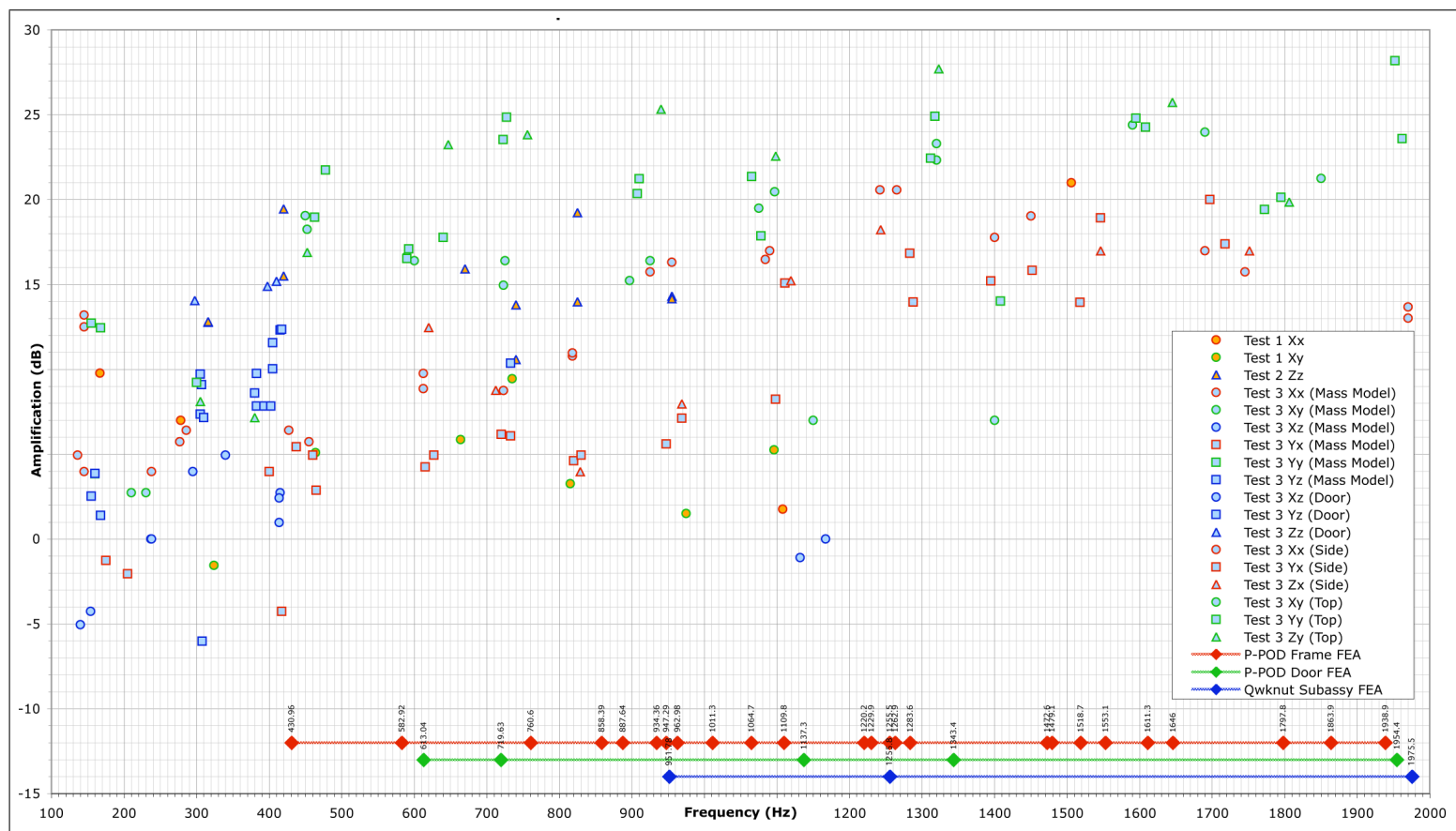


Figure F.6: Composite scatter plot of vibration accelerometer data.

Appendix G

Dnepr Launch Failure Analysis

The Dnepr launch vehicle (the SS-18 missile conversion variant) with a group of spacecraft aboard was launched from Baikonur Cosmodrome on July 26, 2006 at 22 hours 43 minutes, Moscow Standard Time. The launch ended up in a failure during the 73,9th second of flight.

A Ministerial Committee (hereinafter the Committee) chaired by a member of the Russian Academy of Sciences Nikolay A. Anfimov has been set up by the state authorities of Russia to investigate the cause of the Dnepr LV mission failure. Representatives of the Russian Space Agency, Russian Ministry of Defense, SDO Yuzhnoye (the rocket primary design and development entity), the State Enterprise Production Association Yuzniy Machine Building Plant (the rocket primary manufacturing entity), the Scientific and Production Enterprise KHARTRON-ARKOS (the rocket control system primary entity), ISC Kosmotras, FSUE TZNIIMASH and other organizations joined the Committee as its members.

The Committee has come to the conclusion that the emergency was caused by a short-time (0,26 sec) malfunctioning of the pumping hydraulic drive of combustion chamber number 4. The first stage thrust vector is controlled by the nozzle gimbal suspension. The control malfunctioning brought about the disturbances, which led to the roll instability, excessive dispersions of the yaw and pitch angles, and, eventually, the issuance of a command for the emergency shut down of the motor.

It has been determined that the hydraulic drive short-time in-flight malfunctioning occurred because of the heptil overheating inside the pipeline running from the motor to the hydraulic drive. And the heptil overheating was caused by the heat insulation damage resulted from non-compliance with the design and manufacturing documentation. The Dnepr LV launch failure study has not detected any flaws related to the long-term operation of the baseline SS-18 missiles.

Based on its conclusions the Committee has issued the following recommendations in regards to the Dnepr LV operation: to verify the condition of heat insulation of the heptil carrying pipelines of the SS-18 missiles that are being decommissioned and used for the spacecraft launch missions for compliance with the design and manufacturing documentation and, if necessary, modify them.

The conclusions made by the Committee were delivered to the State Committees of Russia and Kazakhstan established with the aim to investigate the Dnepr launch failure consequences.